DEVELOPING A MODEL TO INCREASE QUALITY OF DEM

A THESIS SUBMITTED TO
THE GRADUATE SCHOOL OF NATURAL AND APPLIED SCIENCES
OF
MIDDLE EAST TECHNICAL UNIVERSITY

BY

ONUR PAŞAOĞULLARI

IN PARTIAL FULFILLMENT OF THE REQUIREMENTS
FOR
THE DEGREE OF DOCTOR OF PHILOSOPHY
IN
GEODETIC AND GEOGRAPHIC INFORMATION TECNOLOGIES

FEBRUARY 2013

DEVELOPING A MODEL TO INCREASE QUALITY OF DEM

submitted by **ONUR PAŞAOĞULLARI** in partial fulfillment of the requirements for the degree of **Doctor of Philosophy** in **Geodetic and Geographic Information Technologies Department, Middle East Technical University** by,

Prof. Dr. Canan Özgen
Dean, Graduate School of **Natural and Applied Sciences**

_____

Assoc. Prof. Dr. Ahmet Coşar
Head of Department, **Geographic Information Technologies**

_____

Assoc. Prof. Dr. Nurünnisa Usul
Supervisor, **Civil Engineering Dept., METU**

_____

Examining Committee Members

Prof. Dr. S. Zuhal Akyürek
Civil Engineering Dept., METU

_____

Assoc. Prof. Dr. Nurünnisa Usul
Civil Engineering Dept., METU

_____

Assoc. Prof. Dr. Çağatay Candan
Electrical and Electronics Engineering Dept., METU

_____

 Prof. Dr. Gözde Bozdağı Akar
Electrical and Electronics Engineering Dept., METU

_____

Prof. Dr. Ibrahim Gürer
Civil Engineering Dept., Gazi University

_____

Date: 13 February 2013

I hereby declare that all information in this document has been obtained and presented in accordance with academic rules and ethical conduct. I also declare that, as required by these rules and conduct, I have fully cited and referenced all material and results that are not original of this work.

Name, Last Name   : Onur PAŞAOĞULLARI

Signature   :

ABSTRACT

DEVELOPING A MODEL TO INCREASE QUALITY OF DEM

Onur PAŞAOĞULLARI
Ph.D. Department of Geodetic and Geographic Information Technologies
Supervisor: Assoc. Prof. Dr. Nurünnisa USUL

February 2013, 101 pages

Low resolution (LR) Grid Digital Elevation Models (DEMs) are the inputs of multi frame super resolution (MFSR) algorithm to obtain high resolution (HR) grid DEM. In digital image MFSR, non-redundant information carrying LR image pairs are a necessity. By using the analogy between digital image and grid DEMs, it is proven that, although the LR grid DEMs have a single source, they carry non-redundant information and they can be inputs of MFSR.

Quality of grid DEM can be increased by using MFSR techniques. The level of spatial enhancement is directly related to the amount of non-redundant information that the LR grid DEM pairs carry. It is seen that super resolution techniques have potential to increase the accuracy of grid DEMs from a limited sampling.

Keywords: GIS, DEM, Super Resolution, grid size, spatial resolution enhancement

ÖZ

SYM NİN KALİTESİNİ YÜKSELTMEK İÇİN BİR MODEL OLUŞTURULMASI

Onur PAŞAOĞULLARI
Doktora Jeodetik ve Coğrafi Bilgi Teknolojileri Bölümü
Tez Yöneticisi: Doç Dr. Nurünnisa USUL

Şubat 2013, 101 sayfa

Düşük çözünürlüklü (DÇ) grid Sayısal Yükseklik Modellerinin (SYM) çok görüntülü süper çözünürlük (ÇGSÇ) algoritmasına girdi olarak kullanılmasıyla yüksek çözünürlüklü grid SYM elde edilmektedir. Tekrarlanmayan bilgi içeren DÇ görüntü çiftleri, sayısal görüntülemede ÇGSÇ için bir gerekliliktir. Sayısal görüntüleme ile grid SYM arasındaki benzerlik kullanılarak, aynı kaynaktan elde edilseler bile DÇ grid SYM'lerin tekrarlamayan bilgi içerdikleri ispatlanmış ve ÇGSÇ'de girdi olarak kullanılabilecekleri gösterilmiştir.

Grid SYM'lerin kalitesi, ÇGSÇ teknikleri ile arttırılabilir. Mekânsal zenginleştirmenin seviyesi, DÇ grid SYM'lerin taşıdığı tekrarlanmayan bilgi ile doğrudan ilişkilidir. Yüksek çözünürlük teknikleri, sınırlı örneklemeden elde elilen grid SYM'lerin doğruluğunu arttırmakta yardım etmektedir.

Anahtar Kelimeler: CBS, SYM, Süper çözünürlük, grid boyutu, yersel çözünürlük zenginleştirmesi

To Hülya, Emre and Efe

ACKNOWLEDGEMENTS

TABLE OF CONTENTS

LIST OF FIGURES

LIST OF TABLES

CHAPTER 1

INTRODUCTION

1.1   Statement of the problem

Geographic Information System (GIS) is a very useful tool in modeling discrete and more importantly continuous phenomena; such as topography of an area. The values obtained for continuous phenomenon are interpolated over the study area and a matrix of values for the whole area is obtained. The primary criterion is the unit size that any value of that matrix represents spatial resolution. Higher accuracy can be obtained by using smaller grid sized Digital Elevation Models (DEM) to represent the area. However, decreasing the grid size is limited with sampling size; or generally with the map scale. In other words, sampling accuracy limits the accuracy of the products that will base on this sampling.

On the other hand, another branch of science seems like finding a solution to limited sampling accuracy problem. Signal processing and digital image processing scientists are also using limited samples, but more information can be obtained by using different techniques. Super resolution is one of the techniques that gave great chances to increase the accuracy of the products.

Can the accuracy of the DEM be increased by using super resolution techniques? In this study the answer to the above question is investigated. The main direction of this study is seeking that whether the combination of geography and digital image processing domains will help increasing DEM accuracy or not.

1.2   Aim of the study

Digital Elevation Models are named after the elevation model that is used for modeling topography; however, they are also used for modeling other continuous phenomenon like temperature, rainfall, pollutant concentrations, etc. The 'elevation' term is used instead of the continuous phenomenon throughout this text. Literally DEM is designed to determine value of any point in a given area in digital format. Although there are different models for modeling continuous phenomenon like point, line and Triangulated Irregular Network (TIN) models, the most widely used is the Grid Structured Digital Elevation Model (Grid DEM). Simply Grid DEM is a matrix of values representing the continuous values for a specific area named grid cell. Despite the fact that Grid DEM is most widely used continuous model, it has several disadvantages; the biggest disadvantage is the grid size itself.

Grid size determines the spatial resolution of Grid DEM. Most of the time; the scale of the source data is the primary parameter in choosing the grid size. The interpolation method, boundaries and the distribution of the data are the secondary ones. Scale dependency on the selection of grid size brings new limits to the accuracy of grid DEM.

On the other hand; high resolution (HR) image can be re-constructed from a set of low resolution (LR) images by a method called super resolution (SR). The primary prerequisite condition is that the low resolution images must contain non-redundant information of the same scene. Video sequences, radar images, astronomic or microscopic digital images are the areas that are using super resolution. Improved face recognition, improvement in medical imaging, even discovery of new planets are some of the results obtained by the application of super resolution. The aim of this study is to prove that super resolution is applicable to DEM and this application will result in increasing the resolution of DEM. This proof is stated first as; application multi-frame super resolution on Shuttle Radar Topography Mission (SRTM) data and check the result with Advanced Spaceborne Thermal Emission and Reflection Radiometer (ASTER) data. The second application is the application of multi-frame super resolution on two geometrical surfaces. The third application will be done on METU area with two different scales. The last application is done as multi-frame super resolution with SRTM and ASTER and check the result with elevation data.

The second chapter is introducing the methodology used and the study areas. Digital elevation model, its acquisition and algorithm are discussed. The details for the code and the user interface are also explained. The geometrical surfaces, the actual land and the space-borne DEM data are introduced in chapter 2. The third chapter is on super resolution. Information on digital imaging and the analogy between DEM and digital imaging are explained. The examples of super resolution applications on digital imagery and on DEM are provided. The fourth chapter proves that the low resolution (LR) Grid DEMs obtained from the same algorithm has non redundant information by using similarity measures. The results of super resolution application on different LR grid DEMs are explained in another chapter. The discussions, conclusions and recommendations are covered in the sixth chapter.

1.3   Previous studies

Increase in the accuracy of grid DEM can be assessed by decreasing the error in DEM. Error analysis on DEM and its derivatives are investigated in the literature. In Zhou and Liu's (2004) paper, error is analyzed on derived slope and aspect related to DEM data properties. They found out that high resolution DEM does not assure higher slope and aspect accuracy. Better results had been acquired with high DEM accuracy. They concluded that grid orientation created a directional bias on slope and accuracy calculation. One of the facts that they emphasize on their paper is that diagonal grid calculation (45º or 135º rotation) shows extreme values in slope and aspect calculation. All their calculation had been carried out on two geometrical surfaces. One is ellipsoid surface (for representation of convex slopes) and the other one is Gaussian surface (for representation of complex slopes). This paper gave the inspiration for using the geometrical surfaces in this study. The advantage of using geometrical surface is the ability of finding the exact heights at any point.

The type of interpolation method becomes the main issue that defines the quality of the grid DEM. In conventional grid DEM creation algorithms, one method of interpolation will be used all over the study area. In a study Shi & Tian (2006) proposed a hybrid interpolation method. In this method, they combine the bi-linear and bi-cubic interpolation methods with a hybrid parameter by minimizing Root Mean Square Error (RMSE) of the hybrid model regarding the parent models. They found that this parameter is related to the complexity of the terrain. The hybrid parameter will decrease as the complexity of the terrain increases. However, they reminded that the hybrid parameter has two drawbacks. First, the parameter does not take into account the local behavior of the terrain, which is applied to the whole area. Second drawback is that, the parameter is isotropic. It is selected without considering the different properties of the different directions of the terrain.

Grid DEM has elevation values which represent the areas of the grid cells. Spatial analysis suggests voronoi polygons for area representation of point variables. Voronoi polygons are irregular shaped areas valued by the single point inside. In the case of grid DEM, the area is regular. Assigning values to the regular grid DEM will bring new error resulting from stretching the irregular areas to the regular areas. The error in the conventional grid DEM is spread over the study area and it is highly related to the interpolation. Carlisle (2005)

2

showed that DEM error is spatially variable, spatially correlated and heteroscedastic (an irregular scattering of values in a series of distributions, in this paper it refers that error is related to the form of the terrain), that is error values vary and it is in relation to another variable. It is stated that, although RMSE and standard deviation of error are frequently used for assessing the accuracy of DEM, these measurements only summarize DEM error as a single value. They do not mention about the distribution of error. Using Inverse Distance Weighting method and ArcView's "Spline with Tension" method for DEM creation, it is found out that magnitude and distribution of errors in a DEM are related to the varying character of the terrain. Terrain character, which is found out with DEM derived terrain parameters, and Global Positioning System (GPS) survey of elevation, error can be used in regression model to form a DEM error surface. An accuracy surface which is created with applying a standard deviation filter, gives more complete description of a DEM's accuracy compared to DEM's RMSE.

Every model, including Digital Elevation Model contains errors. Traditionally, DEM errors are found by finding the difference between the calculated elevations and the elevation value measured from the site. The differences for various points are used to find the RMSE or standard deviation of error. These differences, however, reflect not only the difference between DEM and the digital source of DEM, but also it reflects the error between source and real elevation. Also these summarized error figures indicate the error for only the measured points; it does not reflect the error for the whole study area. Carlisle (2005) stated that DEM error is correlated with terrain character which is found out with DEM derived terrain parameters like elevation gradient, aspect, plan curvature, profile curvature, etc. Magnitude and distribution of errors in a DEM are related to the varying character of the terrain. Terrain character and GPS survey of elevation can be used in a regression model to form a DEM error surface. Objection to this article can be stated as; the terrain character is defined by the source data itself. Error of DEM is obviously defined by the source data. Without constraining the source data into some numerical forms of terrain characteristics, source data and DEM must be examined together for error analysis.

The error in grid DEM also affects the derivatives of DEM such as slope, aspect, and basin delineation. Oksanen and Sarjakoski (2005) had investigated the error propagation on the derivatives of DEM, slope and aspect as constrained derivatives, and drainage basin delineation as unconstrained derivative. As expected, increase in DEM error, increased the error in derivatives. They found out that, surprisingly, the spatial autocorrelation models have variable effect on the error propagation. Maximum error in slope and aspect result when the practical range of error's spatial autocorrelation was roughly equal to the window size of the derivation. They concluded that the autocorrelation parameters: practical range and sill are more important than the shape of autocorrelation model: exponential or Gaussian.

The most important source of grid DEM error is the grid size. For any user, ability to decide on the grid size might seem to be a sign of freedom, but as every instance of freedom it has expensive results. Although the elevation is modeled with point or line data, the grid size can be any value greater than zero. There come the questions to be answered: Are the users free to decide in choosing the grid size without taking the distribution of the points or lines into consideration? How much error this freedom brings in creating grid DEM? Is there an optimum grid size where the error is minimal and how this optimum point can be found?

In the master thesis of the author (Paşaoğulları, 2002) grid size was found to be very important on geo-morphological basin parameters. The effect of grid size was observed better as the area of the basin increases. Appropriate grid size for topography dominated studies must be greater than the horizontal accuracy of the source of the data. Depending on the area of the interest, suitable grid size lies between 2 – 30 m for medium size basins and 10 – 50 m for large basins having an area greater than 100 km² and it can be found on a try-error basis with at least three different grid sizes.

The main suggestion of this study is that super resolution may help to increase the accuracy of grid DEM. As stated earlier, super resolution is the method of constructing a high resolution image from low resolution images. It has lots of usage areas such as: image

resolution enhancement, building super resolution video, biomedical image enhancement, etc. If the low resolution images contain non-redundant information of the same scene, a high resolution image can be constructed. In the literature, there are a number of algorithms for super resolution (Baker & Kanade, 2002), (Nguyen & Milanfar, 2001), (Park et al., 2003). In the process of super resolution there are three steps:

- Image registration,
- Projecting the low resolution images onto high resolution grid.
- Image restoration for blur and noise removal.

Most of the studies on super resolution try to solve these three problems. In digital image super resolution, image registration is a major problem that the low resolution images do not have a coordinate system as in the case of Grid DEM. Also lots of algorithms are proposed in the literature for the second problem (Keren, Peleg, & Brada, 1988), (Lucas & Kanade, 1981).

As in the case of applying super resolution techniques to grid DEM, image registration is not a problem to be concerned. The grid DEMs produced from the point, line or TIN data, are in a coordinate system. The resulting high resolution grid DEM will also be on the same projection system, so the image registration problem is solved by the nature of GIS that creates the grid DEM.

Wu et al. (2004) have stated that the projection of low resolution image onto high resolution grid problem is tried to be solved by different approaches which can be categorized into three:

- Frequency domain algorithms,
- Spatial domain algorithms from image generative model,
- Interpolation methods.

Frequency domain algorithms try to reconstruct the high frequency component hidden in the low resolution images.

Super resolution helps in finding the information hidden at sub-pixel level. The aim of this study is the investigation of the information in the sub-pixel level of the grid DEM. The sub-pixel investigation is not a new subject in GIS and RS domain. Flanagan and Civco, (2001) have studied mapping the impervious features using coarse resolution satellite imagery. Tatem et al. (2002) used super resolution techniques for land cover pattern prediction using Hopfield neural network. Also SPOT 5 (2006) satellite uses a sampling technique called "super-mode" which improves resolution in the panchromatic band. This process uses two 5 m resolution images taken at an offset distance of 2.5 m both vertically and horizontally.

In their study, Keeratikasikorn & Trisirisatayawong (2008) say that 90 m DEM of SRTM data can be refined to 30 m DEM, which results in small RMSE. They applied bivariate cubic polynomial equations in order to obtain finer grid. SRTM DEM is publicly available at two resolutions 30 m and 90 m, former is for United States and latter is for all. The study area formed as an east - west band from gently-slope flat land in western part of Kansas to mountainous region in eastern Colorado. They interpolated the 90 m SRTM grid to 30 m grid size. The interpolation errors are computed as the height differences between the 30 m SRTM DEMs and the 30 m corresponding interpolating DEMs. They claim that statistics show that the interpolation results are extremely good. For all reconstructed 30 m DEMs, the RMS errors are between 0.817 and 2.330 m. The larger RMS errors are resulted in mountainous areas, while in flat and smooth terrains RMS error is less than 1.2 m. They conclude that for most cases using 90 m SRTM DEMs as a source, the generation of 30 m resolution DEMs of the same quality as the original 30m SRTM DEMs can be achieved by using the bi-cubic polynomial interpolation technique.

Bulyshev et al. (2010) propose a new super resolution algorithm on flash Light Detection and Ranging (LIDAR) data for DEM creation. Flash LIDAR is on the center of NASA Autonomous Landing and Hazard Avoidance (ALHAT) project for detecting of terrain features that can be

dangerous for spacecraft landings. They offer to use hi-fidelity model of a flash LIDAR to produce input range images to test the algorithm. Algorithm starts with projecting focal plane array (FPA) to zero elevation level. Overlapping cell coordinates and elevations are calculated by the range data and the surface angle. The operation is continued for each detector in the frame and in the end normalization is applied. The process is repeated for all frames. They concluded that the proposed algorithm results in improved resolution in DEMs with high accuracy and precision. They also claimed that the algorithm is also robust to different viewing angles.

There are other studies on SRTM DEM resolution achievement using variogram modeling and krigging (Grohmann 2006 and Valeriano et al., 2006).

Major argument on application of super resolution on Grid DEM is that; multi frame super resolution techniques require non redundant information in low resolution. The low resolution Grid DEMs are produced from the same source so it must be cleared that low resolution Grid DEMs have non redundant information even if they are created from the same algorithm. In order to show that Grid DEMs are carrying non redundant information of the same scene, it is essential to verify the difference between the Grid DEM pairs. The similarity measures of the images are used with the help of the analogy between the image and Grid DEM. Similarity measures show how much the pairs are similar or dissimilar.

There are a large number of studies on the similarities of the images. Especially medical imaging and image fusion studies are using image similarity measures. Medical imaging needs image registration. It is the key process in order to use in different image needs like; biomedical image analysis, feature extraction, tissue characterization, etc. Among the other registration methods; intensity-based registration methods in medical imaging require similarity measures in order to register two 2D or 3D images. Registration transformation is determined by some similarity measures that are calculated using the whole images or part of the images. In their book chapter Fitzpatrick et al. (2000), list eight similarity measures:

1. Image Subtraction
2. Correlation coefficient
3. Ratio-Image Uniformity
4. Partitioned Intensity Uniformity
5. Joint Histograms and Joint Probability Distributions
6. Joint Entropy
7. Mutual Information
8. Normalization of Mutual Information

In another study concentrated on image quality measures, statistical image quality metrics are categorized into six groups according to the type of information they use (Avcıbaş and Sankur, 2000; Avcıbaş et al., 2002). One of the aims of these studies is to investigate metrics' statistical performance. These metrics are used to compare image compression applications. 10 three-band remote sensing images, 10 color face images, and 10 texture images are compressed with JPEG and SPHIT compression algorithms and the results are compared with the originals. 26 different metrics categorized into six groups as pixel difference-based, correlation-based, edge-based, spectral distance-based, context-based and human visual system (HVS)-based measures. These measures show how two images differ and the amount of non-redundant information that a single image carries.

CHAPTER 2

METHODOLOGY AND STUDY AREAS

In this chapter, Digital Elevation Model (DEM) and Triangulated Irregular Network (TIN) algorithms are explained and the study areas are given next. The geometrical surfaces, selected actual land and satellite based DEM areas are explained.

2.1   Digital Elevation Model

In this study, elevation modeling is achieved with grid digital elevation model. As expressed in previous section, any kind of continuous variable can be modeled with DEM; however the most common name for continuous phenomenon modeling has the word "elevation" for representing continuous variable. It is designed to determine the continuous value of any point in a given area. There may be infinite numbers of points in an area, so some values are represented by observed measurement points, while the others are obtained by interpolation.

GIS is an essential tool for collecting, storing, controlling, processing, retrieving, and analyzing spatial information (Aranoff, 1995). Digital representation of elevation can be achieved with GIS which can easily and effectively be done. Besides the other models like point model, line model and Triangulated Irregular Network model, the most widely used one is 'Grid Model'.

As mentioned before, elevation over an area is modeled by DEM. For this, regular sized elemental cells valuated by an algorithm, covers the study area. Grid size decision and valuating process are the main parameters of DEM.

Valuating the grid cell for a defined regular area is mathematically formulated as;

$$Z_g = \int\limits_{y=y_1}^{y_2} \int\limits_{x=x_1}^{x_2} dz \qquad (1)$$

Equation 1 defines that grid cell value must be defined by the part of the phenomena that falls inside the grid cell as seen in Figure 1.
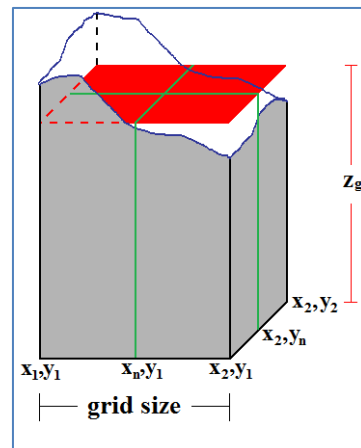
Figure 1 Grid cell Cross Section

The addition property of integral is;

$$\int_{x=x_1}^{x_2} dx = \int_{x=x_1}^{x_n} dx + \int_{x=x_n}^{x_2} dx \tag{2}$$

provided that x_n is an element of $[x_1,x_2]$.

Applying Equation 2 to Equation 1, the following equation is obtained;

$$\int_{y=y_1}^{y_2}\int_{x=x_1}^{x_2} dz = \int_{y=y_1}^{y_n}\int_{x=x_1}^{x_n} dz + \int_{y=y_1}^{y_n}\int_{x=x_n}^{x_2} dz + \int_{y=y_n}^{y_2}\int_{x=x_1}^{x_n} dz + \int_{y=y_n}^{y_2}\int_{x=x_n}^{x_2} dz \tag{3}$$

Regularly spaced elemental area represents a single continuous surface value. The area of interest is divided into elemental areas like triangle, square or regular angular polygons. Most of the time; the mathematical representation of the surface is impossible to be known. "Mean Value Theorem" (Figure 2) states that if f (a, b) is continuous on the closed interval [a, b], and if f (a, b) is differentiable on the open interval (a, b), where a < b then

$$F(x)dx = f(x) \tag{4}$$

$$\int_a^b f(x) = F(b) - F(a) \tag{5}$$

there exists some c in the interval (a, b) (that is a < c < b) such that:

$$f(c) = \frac{F(b) - F(a)}{b - a} \tag{6}$$

If mean value theorem is applied to the mathematical definition of the DEM, at least one point (x_c, y_c) where $x_1 <= x_c <= x_2$ and $y_1 <= y_c <= y_2$ exists such that:

$$f(x_c, y_c) = \frac{F(x_2, y_2) - F(x_1, y_1)}{area} \tag{7}$$
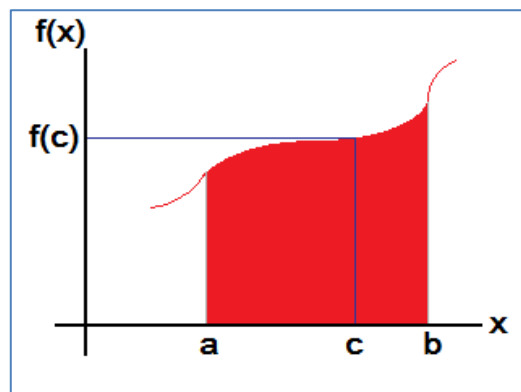
Figure 2   Mean Value Theorem

Rather than finding the mean value for each grid cell, a representation value is appointed, which forms a matrix consisting of numbers. In raster based GIS the elemental area is a square. Nearly all GIS packages use the center point as the mean value.

The regular grid method has the advantage of simplicity of data storage. The starting part of raster based grid DEM file called the "heading"; contains starting point, grid spacing, coordinate system information, meta-data, etc. The rest of the file has the values as matrix elements. This simplifies creating, storing, retrieving, and creation of DEM. Any point whose continuous value is to be found, will fall in one grid cell. The value of the interest point will be the value of the cell.

The most important part of DEM creation is the "cell size", "grid spacing" or naming differently "spatial resolution". When the cell size is relatively large and the change of the elevation is high; in the creation process, there will be more than one data point per cell; in this case the algorithm must cope with the interpolation problem inside the grid cell. On the contrary; when the cell size is relatively small and the change in elevation is less, for some cells there may not be any data point and the same algorithm must find the elevation data by grid cell extrapolation.

These interpolations will bring an error between the grid cell value and the original terrain elevation. By the definition of Grid DEM, the cell size is fixed for all over the research area. If small grid cells in size can be applied to the steeper areas and large grid cells in mild areas, then applying two interpolations will be reduced to one. However; interpolation, which is one of the disadvantages of the grid DEM, is inevitable.

The algorithm that is employed in DEM creation process is the second key player. The characteristic of the surface is approximated by the algorithm. There are several algorithms in the literature like spline with tension, krigging, trend surfaces, etc. The following section explains the algorithm that is employed in this study.

2.2   Triangulated Irregular Network

As the name implies, Triangulated Irregular Network consists of triangles, made with natural neighbor data points that are arranged in a network of contiguous, irregularly distributed and non-overlapping manner. Although TIN model is said to be a significant alternative to grid DEM, it is also an interpolation base for grid DEM. TIN represents the surface with a finite number of triangular surface components, within each triangle the surface is represented by a plane having its own slope and aspect.

Construction of TIN by Delaunay triangulation starts with finding a starting point and its nearest point. The nearest points of each data point make one of the sides of the triangles. A third point is selected (Figure 3). These three points create a triangle. Then circumscribed circle, passing from these three points is obtained in order to find the natural neighbors. If there is any point in that circle other than the corners of the triangle, then that triangle is rejected. The third point is changed with the one that is inside the circle. The process is repeated until there are no points in circumscribed circle. In this case the triangle is accepted. The process is continued until all the points in that data set are checked to form triangles. The formation of grid centers for a particular triangle can also be seen in Figure 3.
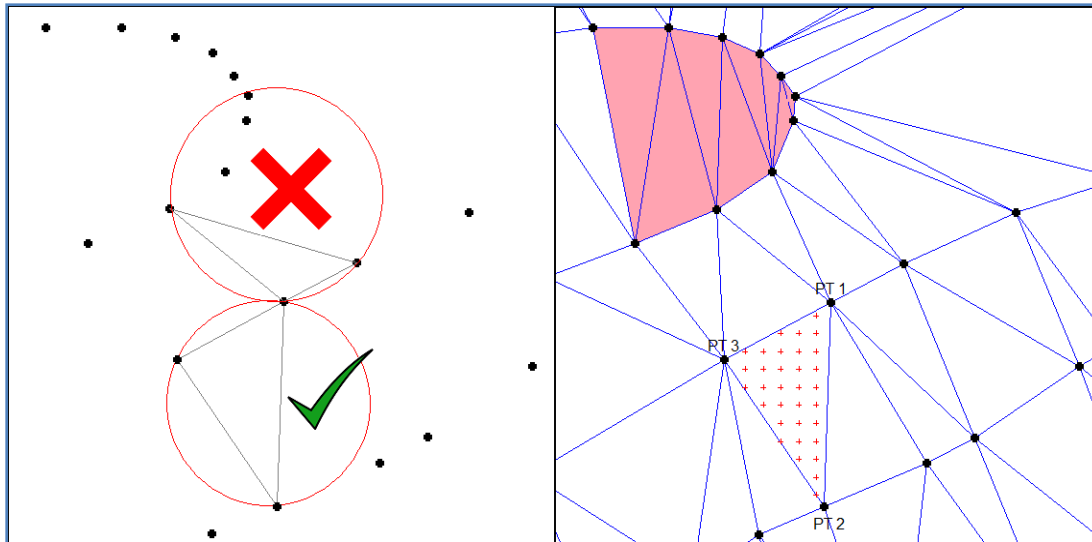
Figure 3   Construction of TIN and obtaining values from TIN

After creating TIN surface, the grids are formed and the value of the center of each grid cell is calculated with slopes. For each triangle, the slope matrix (equation 8) is formed by multiplying the coordinate matrix (equation 9) and the value matrix (equation 10). The grid center coordinates are formed as a matrix (equation 11) and the grid value (equation 12) is found by multiplying it with the slope matrix.

$$\mathbf{s} = |\mathbf{c}|^{-1} \times \mathbf{z} \tag{8}$$

$$\mathbf{c} = \begin{vmatrix} x_1 & y_1 & 1 \\ x_2 & y_2 & 1 \\ x_3 & y_3 & 1 \end{vmatrix} \tag{9}$$

$$\mathbf{z} = \begin{vmatrix} z_1 \\ z_2 \\ z_3 \end{vmatrix} \tag{10}$$

$$\mathbf{g_c} = |x_g \quad y_g \quad 1| \tag{11}$$

$$\mathbf{z_c} = \mathbf{g_c} \times \mathbf{s} \tag{12}$$

Although TIN is a very good representation of the surface and helps to create grid DEMs, it has also problems. The nature of Delaunay triangulation and using contour lines for TIN often creates flat triangles. Flat triangles are created by three nodes with the same elevation value and having a slope of 0 and consequently having no defined aspect. They are frequently generated along contours when the third sample points occur along the same contour at a distance that is less than the distance of any point on another contour. TIN creation algorithm discovers that for any side of the triangle, the closest point is on the same contour, causing the generation of flat triangles. They might cause problems when the surface is used for modeling. Flat triangles can be seen as painted in pink on top part of Figure 3.

2.3   Study Areas

The study is conducted on three types of surfaces. In one of them, there are two surfaces which are expressed by mathematical equations. The last two are actual existing areas.

10

2.3.1 Geometrical Surfaces

In their research, Zhou & Liu (2004) had worked on two geometrical surfaces to show the error analysis on slope and aspect. One of the surfaces is the ellipsoid and the other one is the Gaussian surface. The advantage of using these surfaces is that they provide the calculation of the real elevation at every point.

Grid DEM super resolution application and evaluation also need the real continuous values for every grid cell, the same two geometrical surfaces are chosen for applying grid DEM super resolution. The contour lines are obtained by solving equations for each contour value (elevation). The contour data are formed for 10 m and 5 m contour interval in order to compare the effect of super resolution result with a finer grid DEM. First geometrical surface is half ellipsoid, expressed as:

$$\frac{x^2}{A^2} + \frac{y^2}{B^2} + \frac{z^2}{C^2} = 1 \tag{13}$$

where A=500, B=300 and C=300. The surface obtained from MatLab program and 10 m interval contour lines can be seen in Figures 4 and 5 respectively.
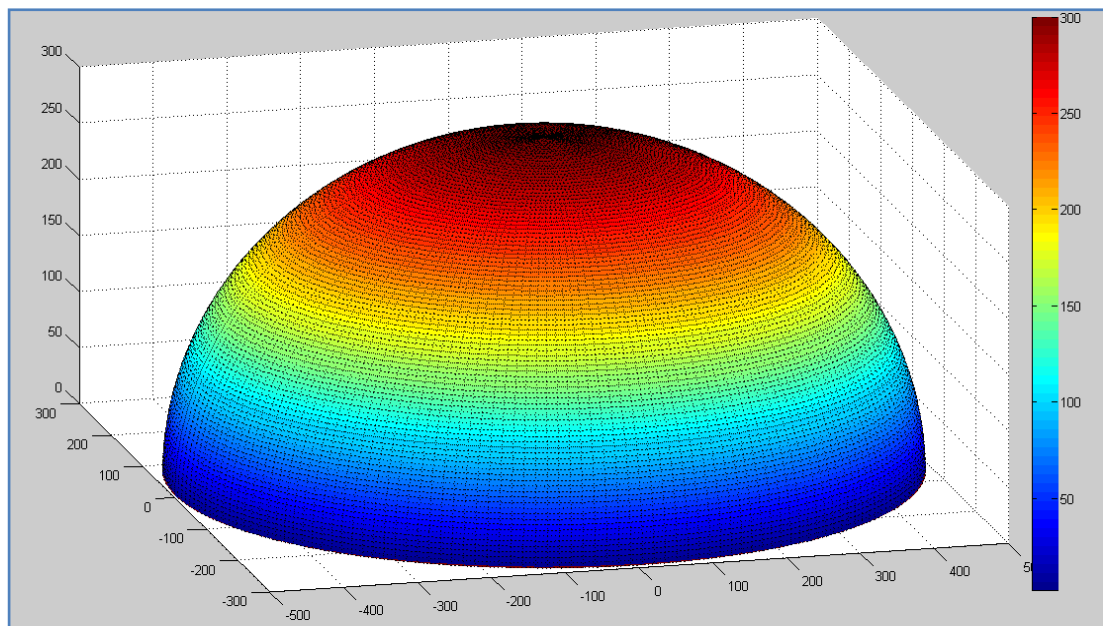
Figure 4 Ellipsoid surface
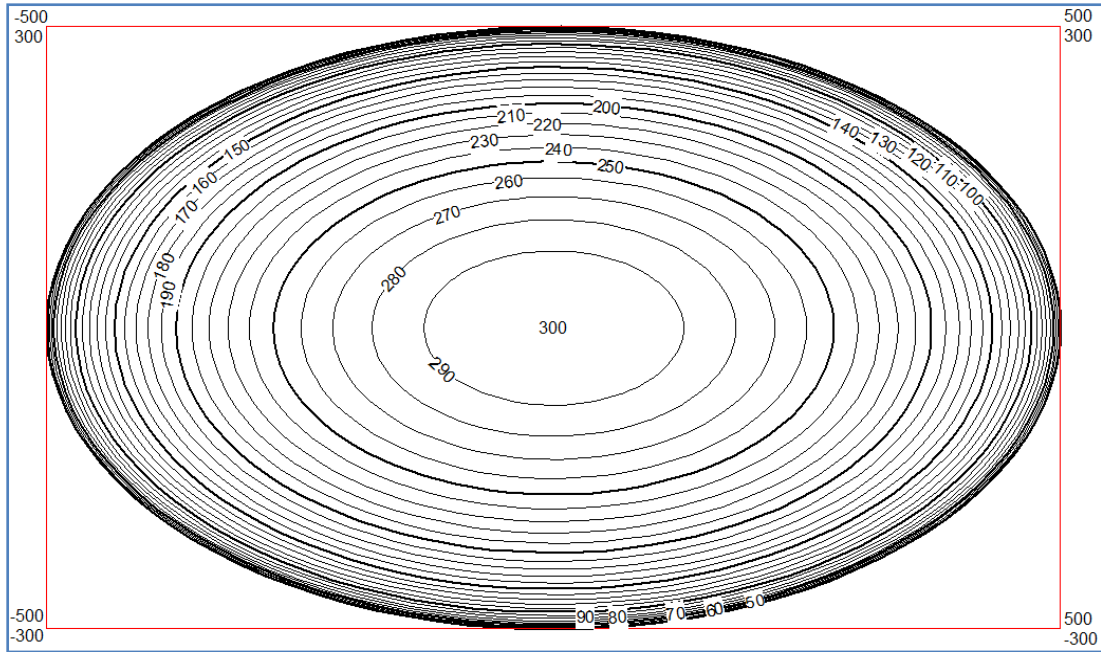
Figure 5 Ellipsoid surface contour lines with 10 m interval

The other one is a Gaussian surface:

$$
z = A\left[1 - \left(\frac{x}{m}\right)^2\right] e^{\left[-\left(\frac{x}{m}\right)^2 - \left(\frac{y}{n}+1\right)^2\right]}
$$

$$
- B\left[0.2\left(\frac{x}{m}\right) - \left(\frac{x}{m}\right)^3 - \left(\frac{y}{n}\right)^5\right] e^{\left[-\left(\frac{x}{m}\right)^2 - \left(\frac{y}{n}\right)^2\right]}
$$

$$
- Ce^{\left[-\left(\frac{x}{m}+1\right)^2 - \left(\frac{y}{n}\right)^2\right]} \tag{14}
$$

where A=12, B=50, C=10. The constants m and n are used for defining the boundaries of the surface. The surface and 5 m interval contours are shown in Figures 6 and 7 respectively.

12
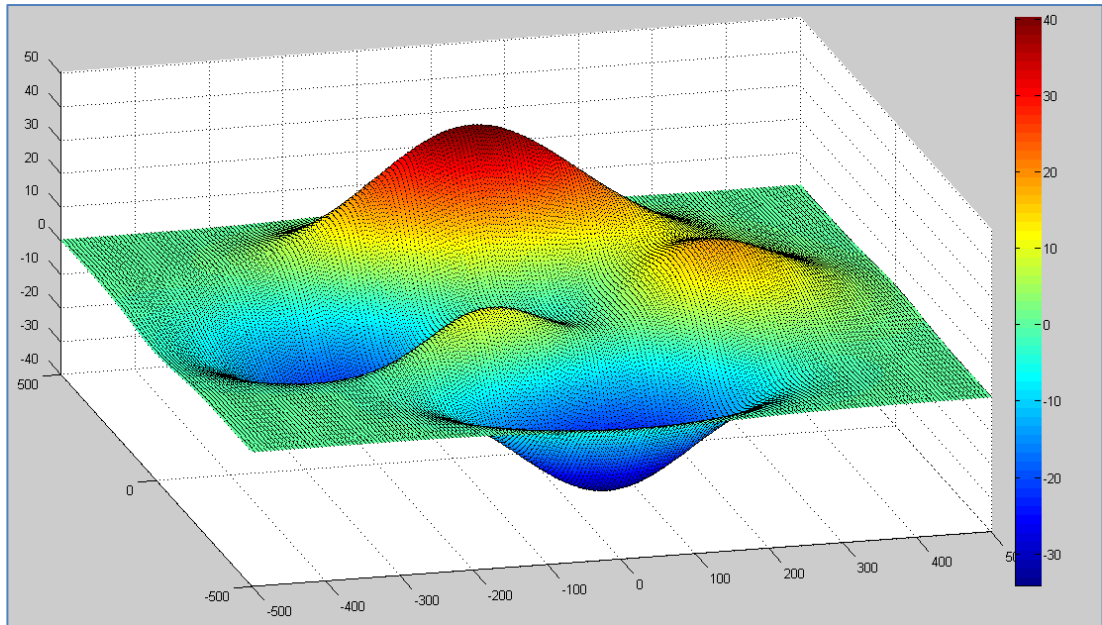
Figure 6   Gaussian Surface
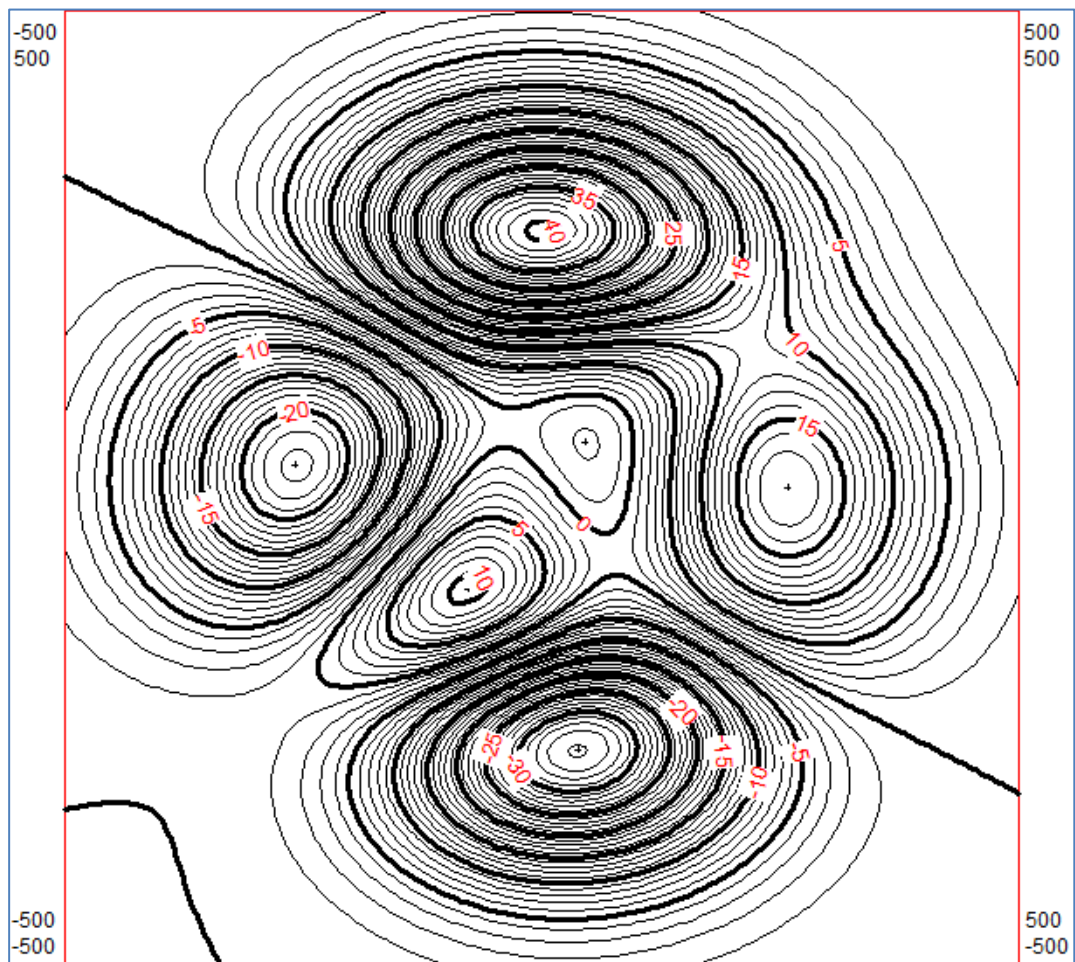
Figure 7   Gaussian surface contour lines (Thick lines with 5 m, others with 1 m interval)

2.3.2   Actual Land

The real surface application has been carried on a part of the elevation data of Middle East Technical University campus area. The data had been acquired from University administration as 1/25000 and 1/5000 scaled contour maps having 10 m and 5 m contour intervals respectively. Most common method of acquiring elevation data in digital raster format is often the least accurate one, digitizing of contour lines from a topographic map. In this study the real case data are the only data so the integrity and quality issues about the data are neglected.

In order to see the effect of multi-frame super resolution SRTM and ASTER data sets are also checked with METU area data. The information about SRTM and ASTER data sets are given in following sub sections. METU area contour data obtained from 1/25000 scaled map with 10 m interval can be seen in Figure 8 with SRTM data (N 39 E 32). 5 m interval contour lines obtained from 1/5000 scale map and corresponding ASTER data (N 39 E 32) can be seen in Figure 9.
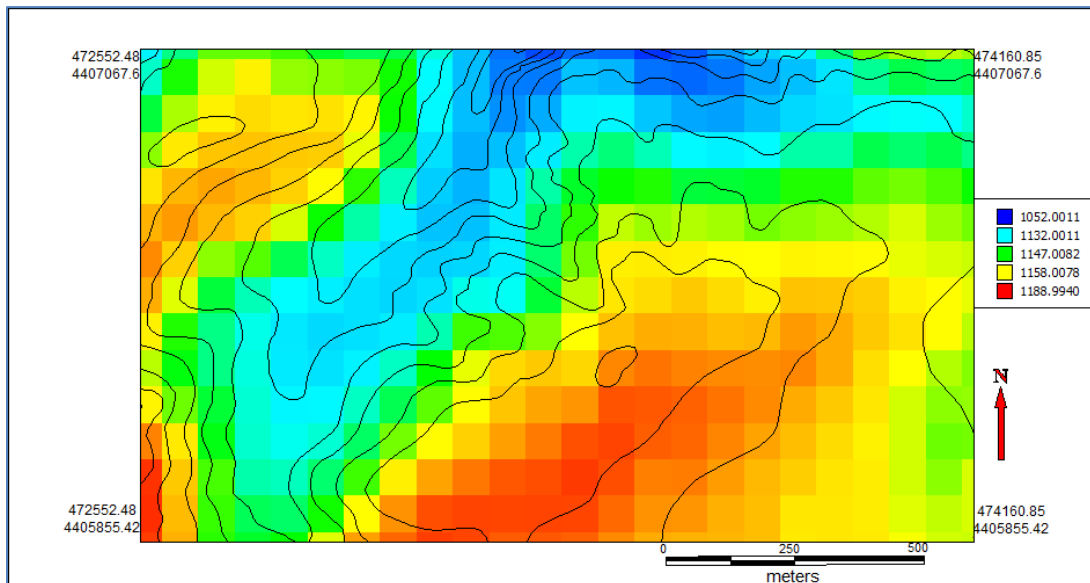
Figure 8   METU area (Scale: 1/25000, Contour interval: 10 m, SRTM data (N39E32)).

2.3.3   Space-borne DEMs

In this study, the improvement in spatial resolution of multi-frame super resolution is also proven by space-borne DEMs. Regarding the objective of "single source of data", most common space-borne DEMs SRTM and ASTER data are used. The next two subsections are about these datasets.

2.3.3.1 SRTM

Space Shuttle Endeavour flew to space with Shuttle Radar Topography Mission (SRTM) payload onboard in February 2000. In the orbit, SRTM system was placed with two radar antennas, one is inside the shuttle's payload bay, and the other one was on the end of 60 meter mast. This SRTM configuration was set to acquire elevation data, and on its 11-day mission these radars swept most of the Earth's surface. The resulting product gave most complete near-global database of the Earth's topography.
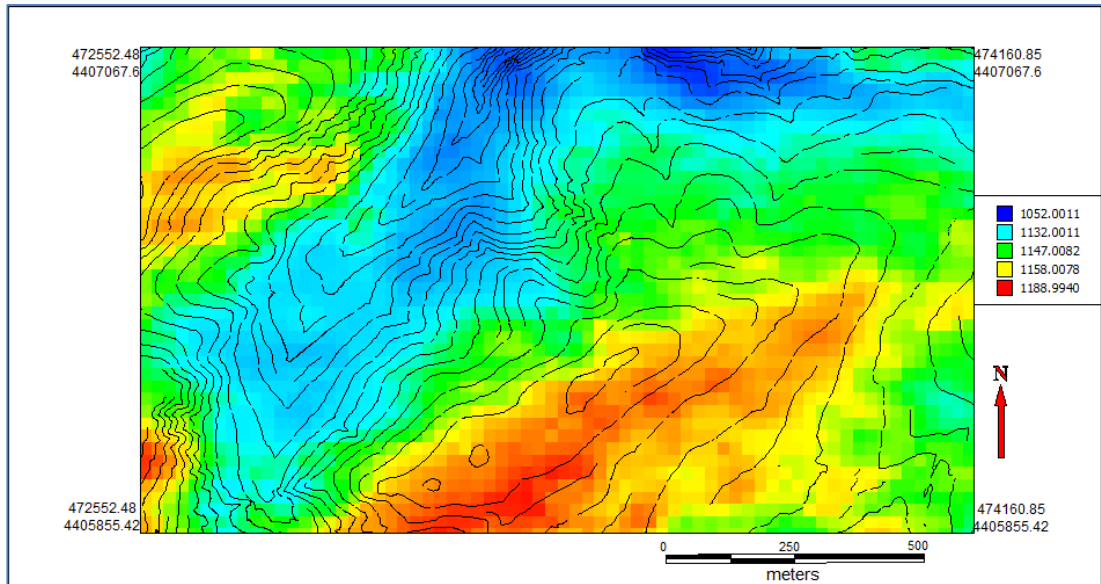
Figure 9 METU area (Scale: 1/5000, Contour interval: 5 m, ASTER data (N39E32)).

The SRTM DEMs are arranged into tiles, each covering one degree of latitude and longitude, named according to their south western corners. For Turkey, only three arc-second (~90 m) data are available. The dimensions of the three arc-second tiles are 1201 x 1201. SRTM and ASTER naming convention is done on lower left corner basis. In Figure 10 N39E32 SRTM dataset for N39-N40 and E32-E33 is shown.
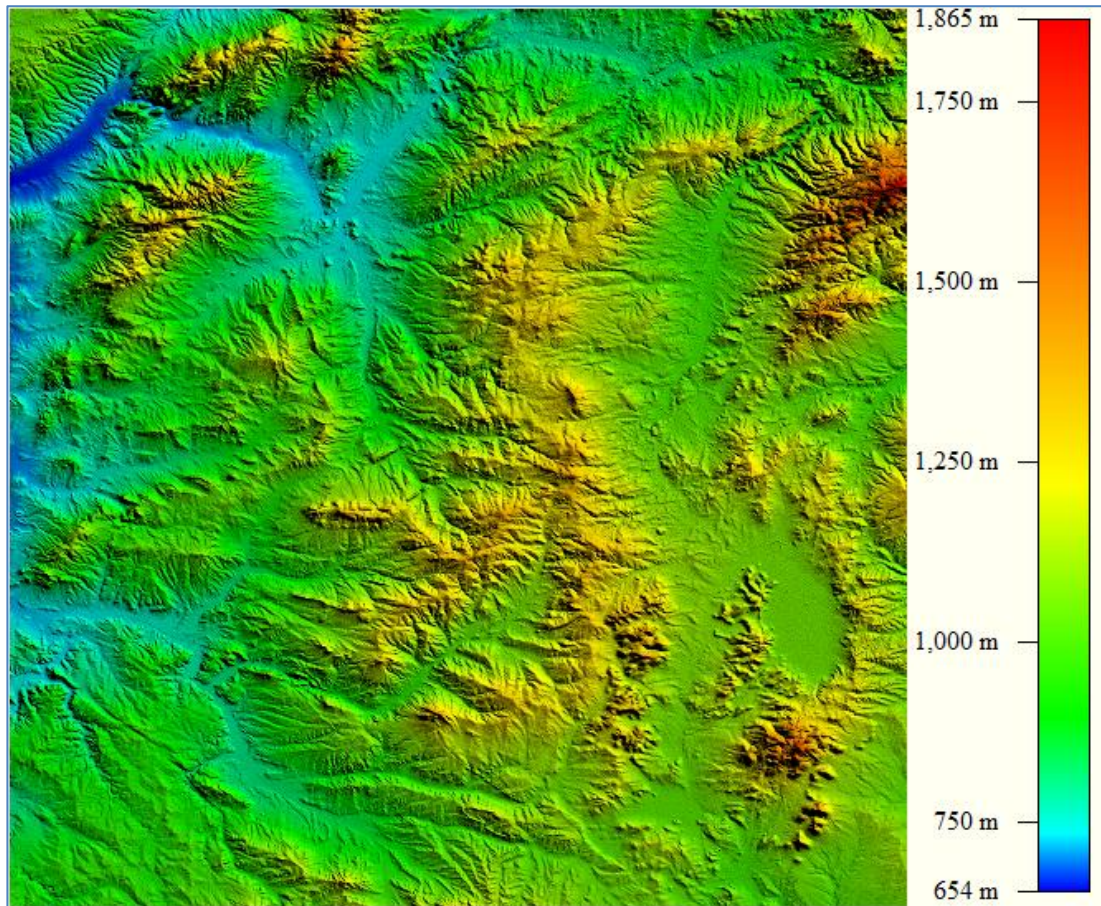
Figure 10   SRTM DEM (N 39 E 32)

2.3.3.2 ASTER

At an altitude of 705 kilometers, Terra satellite carries five instruments; one of them is Advanced Spaceborne Thermal Emission and Reflection Radiometer (ASTER). With its three subsystems: Visible and Near Infrared (VNIR), Shortwave Infrared (SWIR), and Thermal Infrared (TIR); it captures high spatial resolution data in 14 bands, from the visible to the thermal infrared wavelengths, and provides stereo viewing capability for digital elevation model creation. Terra satellite has a period of 99 minutes which means 16 orbits per day.

ASTER GDEM was first released in June 2009, covering 99 percent of the Earth's landmass from 83 degrees north to 83 degrees south. Improved GDEM V2 was publicly released in October 2011, with data-voids filled and many artifacts are removed. ASTER GDEM data are in 1 x 1 degree tiles and for Turkey, one arc-second (~30 m) data are available. The dimensions of the one arc-second tiles are 3601 x 3601. ASTER DEM dataset that is used in this study can be seen in Figure 11.
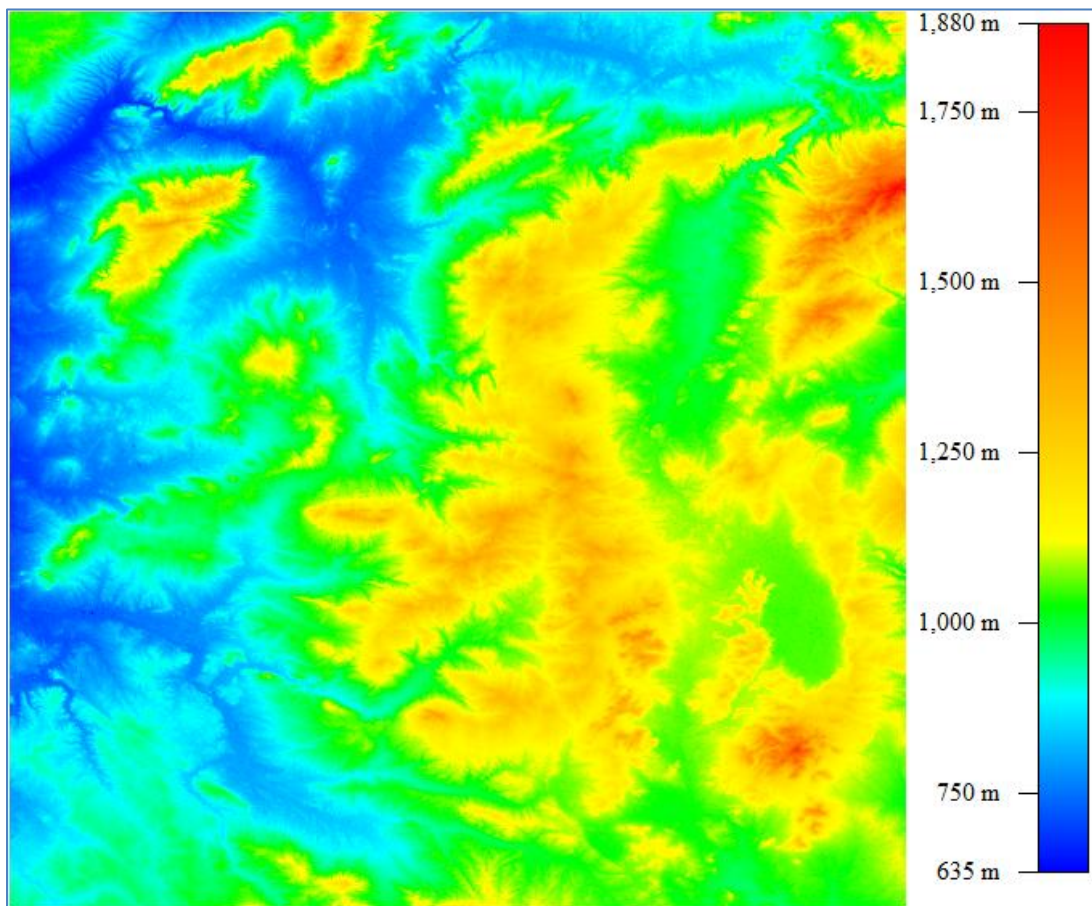
Figure 11 ASTER DEM (N 39 E 32)

Code development, tests, and initial applications are done on geometrical surfaces. The results are checked with the calculated elevation values on these surfaces. The completed code is then applied on the METU area data and space-borne DEM data. 5 m contour interval data is assumed as the reference data for super resolution application on 10 m contour interval data.

CHAPTER 3

SUPER RESOLUTION

3.1 Digital Image

Any kind of sensor, for example a Charge Coupled Device, collects the amount of light coming from the scene via the optics. The scene is divided into elemental areas and the sensor quantizes the brightness of light coming from these elemental areas. This quantization results are converted into numeric representation. This representation is the "digital image", or "raster image" or "bitmap image". Raster images have a finite set of digital values, called picture elements or pixels. They have fixed number of rows and columns of pixels. Pixels are the smallest individual elements in an image, holding quantized values that represent the brightness of a given color at any specific point.

The sources of raster images can be numerous; such as digital cameras, scanners, coordinate-measuring machines, seismographic profiling, airborne radar, etc. Raster images can also be synthesized from arbitrary non-image data, such as mathematical functions or three-dimensional geometric models.

Most widely, color representation is done by three bands of visible part of the spectrum, namely Red, Green, and Blue (RGB). The raster image is stored as three band quantization numbers for every pixel.

3.2 Digital Elevation Model and Digital Image Analogy

Digital images are the numerical representation of the brightness values in a scene. The light coming from the scene is collected on a lens and transferred to a device which converts this analog light signal into quantized brightness values. The result is a matrix of digital numbers containing the brightness values. In order to make an analogy between the digital image and the grid DEM the following conditions can be considered:

- The lens size is as large as the study area, so there is no zooming or loss of region of interest (ROI) in grid DEM,

- The effect of earth curvature is neglected,

- The elevation value in DEM is equivalent with the amount of energy that the sensor measures in digital image,

- The quantization level of digital image is the unit of the elevation values in DEM.

DEM creation is the collecting, interpolating and storing elevation values for the study area. Digital grid DEM maker will measure or interpolate the values of phenomena like a digital image camera sensor measures and interpolates the light coming from the source. In Figure 12 elevation values are analogous to the brightness level of that in digital image. The

similarities between digital imaging and DEM are so much that DEM can be called as "single band, infinite quantization leveled digital imagery". The above definition emphasizes the only difference between DEM and digital imagery, which is infinite quantization.
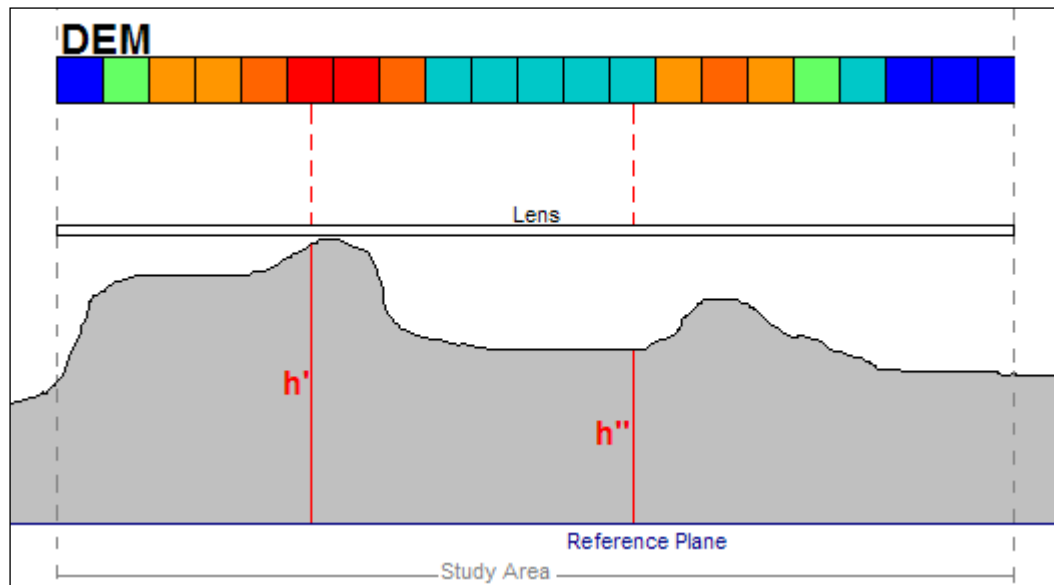
Figure 12 DEM Creation and digital image analogy

3.3   Super Resolution

Super resolution (SR) is the method of constructing a high resolution (HR) image from low resolution (LR) images. If the low resolution images contain non-redundant information of the same scene, a high resolution image can be constructed. As seen in Figure 13, most SR methods consist of three stages: registration, interpolation, and restoration (Park et al., 2003).

These steps can be implemented separately or simultaneously according to the reconstruction methods adopted. In the registration stage (Figure 14), LR images are registered to HR image or to the reference LR image. Image registration is done by pixel enlargement and referencing. Enlarged pixel coordinates are referenced to those of HR images. Obviously, registration is very important for the success of the SR image reconstruction algorithm. For the second stage; since the shifts of the pixels between LR images are arbitrary, the registered HR image will not always match up to a uniformly spaced HR grid. Thus, non-uniform interpolation is necessary to obtain a uniformly spaced HR image from non-uniformly spaced composite of LR images. Finally the last stage, image restoration is applied to the up-sampled image to remove blurring and noise.

Among different super resolution techniques, Iterative Back Projection (IBP) approach has been studied. It is an iterative approach that minimizes the error between the simulated LR images and the observed image (Figure 15). The LR images are simulated from the HR image. Simulated errors are obtained by subtracting the simulated LR images from the corresponding observed LR images. Each simulated error is then added to the HR image as back projection. The advantage of IBP is that it is understood intuitively and easily. However, this method has no unique solution due to the ill-posed nature of the inverse problem and it is difficult to apply constraints.
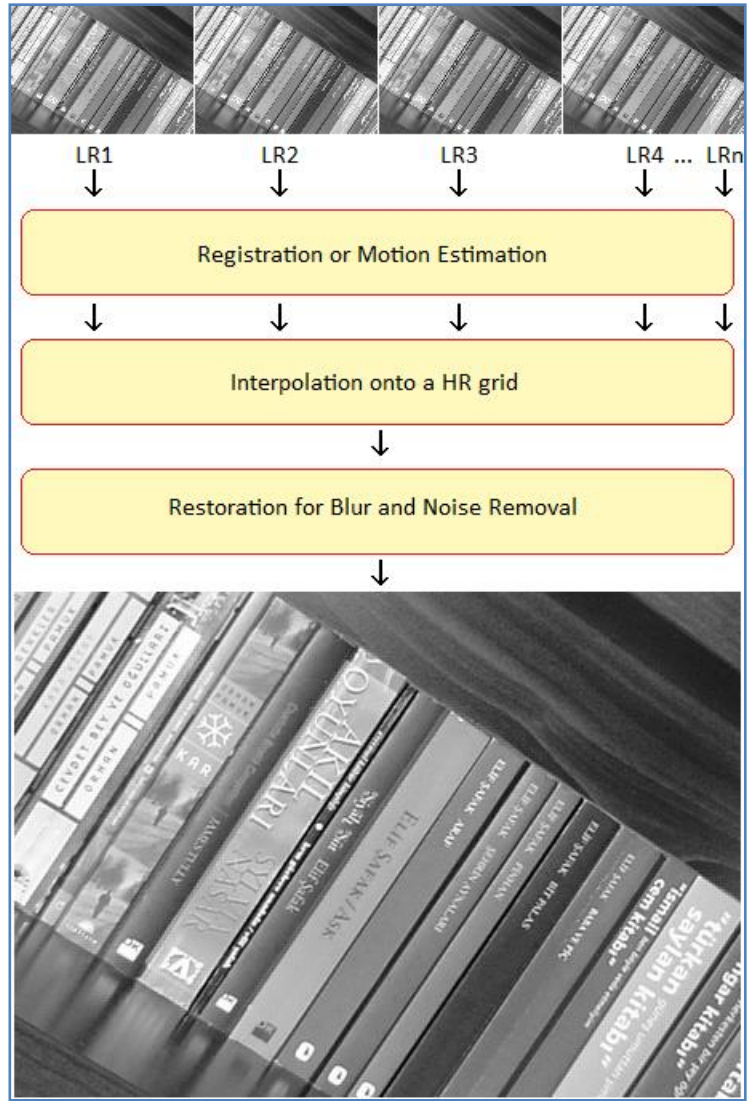
Figure 13 Super resolution scheme
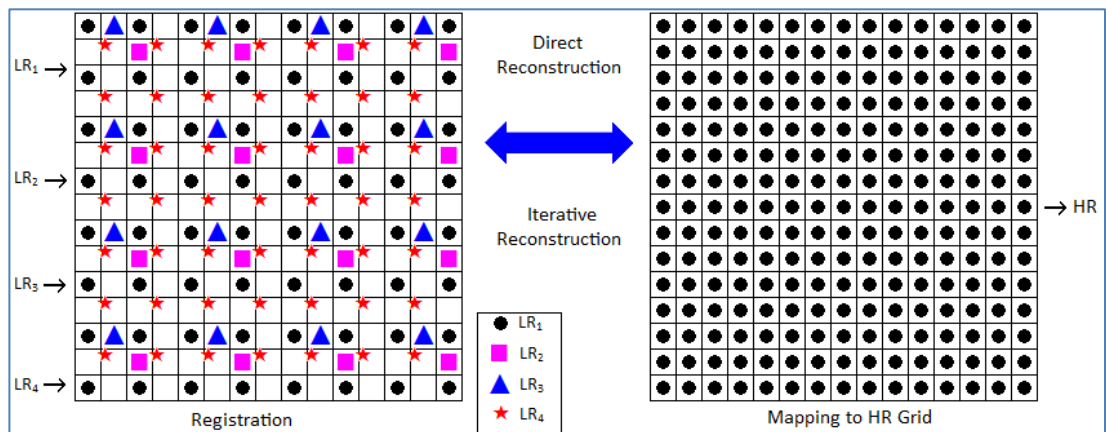
Figure 14 Registration of LR images
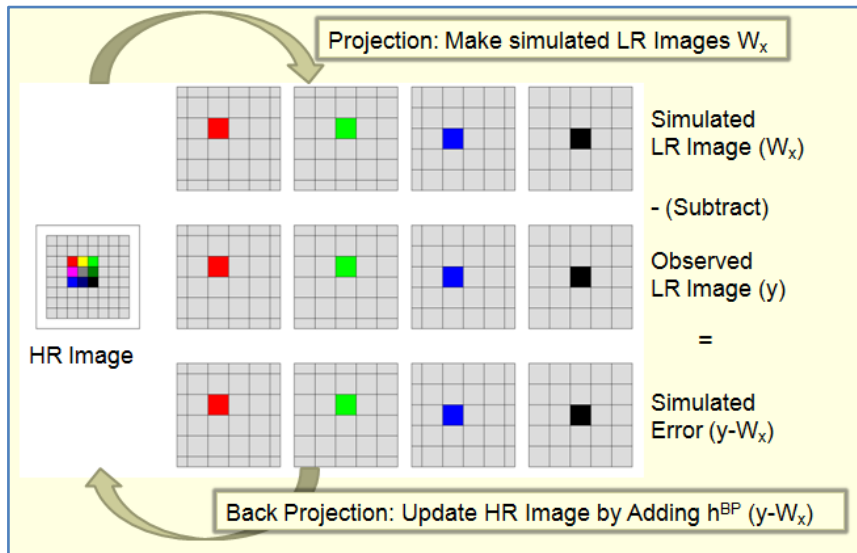
Figure 15 Iterative Back Projection

In grid DEM super resolution; LR grid DEMs are exactly geo-referenced to coordinate system, so non-uniform interpolation is not a necessity for grid DEM interpolation. Also restoration for blur and noise removal cannot be done on grid DEM super resolution because; as stated in the previous section, the zoom is infinite for grid DEM generation. There is no zooming or loss of ROI in grid DEM, so the third step in image super resolution is neglected in grid DEM super resolution.

3.3.1 Super Resolution Application on Digital Imagery

Super resolution is the backbone of this dissertation. The succes of the study will mainly depend of the robustness of the application of super resolution algorithm. The implementation of the super resolution is done by a program coded by the author. The program is written in Delphi language. The SR program is around 1000 lines and uses two different Dynamic Link Libraries (DLL) in order to handle repeated jobs. It starts with acqusition of LRs, and lets the user to define the relative displacements to the reference LR image. Then the program defines the HR image size and starts interpolation. The code is full consistent with the flow chart of IBP given in Figure 15.

SR program is applied on a real image (Figure 16). The image is an air-borne image of METU area. The area covers the buildings of Chemical Enginnering Department, Environmental Enginnering Department. Also some buildings of Civil Engineering Department and some part of Metallurgical and Materials Enginnering Department building and Geological Engineering Depratmen buildings can be seen in the image.

The important part of the super resolution is the image registration as stated previously. It has a key role that affects the success of super resolution. Grid DEMs are referenced to a coordinate system, so image registration part of coding is omitted. The low resolution images had been obtained manually by pixel shifting. In Figure 17 the shifted low resolution images are given.

As explained in section 3.3, the IBP algorithm has been implemented in the code. The results can be seen in Figures 18 to 21 In Figure 18 the result of super resolution with 16 LRs can be seen. In Figure 19 the LR number is 9. The Figures 20 and 21 are the result of 4 LRs. The best result is achieved with 4 LR images.
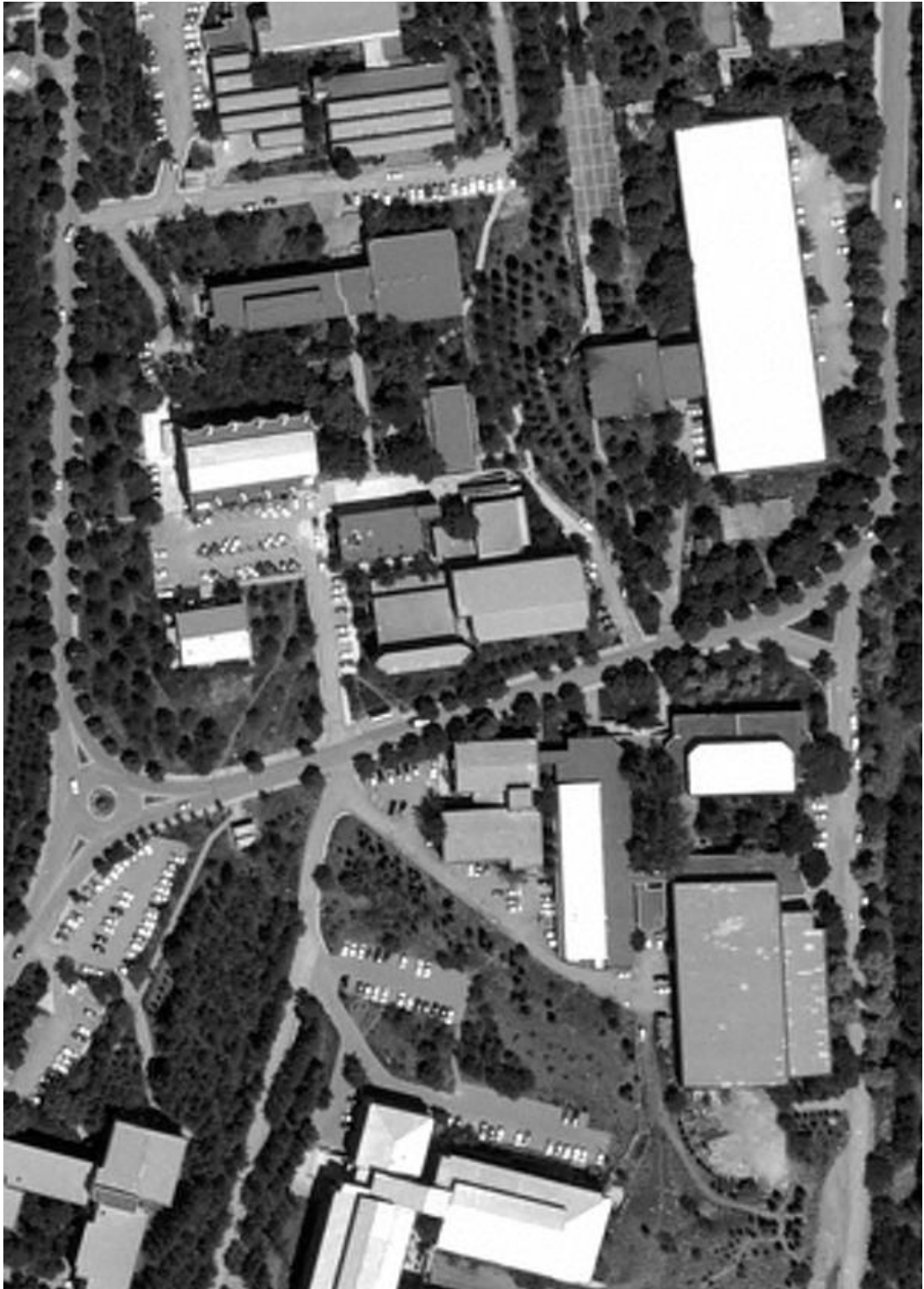
Figure 16 The image chosen for super resolution program control

a) Low resolution image produced from Figure 16 (Reference LR)

b) Low resolution image (dx=1, dy=0)

c) Low resolution image (dx=0, dy=1)

d) Low resolution image (dx=1, dy=1)

Figure 17 Low resolution images produced from Figure 16
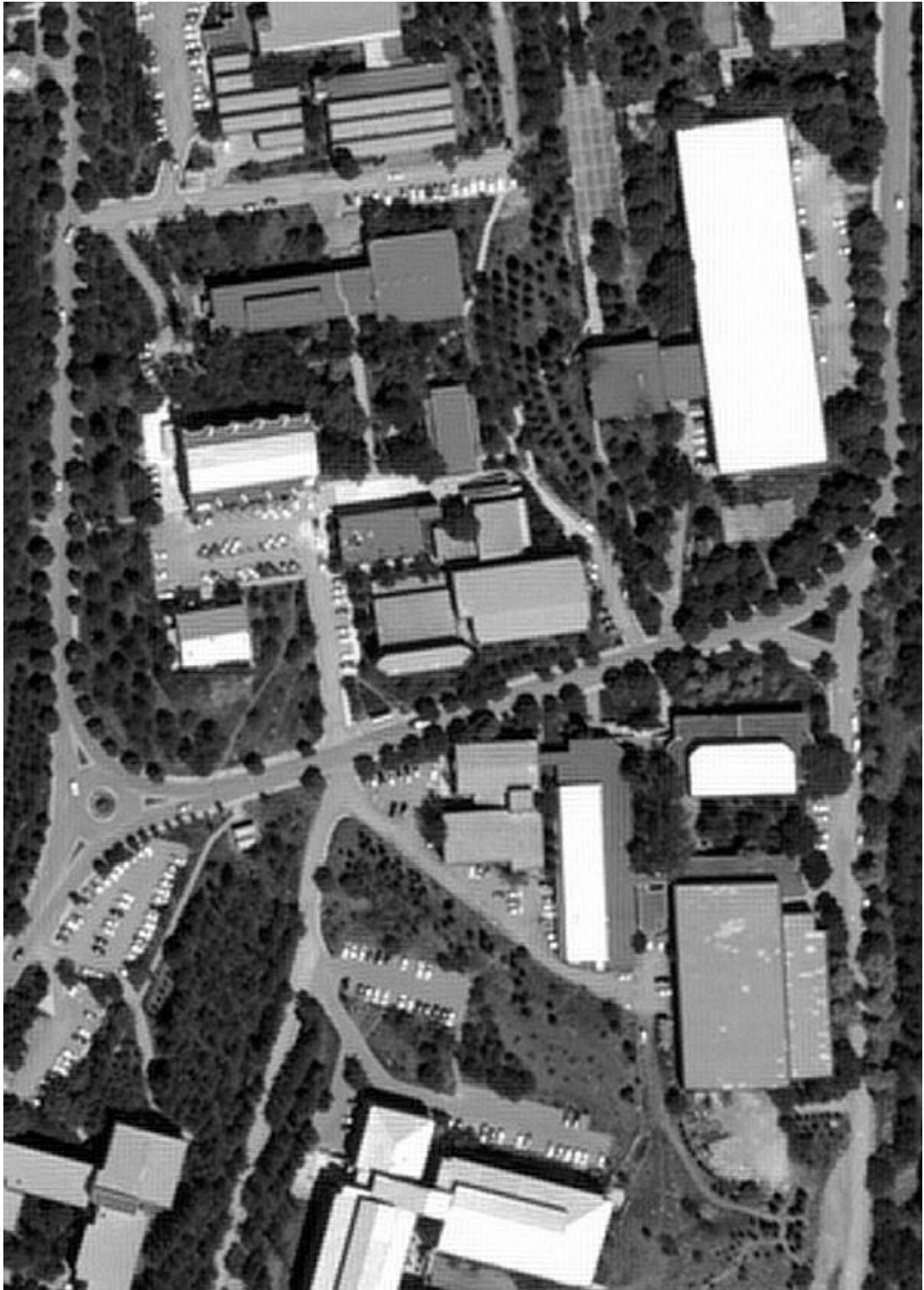
Figure 18 The result of the super resolution program with 16 LR images
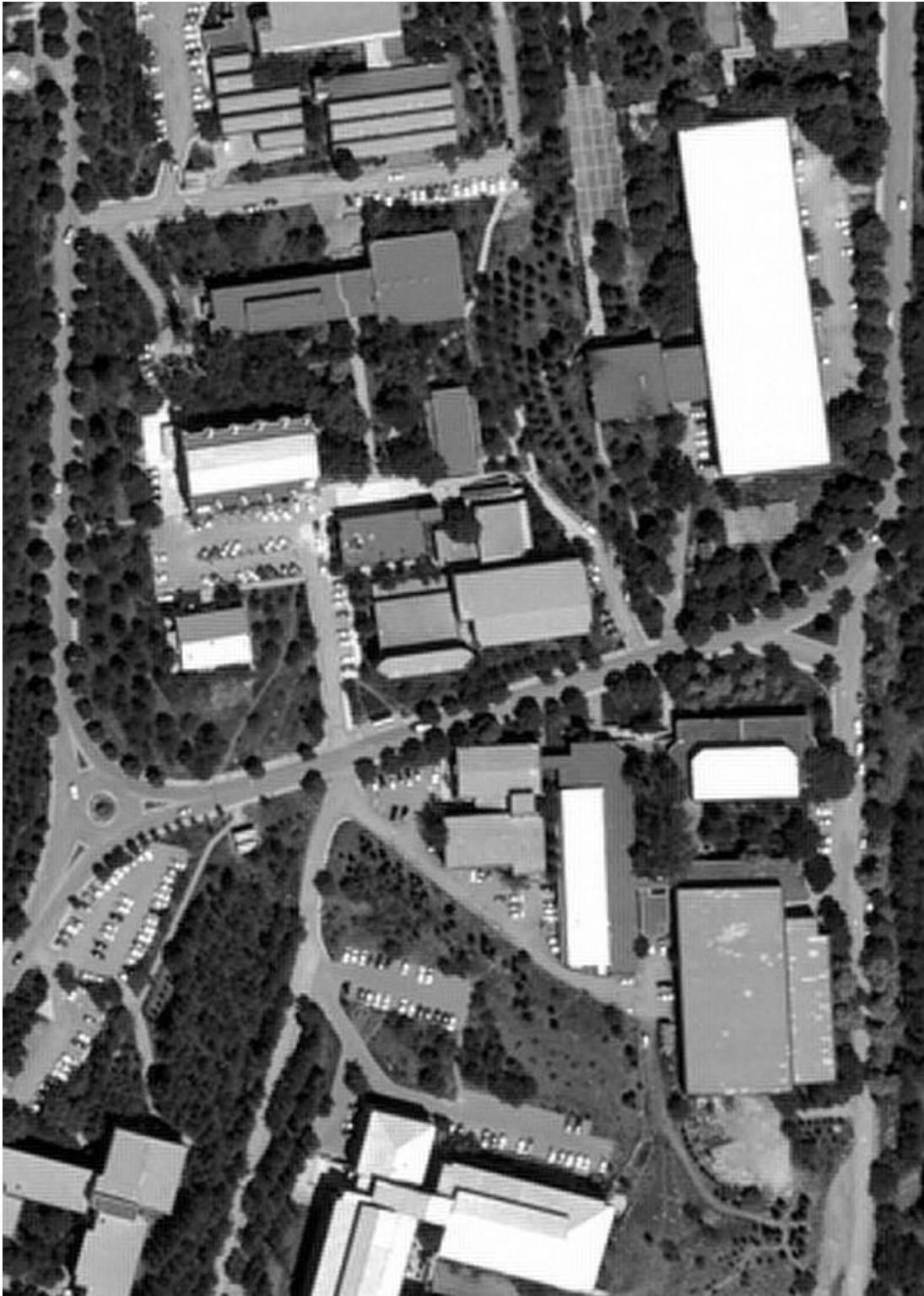
Figure 19 The result of the super resolution program with 9 LR images
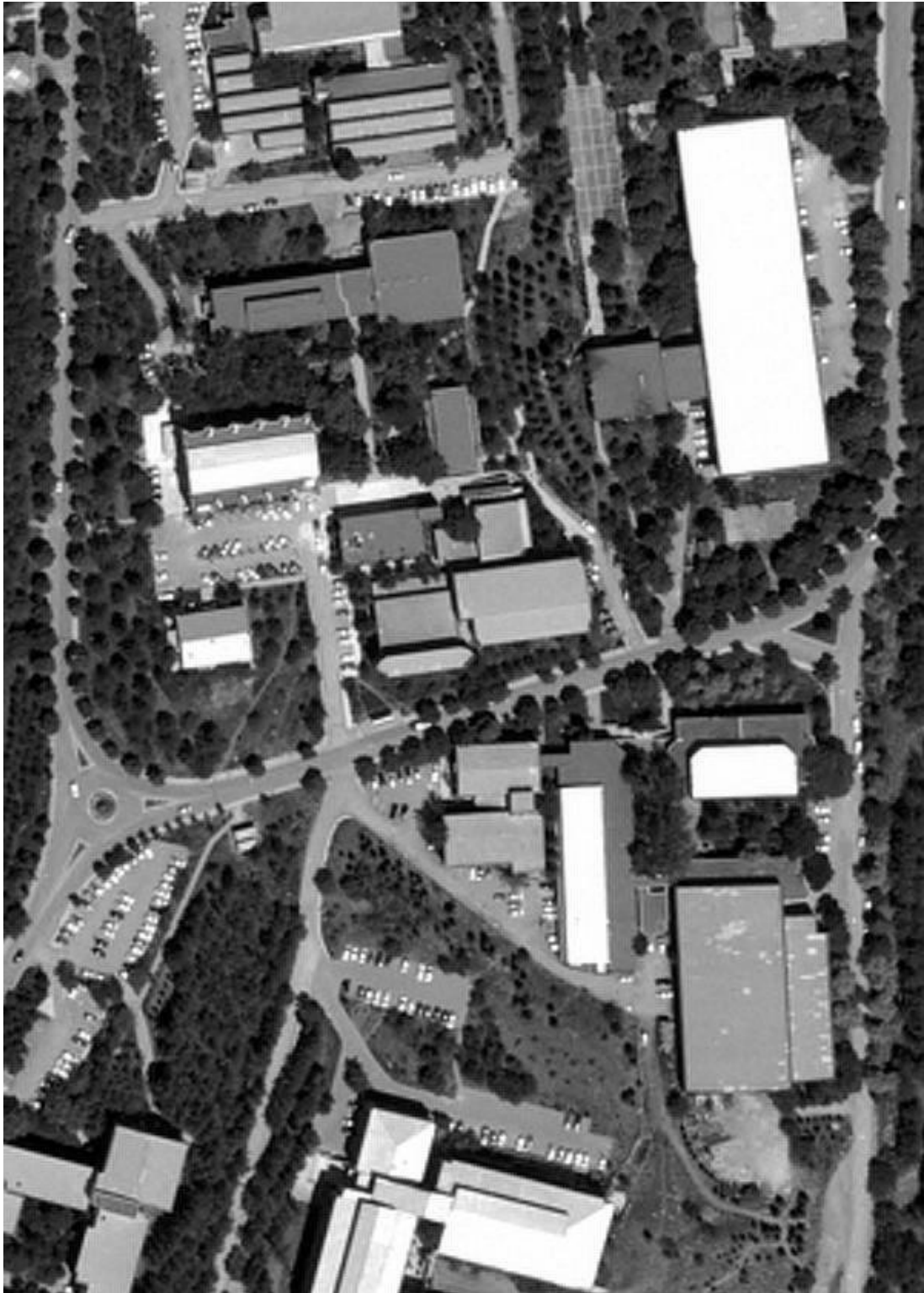
Figure 20 The result of the super resolution program with 4 LR images in Figures 17 - 20 (without boundary conditions)
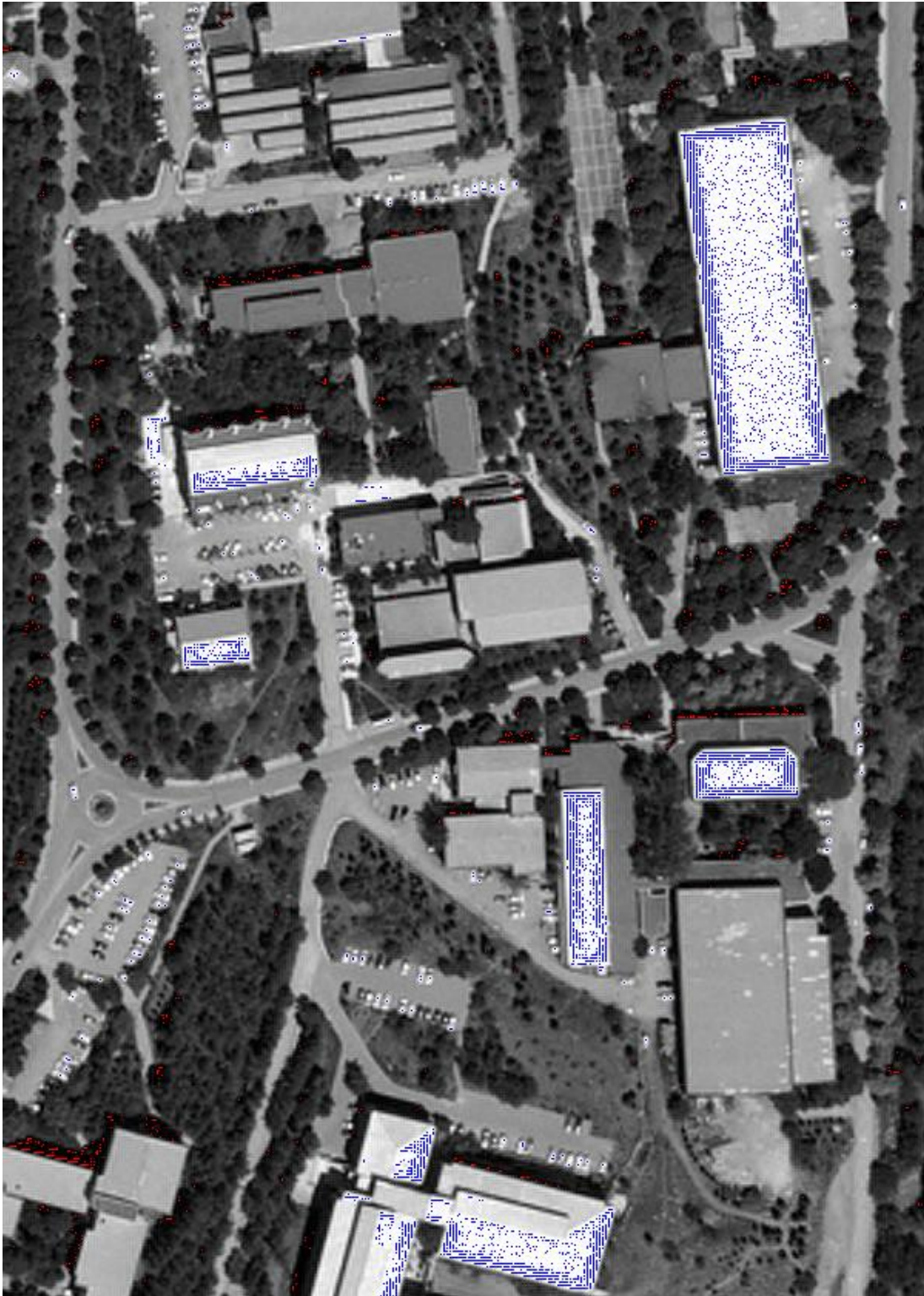
Figure 21 The result of the super resolution program with 4 LR images in Figures 17 - 20 (with boundary conditions)

In order to use the code in DEM super resolution, the number domain has been implemented as real numbers. However quantization level in imaging domain is usually 0-255. In making the image of the real number data set, the outlier numbers had been mapped to quantization level. Although IBP method had been referred as difficult to apply a priori constraints (Park, Park, & Kang, 2003), this boundary condition is common and it is posteriori. In Figure 20, super resolution result can be seen as the boundary condition applied. In Figure 21 the outlier pixels are colored as blue for the ones having a value below 0 and as red for the ones having a value over 255. This will lead the boundary conditions in DEM SR which will be discussed later.

As stated earlier, image registration is very important in super resolution. Luckily, DEMs are naturally registered to a reference system. However, proper sizing is very important also. Figure 22 shows that how improper size calculation may result in ringing effect. Ringing effect is defined as the spurious signals near sharp edges. This effect results as the stripes at the ends of the image.

3.3.2 SR Application on DEM

"Single band, infinite quantization leveled digital imagery" definiton and the right side of equation 3 in section 2.1 states that, a larger grid can be divided into smaller grids. This statement concludes that super resolution can be applied to DEM.

The digital grid DEM algorithm will measure and interpolate the elevation values to create a surface. The resulting image is regarded as grid DEM. The above analogy also enables us that two or more grid DEMs can be inputs to the super resolution algorithm and the result would be a finer resolution grid DEM. The ruling part of the conventional grid DEM is the interpolation. The motivation of this research is to minimize the effect of interpolation by the help of super resolution.

Application of grid DEM resolution is done by the combination of DEM creation program and super resolution program. This combination is obtained in the main program which is around 1500 lines and uses 7 different DLLs in order to handle repeated jobs. It starts with acqusition of points, and lets the user to define the geometry of the grid. Then interpolation method is chosen. Depending on the interpolation method, various options are defined by the user. User decides whether this grid is calculated by using super resolution or not. Depending on this choice super resoltion options are selected and finally the result is written on a grid file.

Image super resolution deals with integer numbers, and the DEM creation works with real numbers. In order to combine them, the super resolution program had been customized to work in real number domain. In image case, super resolution iterates on real numbers, at last the result is converted to integer numbers. The outliers mapped to quantization level boundaries. As stated in section 3.2, DEM is a single band, infinite quantization leveled digital imagery. In DEM case integer conversion is omitted. Infinite leveled quantization has no limit, so boundary conditions cannot be applied.

As stated, grid DEM can be accepted as a digital image and super-resolution techniques can be used for enhancement of grid DEM. It is also stated that if the low resolution images have non-redundant information, then super-resolution techniques can be successful in creating high resolution images. If the low resolution grid DEMs can be organized in a way that they have non-redundant information, then super resolution techniques will enable to create a high-resolution grid DEM. Luckily grid DEMs are referenced to a coordinate system, so there is infinite number of different organization schemes that can be applied on LR grid DEMs. As stated in section 3.3.1 and seen in the figures of that section, the best result is achieved with 4 LRs. In order to give the user more choices, in Graphical User Interface (GUI) of SR part, more than one low resolution level is offered. The minimum of low resolution level is 2x2 and the maximum is 5x5. Also the number of iteration can be chosen on GUI which is limited by 100 (Figure 23).
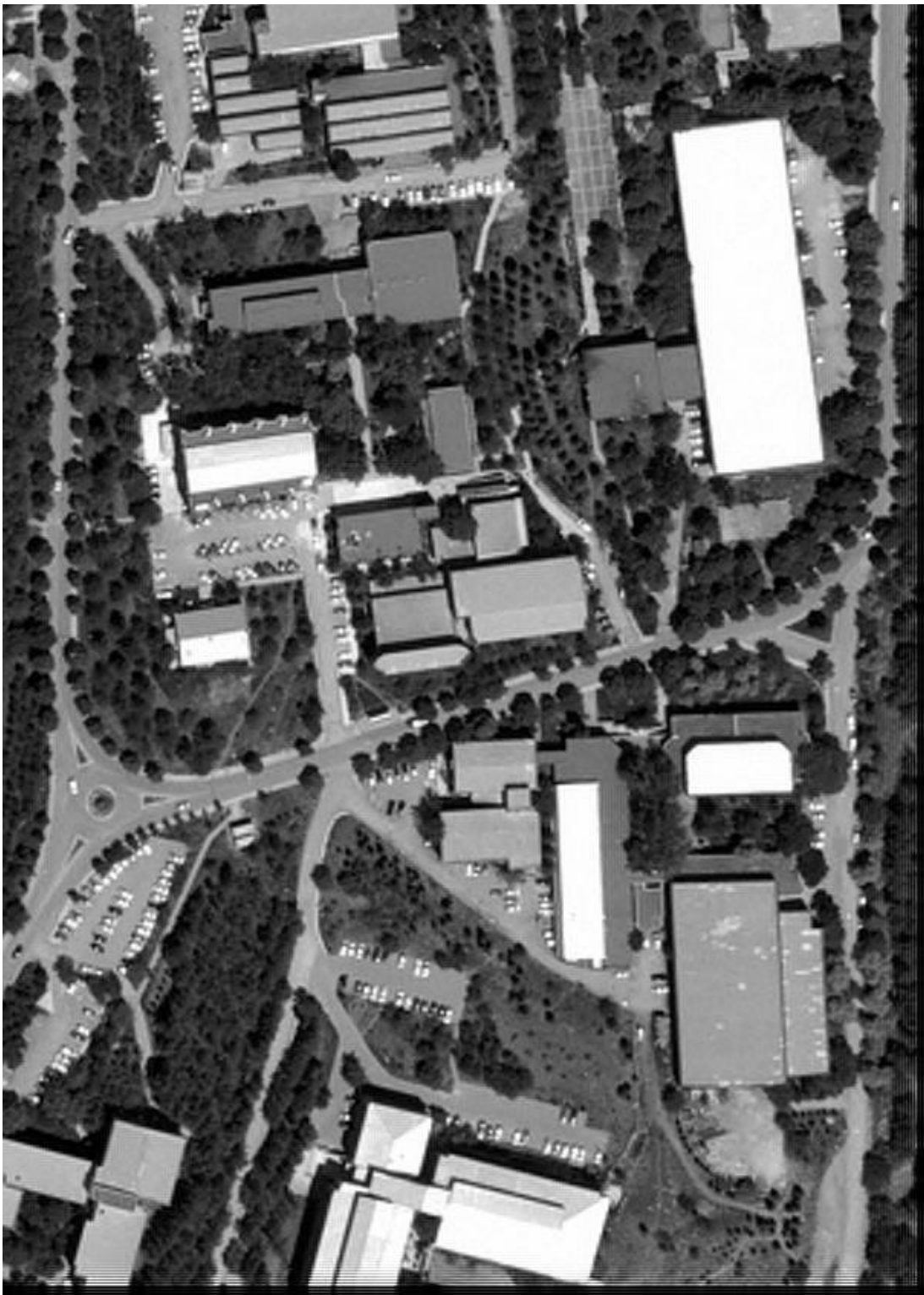
Figure 22 The result of improper size calculation
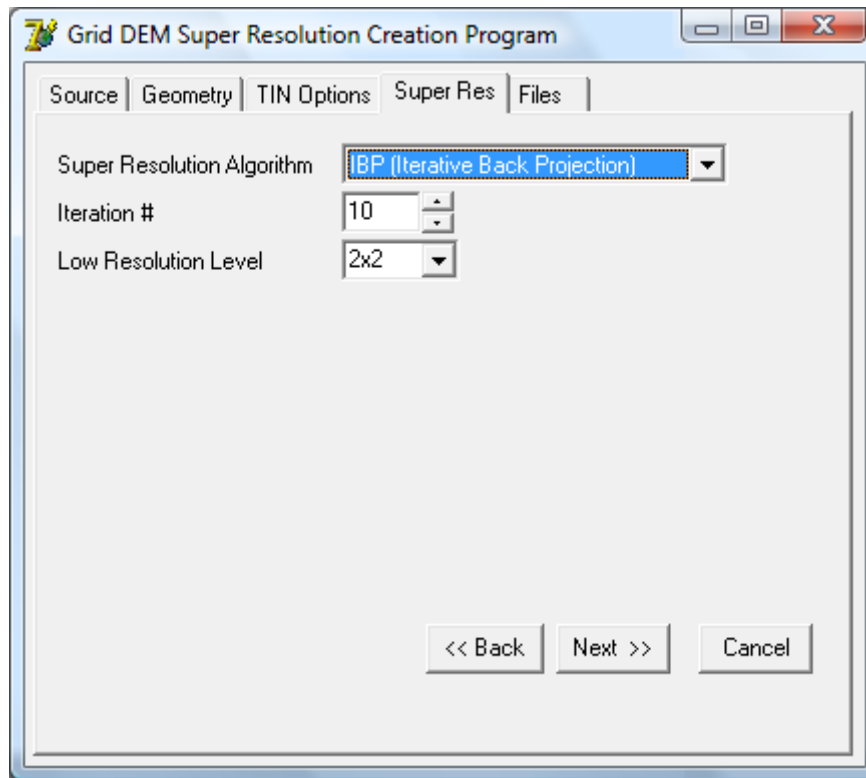
Figure 23 GUI of Grid DEM Super Resolution

Digital images are always presented in rectangular forms. On the other hand Gird DEMs, may not always be presented in rectangular form. There may also be parts which have no values. These non-valued grid cells are handled as Not A Number (NAN) type in grid DEMs. On the early trials the ringing effect occurred as the stripes at the edges. The values at the borders are calculated including the non-valued grid cells. This error is iterated through the center part where there are no non-valued grid cells. The source of the striping effect is that in iteration one; these grid cells are calculated as the lowest value. In the preceding iteration these values are calculated as the highest value. This lowest-highest calculation is repeated as the iteration continues. The limits of the whole grid DEM are violated because of this ringing effect.

In their study; Song, et al., (2010) proposed improved iterative back projection (IBP) algorithm. In SR reconstruction process, ringing artifacts may occur in the reconstructed images. In order to reduce the dominant effect high frequency components, the second-order differential revised term is formed by the difference between the Laplace transform of the iterated LR and the Laplace transform of the reference image. Simulated LR images and standard test video sequence experiments result in reduced ringing effects and improved visual quality. They concluded that employing of this term in IBP algorithm effectively reduces the ringing artifacts and preserves the edge and texture.

Ringing effect problem is solved by employing bi-cubic interpolation. Before the first IBP iteration, bi-cubic interpolation is applied to one of the LR grid DEMs. The bounding grid cells are identified using the result of bi-cubic interpolation. The values on the bounding cells are used as the iteration values and they are not changing as the iteration progresses. This operation is called "boundary adjustment".

In order to see the effect of super resolution with boundary adjustment, the low resolution grid DEMs are obtained. One of the low resolution ellipsoid 10 m grid DEMs can be seen in Figure 24 and corresponding results of the super resolution with 5 m grid can be seen in

Figure 25. One of the low resolution 10 m grid DEM of METU area can be seen in Figure 26 and corresponding super resolution result can be seen in Figure 27.
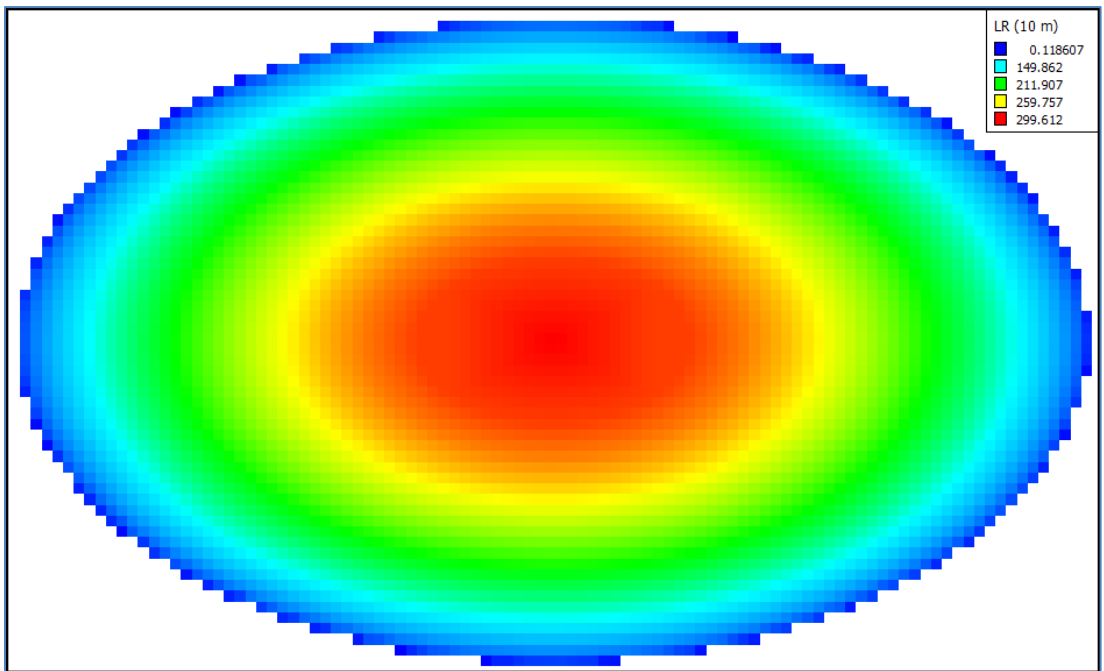
Figure 24 Low Resolution Ellipsoid Grid DEM (10 m grid DEM)
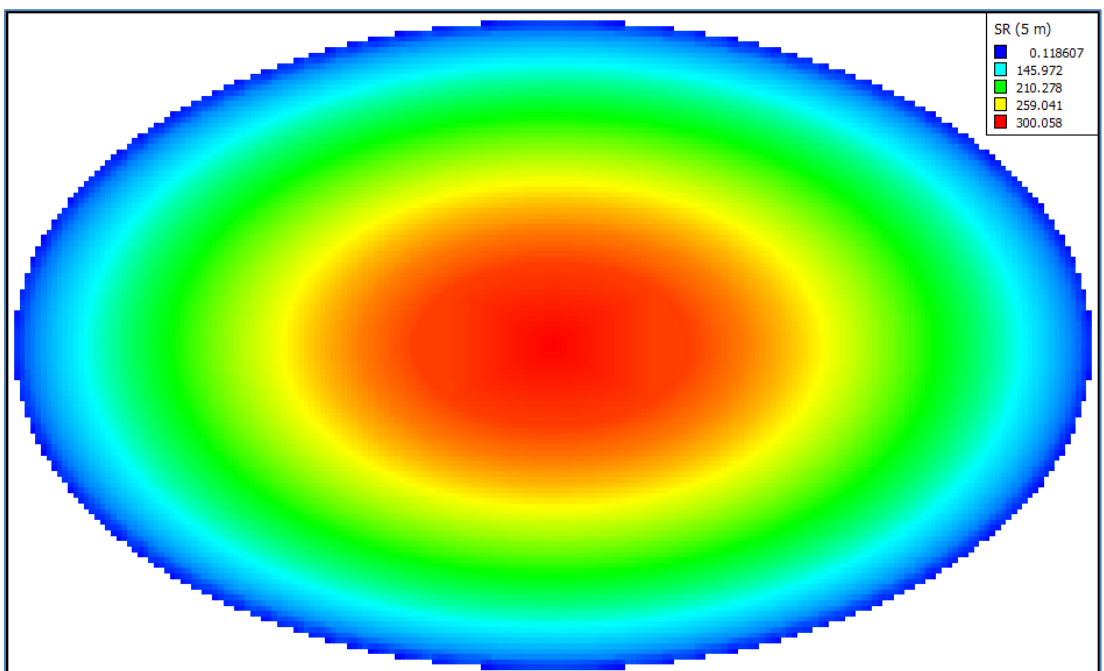
Figure 25 High Resolution Ellipsoid Grid DEM (5 m grid DEM)
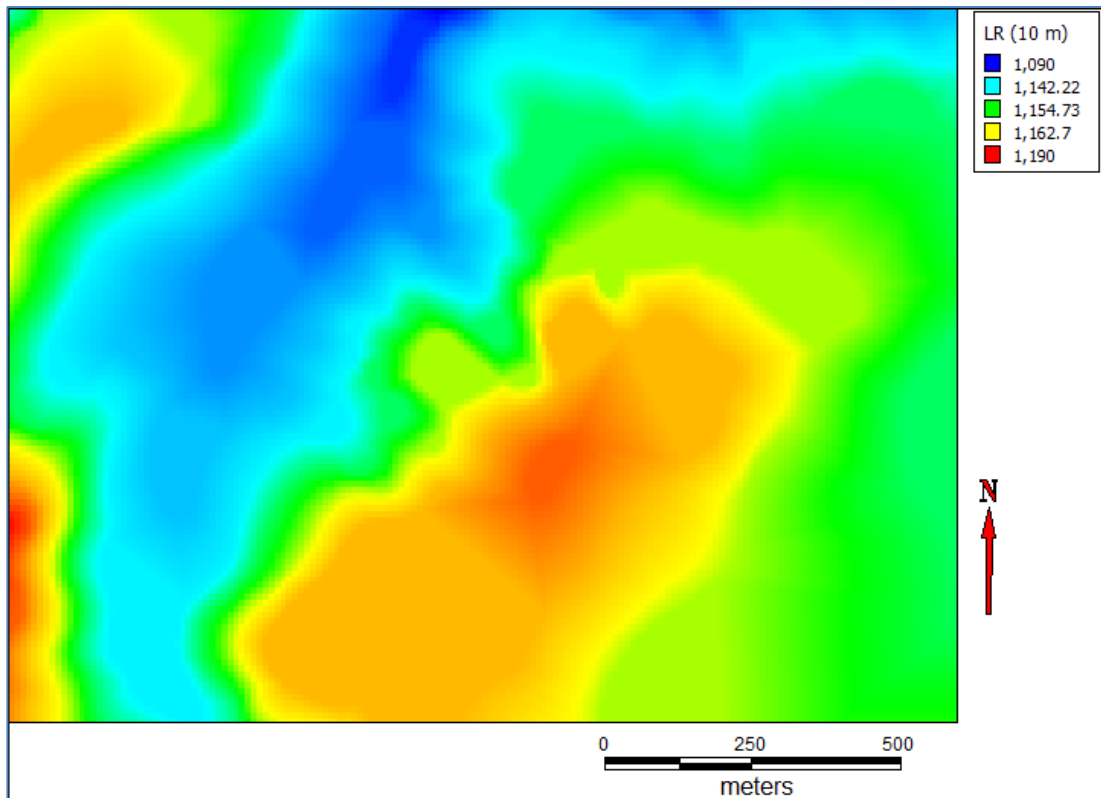
Figure 26 Low Resolution METU Grid DEM (10 m grid DEM)
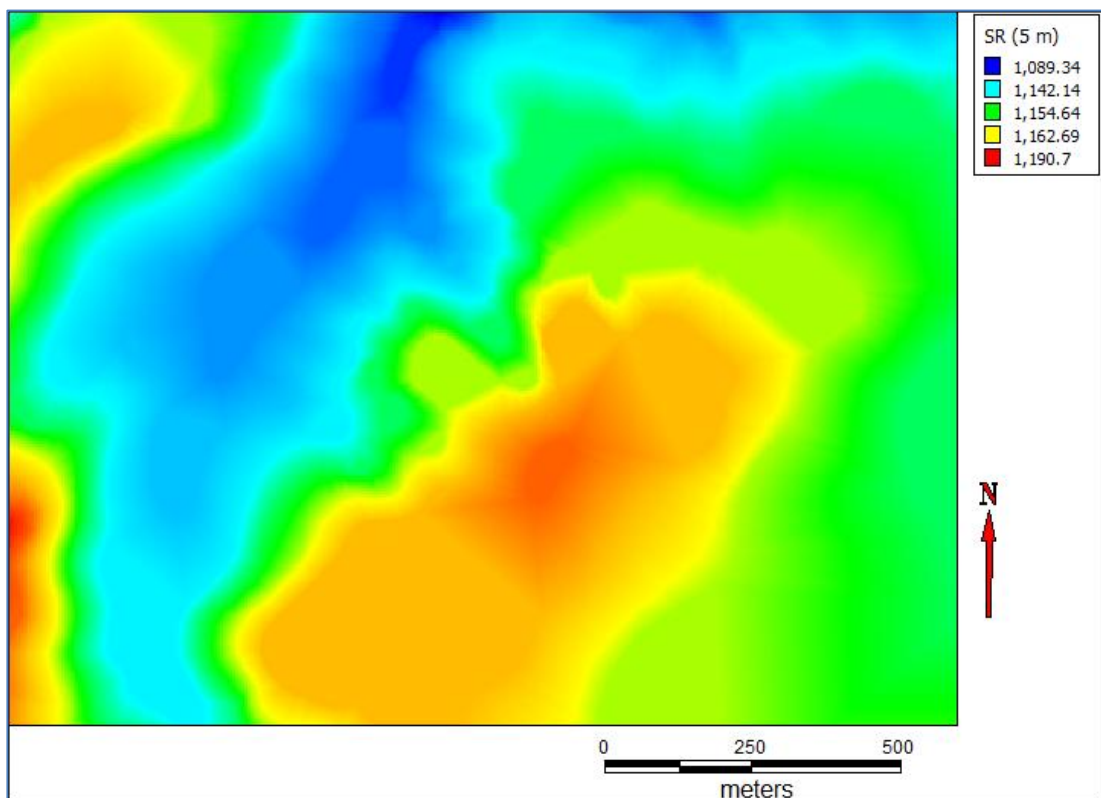
Figure 27 High Resolution METU Grid DEM (5 m grid DEM)

The main concern in application of multi-frame super resolution on grid DEM is that low resolution DEMs have single source. This may result as the LR grid DEMs may not carry non-redundant information. Before presenting the results of multi-frame super resolution application, it is necessary to show that LR grid DEMs having single source data, carry non-redundant information. The next chapter explains the similarity measures and the non-redundancy situation of LR grid DEMs.

CHAPTER 4

SIMILARITY MEASURES AND CHECKING THE DEM PAIRS FOR NON REDUNDANT INFORMATION

In order to show that DEMs are carrying non redundant information of the same scene, it is essential to verify the difference between the DEM pairs. As stated in section 1.3, the similarity measures of the images are used with the help of the analogy between the image and DEM to prove that DEM pairs are similar or dissimilar.

In digital imaging there are three bands. These bands form a new space having three dimensions of color. Grid DEM has only one dimension so spectral dimension based metrics like multi-resolution similarity, mean angle similarity, mean angle-magnitude similarity, block spectral phase-magnitude similarity, rate distortion measure, etc. cannot be applied to DEM. The rest of the measures stated in Avcıbaş et al. (2002), and Fitzpatrick et al., (2000) are investigated and with the similarity measures expressed below, possible applications on DEM are explored. First preliminary condition is coinciding grid center points. The second sub section of this chapter is explaining how the low resolution grid DEMs and high resolution grid DEM had been arranged for coinciding grid centers. The second preliminary condition is the intersection set between the subject DEMs. In order to apply similarity measures to any two LR DEMs, the intersection set is found. However, as seen in Figure 24 and the rest of figures, z value of some part of the ellipsoid area cannot be calculated. These grids are stored as NAN in the code. While calculating the intersection areas, it is crucial that these grids are excluded in DEMs.

4.1   Similarity Measures

A list of suitable measures and corresponding application results are given at the end of the section. Before discussing the similarity measures, common nomenclature is given below. Additional figures are explained in appropriate items.

   A (i,j) : Individual pixel value at i^{th} column and j^{th} row of image or DEM A.

   B (i,j) : Individual pixel value at i^{th} column and j^{th} row of image or DEM B.

   μ_A : The mean of all pixel values of image or DEM A.

   σ_A : Standard deviation of all pixel values of image or DEM A.

   M, N : Image or DEM has M columns and N rows.

   w   : Kernel size can be 3x3, 5x5, or 7x7 even larger. It must be an odd number.

   l, m   : Pixel positions in kernel.

4.1.1 Image Subtraction

This measure calculates the distortion between two images on pixel-wise difference. If two images are identical, the sum of squares of intensity difference (SSD) will be zero. As the images differ SSD will increase. The theory of SSD lies on Minkowsky distance as stated in Avcıbaş et al. (2002). Mean absolute difference (MAD) and modified infinity norm of Minkowsky distance measures can also be found by image subtraction; however, the latter refers to the spectral dimension, so it cannot be applied on DEM. SSD and MAD measure formulas, that can be applicable on DEM, are given below:

$$SSD = \frac{1}{MxN} \sum_{i,j}^{M,N} \left(A(i,j) - B(i,j)\right)^2 \tag{15}$$

$$MAD = \frac{1}{MxN} \sum_{i,j}^{M,N} \left|A(i,j) - B(i,j)\right| \tag{16}$$

The square root of SSD leads us to the well-known metric root mean square difference (error). RMSD has the same unit with the images, in our case DEMs. This value gives an idea of difference in variation.

Another measure based on the image subtraction is the "difference over a neighborhood" (DON) as stated in Avcıbaş et al. (2002). This measure shows the difference of two images because of any shift of the pixels.

$$DON = \sqrt{\frac{1}{2(MxN-w^2)} \sum_{i,j}^{M-\frac{w}{2},N-\frac{w}{2},} \left(\min\{d[A(i,j),B(l,m)]\}\right)^2 + \left(\min\{d[A(l,m),B(i,j)]\}\right)^2} \tag{17}$$

where, $d[.,.]$ is an appropriate distance metric. The measure works with kernel. A kernel size of 3x3 or 5x5 (w=3 or w=5 respectively) on both images finds the minimum distance of pixels having the minimum intensity difference. Note that for w=1, this metric becomes mean square error. DON value 0 shows two identical images, deviation from this value shows the level of dissimilarity.

4.1.2 Correlation coefficient

In digital imaging; the brightness values of the same scene may differ due to the sensor change. This results a change in pixel values. In order to see whether the brightness values in images are linearly related, the correlation coefficient (CC) is calculated. If images A and B are totally similar then correlation coefficient will be 1. The deviation from 1 will show the degree of dissimilarity. The formula of correlation coefficient is given below:

$$CC = \frac{\sum\limits_{i,j}^{M,N} \{A(i,j) - \mu_A\}\{B(i,j) - \mu_B\}}{\sqrt{\sum\limits_{i,j}^{M,N} \{A(i,j) - \mu_A\}^2 \sum\limits_{i,j}^{M,N} \{B(i,j) - \mu_B\}^2}}$$ (18)

In their study, Avcıbaş et al. (2002) added different definitions of correlation coefficients like structural content (SC), normalized cross-correlation measure (NCC), and Czenakowski distance (CD) whose equations are given below respectively:

$$SC = \frac{\sum\limits_{i,j}^{M,N} A(i,j)^2}{\sum\limits_{i,j}^{M,N} B(i,j)^2}$$ (19)

$$NCC = \frac{\sum\limits_{i,j}^{M,N} A(i,j)B(i,j)}{\sum\limits_{i,j}^{M,N} A(i,j)^2}$$ (20)

$$CD = 1 - \left\{ \frac{2 \sum\limits_{i,j}^{M,N} \min(A(i,j), B(i,j))}{\sum\limits_{i,j}^{M,N} [A(i,j) + B(i,j)]} \right\}$$ (21)

First two measures get a value of 1 if both images are identical whereas the last measure, Czenakowski distance, gets 0. For the first two measures as the measure diverges from 1 (0 for the last one) the level of similarity decreases.

4.1.3   Ratio-Image Uniformity

The ratio image (R) is obtained by dividing image B values by image A for each pixel. Ratio – image uniformity (RIU) is calculated by the normalized standard deviation of R.

$$R(i,j) = \frac{B(i,j)}{A(i,j)}$$ (22)

$$\mu_R = \frac{1}{MxN} \sum_{i,j}^{M,N} R(i,j)$$ (23)

$$\sigma_R = \frac{1}{MxN} \sum_{i,j}^{M,N} [R(i,j) - \mu_R]^2$$ (24)

$$RIU = \frac{\sigma_R}{\mu_R}$$ (25)

Diverging values of RIU from 0 show the level of difference between the images.

4.1.4 Partitioned Intensity Uniformity

The idea behind partitioned intensity uniformity (PIU) comes from medical imaging: "the same tissues must have the similar values in MR and PET respectively". This measure is calculated by using image histograms. Image A's histogram is constructed for some intensity values. For each intensity value, pixel coordinates are obtained and corresponding pixel values of image B are collected.

Corresponding pixel values of image B are used to calculate the normalized standard deviation. For each intensity value; histogram proportion is multiplied with normalized standard deviation and the sum of this multiplication gives the PIU measure.

$$PIU = \sum_a \frac{n_A(a)}{MxN} \frac{\sigma_B(a)}{\mu_B(a)}$$ (26)

where, $n_A(a)$ is the number of pixels having the value of a, $\mu_B(a)$ and $\sigma_B(a)$ are average and standard deviation of the co-occurring pixels in image B.

4.1.5 Joint Histograms and Joint Probability Distributions

A joint histogram is n-dimensional where n is the number of images used to generate it. In one dimension (image A); the number of pixels and pixel coordinates having a specific value of intensity (or intensity partition) is counted. Pixel coordinates are used for finding the second dimension (image B) values. If two images are similar then histograms of these images must be similar. Also the joint histogram must be a multi-dimensional straight line. Deviation from this line shows the degree of dissimilarity. Normalized joint histogram gives an estimate of the joint probability distribution function (JPDF) of intensities.

$$JPDF = \frac{HIST[i,j]}{\sum\limits_{i,j}^{K} HIST[i,j]} \qquad\qquad\qquad \textbf{(27)}$$

where *K* is the total number of intensity intervals. Rather than a single value, probability distribution function is given as a two dimensional graph. Dispersion from the diagonal line shows the dissimilarity of the images.

4.1.6　Joint Entropy

Joint entropy is a measure of the uncertainty or information associated with them. Before defining joint entropy, the definition of entropy must be given. Hartlry (1928) defined the first information measure as:

$$H = n \log s \qquad\qquad\qquad \textbf{(28)}$$

where n is the length of the message and s is the number of possible values for each symbol in the message. This measure assumes that all symbols have the same probability to occur.

Shannon (1948) proposed another measure for information entropy. It is stated as follows:

$$H = -\sum_{i} p_i \log p_i \qquad\qquad\qquad \textbf{(29)}$$

where p_i is the probability of an event to occur. This probability is normalized by the inverse of the probability of occurrence. If events have equal probability, then entropy will be at maximum. If one event has a probability of 1 and all others have a probability of zero, then entropy will have a minimum value. Rarely occurring event contributes to entropy more than a frequently occurring event.

Two images have their own entropies; together they have a joint entropy which shows how much information they have together. As in the previous measure we provide that the probability of any pixel to occur is found by the histograms. The joint histogram shows probability distribution of both images. The joint entropy definition is given as follows:

$$H = \sum_{i,j}^{K} JPDF[i,j] \log \frac{1}{JPDF[i,j]} \qquad\qquad\qquad \textbf{(30)}$$

where *K* is the total number of intensity intervals and $JPDF[i,j]$ is the joint probability distribution function.

4.1.7 Mutual Information

Mutual information is the measurement of uncertainty in two related information sets when the second is known and information is reduced from the first one. It shows how much one random variable tells us about another. It can be regarded as the reduction in uncertainty about one random variable given knowledge of another and it is a dimensionless quantity with (generally) units of bits. Mutual information value 0 shows that two random variables are independent, as the measure increases, the level of dependency (or similarity) increases. Mutual information formula is given below:

$$MI = \sum_{i,j} JPDF[i,j] \log \frac{JPDF[i,j]}{PDF[i]PDF[j]} \tag{31}$$

where $PDF[i]$ and $PDF[j]$ are joint probability distribution function of a single images. $JPDF[i,j]$ is the joint probability distribution function of both images. Below properties of information gain help to prove the calculations:

$$MI(A,B) = H(A) - H(A|B) \leq H(A) \tag{32}$$

$$MI(A,B) = H(B) - H(B|A) \leq H(B) \tag{33}$$

$$MI(A,B) = H(A) + H(B) - H(A,B) \tag{34}$$

where $H(A)$ and $H(B)$ are entropies of images A and B and $H(B|A)$ is part of the entropy of B where the mutual information with A is excluded. $H(A,B)$ is the joint entropy of image A and B. The relations between entropy, joint entropy and mutual information are shown in Figure 28.
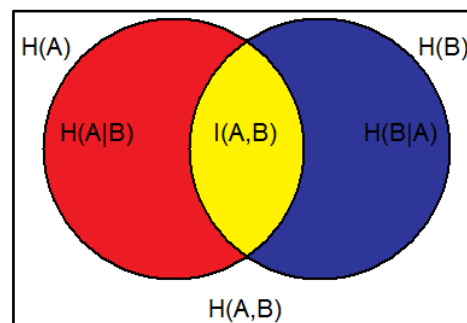
Figure 28 Relation between entropy, joint entropy and mutual information

4.1.8   Normalization of Mutual Information

Mutual information is highly dependent on entropies of the source images; however it does not give a constant value for similarity or complete dissimilarity. Normalization of mutual information will give a constant figure. There are lots of normalization schemes for normalized mutual information; the one given below is the most common:

$$NMI = \frac{H(A) + H(B)}{H(A,B)}$$ (35)

Mutual information can be normalized between [1, 2] resulting in 1 for never occurring together, and in 2 for complete co-occurrence. Besides the normalized mutual information definition, also redundancy and symmetrical uncertainty definitions are given in Witten and Frank (2005). Redundancy between the images is defined as the ratio of mutual information to sum of entropy of the images, and symmetrical uncertainty is twice the redundancy:

$$RD = \frac{MI(A,B)}{H(A) + H(B)}$$ (36)

$$SU = 2xRD = 2\frac{MI(A,B)}{H(A) + H(B)}$$ (37)

As extracted from the formula; if two images are identical, RD value is 0.5 and SU value is 1. Deviation from these values shows the level of dissimilarity.

As a summary of this section, the list of the measures that are used for assessing (dis)similarity of DEMs is given in Table 1. The formulas of the measures and the values for identical image pairs are supplied. As stated in section 4.1.5, joint probability distribution function results are mostly given as a two dimensional graph. JPDF result for identical DEM pair is given in Figure 29. The next section will be concentrating on the application of these measures to DEM pairs.

Table 1 List of measures

#	Measure	Formula	Val
15 SSD	Squares of Intensity Difference	$$SSD = \frac{1}{MxN} \sum_{i,j}^{M,N} \big(A(i,j) - B(i,j)\big)^2$$	0
16 MAD	Mean Absolute Difference	$$MAD = \frac{1}{MxN} \sum_{i,j}^{M,N} \big|A(i,j) - B(i,j)\big|$$	0
17 DON	Difference Over a Neighborhood	$$DON = \sqrt{\frac{1}{2(MxN - w^2)} \sum_{i,j}^{M-\frac{w}{2},N-\frac{w}{2}} (\min\{d[A(i,j),B(l,m)]\})^2 + (\min\{d[A(l,m),B(i,j)]\})^2}$$	0
18 CC	Correlation Coefficient	$$CC = \frac{\sum_{i,j}^{M,N}\{A(i,j) - \mu_A\}\{B(i,j) - \mu_B\}}{\sqrt{\sum_{i,j}^{M,N}\{A(i,j) - \mu_A\}^2 \sum_{i,j}^{M,N}\{B(i,j) - \mu_B\}^2}}$$	1
19 SC	Structural Content	$$SC = \sum_{i,j}^{M,N} A(i,j)^2 \Big/ \sum_{i,j}^{M,N} B(i,j)^2$$	1
20 NCC	Normalized Cross-Correlation	$$NCC = \sum_{i,j}^{M,N} A(i,j)B(i,j) \Big/ \sum_{i,j}^{M,N} A(i,j)^2$$	1
21 CD	Czenakowski Distance	$$CD = 1 - \left\{ 2\sum_{i,j}^{M,N}\min(A(i,j),B(i,j)) \Big/ \sum_{i,j}^{M,N} A(i,j) + B(i,j) \right\}$$	0
25 RIU	Ratio Image Uniformity	$$RIU = \frac{\sigma_R}{\mu_R}$$	0
26 PIU	Partitioned Intensity Uniformity	$$PIU = \sum_a \frac{n_A(a)}{MxN} \frac{\sigma_B(a)}{\mu_B(a)}$$	NA
27 JPDF	Joint Probability Distribution Function	$$JPDF = \frac{HIST[i,j]}{\sum_{i,j}^{K} HIST[i,j]}$$	
30 JE	Joint Entropy	$$H = \sum_{i,j}^{K} JPDF[i,j] \log \frac{1}{JPDF[i,j]}$$	NA
31 MI	Mutual Information	$$MI = \sum_{i,j} JPDF[i,j] \log \frac{JPDF[i,j]}{PDF[i]PDF[j]}$$	NA
35 NMI	Normalized Mutual Information	$$NMI = \frac{H(A) + H(B)}{H(A,B)}$$	2
36,37 RD & SU	Redundancy & Symmetrical Uncertainty	$$RD = \frac{MI(A,B)}{H(A) + H(B)}$$ $$SU = 2xRD = 2\frac{MI(A,B)}{H(A) + H(B)}$$	0.5 & 1
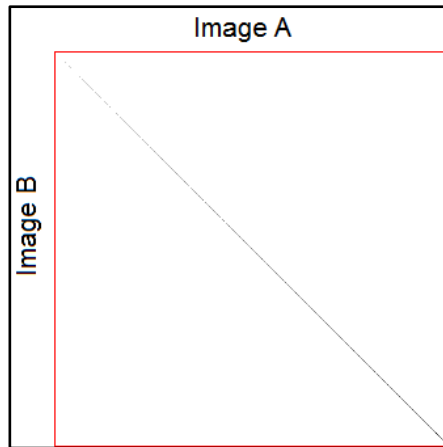
Figure 29 JPDF for an identical image pair

4.2 Application of Similarity Measures

Similarity measures expressed in the previous section are applied on the synthetic half ellipsoid surface and part of the METU area. The main problem of this study is the redundancy of DEMs from the same interpolation algorithm, so a "Similarity and Redundancy Report Tool" is employed on the code. Difference DEMs, similarity measures, and JPDF graph make the similarity and redundancy report. Grading levels and histogram intervals are pre-arranged by the report tool but they are controlled by the user. The Graphical User Interface (GUI) of the report tool can be seen in Figure 30.
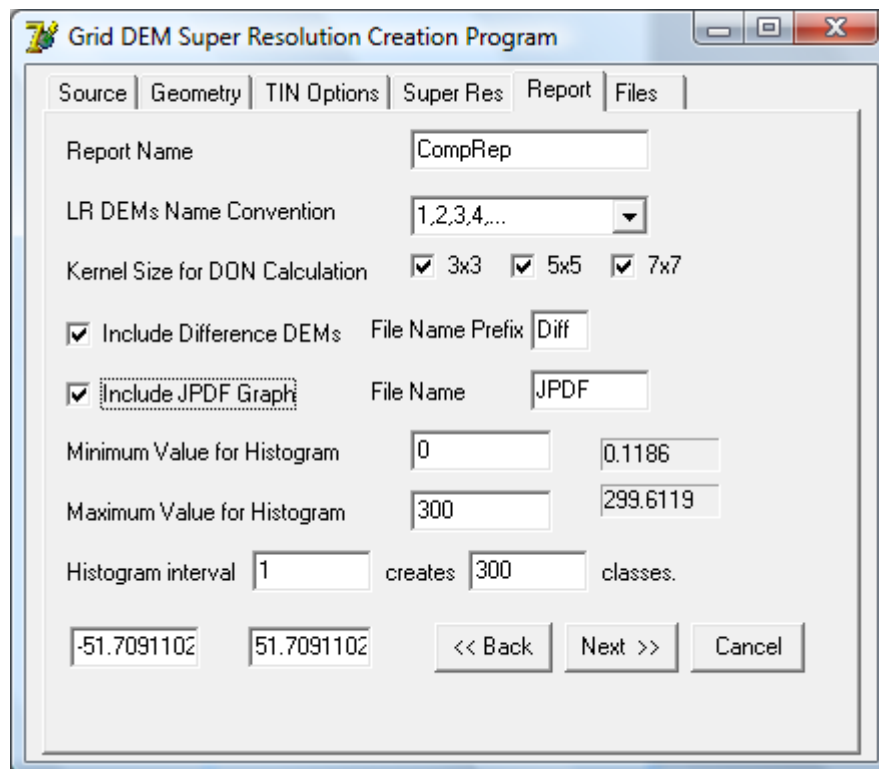
Figure 30 Graphical User Interface for Similarity and Redundancy Report Tool

41

The main point in multi-frame DEM super resolution is the difference in the grid cell center arrangement of LR DEMs. Application of similarity measures directly on the LR DEM set will not give correct results because the grid cell centers are not intersecting. This problem is solved by projecting the LR DEMs into high resolution grids. This application can be seen in Figure 31 and typical grid center arrangement of LRs can be seen in Figure 32.
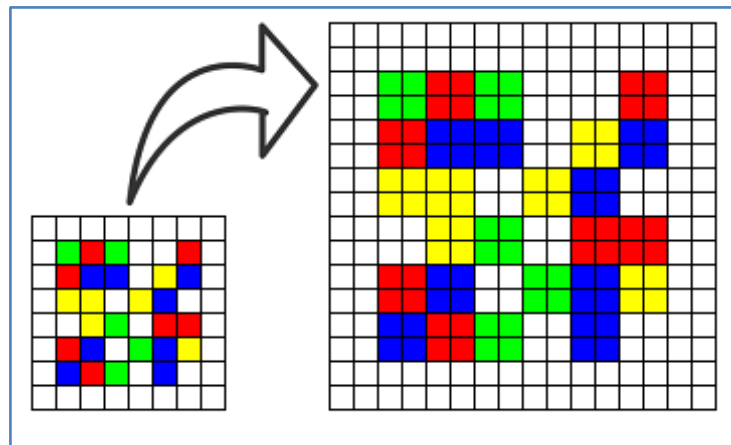
Figure 31 Projecting LR image to HR grid
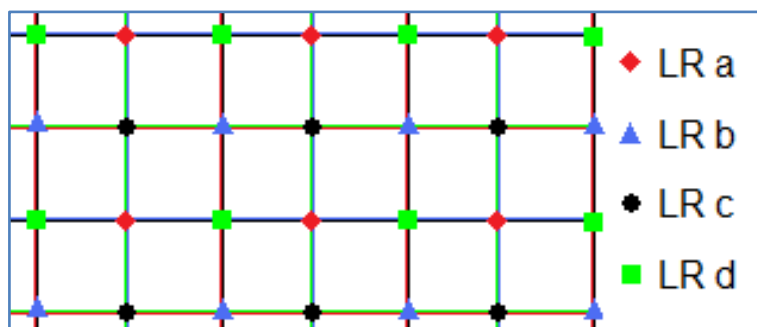
Figure 32 Arrangement of LR grid centers

The organization of the similarity and redundancy report is as follows: The subjects (LR grid DEMs) are given first, then the difference of the subjects and the similarity measures are given. Finally JPDF graphs are provided. Normalized cross-correlation (NCC) measure takes one of the images as master, so it is calculated two times with changing the master in each time. The measures for identical grid DEMs for partitioned intensity uniformity (PIU), joint entropy (JE), and mutual information (MI) measures will be used in comparing. In order to see the dissimilarity of two different LR DEMs; these measures are also calculated for identical grid DEMs and supplied as the diagonal values in the tables.

4.3   Similarity Measures Application on Synthetic Surface

Low resolution DEM for synthetic surface is constructed by forming four different 10m LR grid DEMs. The center of grids in each LR grid DEM is half pixel apart from each other. These LR grid DEMs are given in Figures 33 to 36.
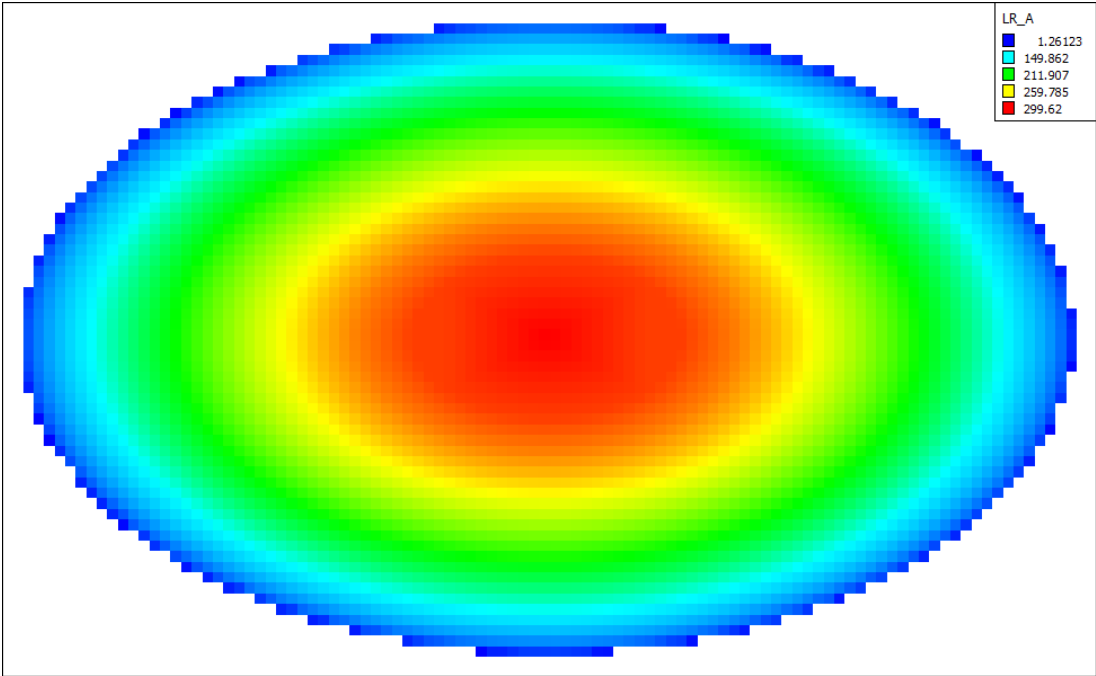
Figure 33 LR grid DEM A
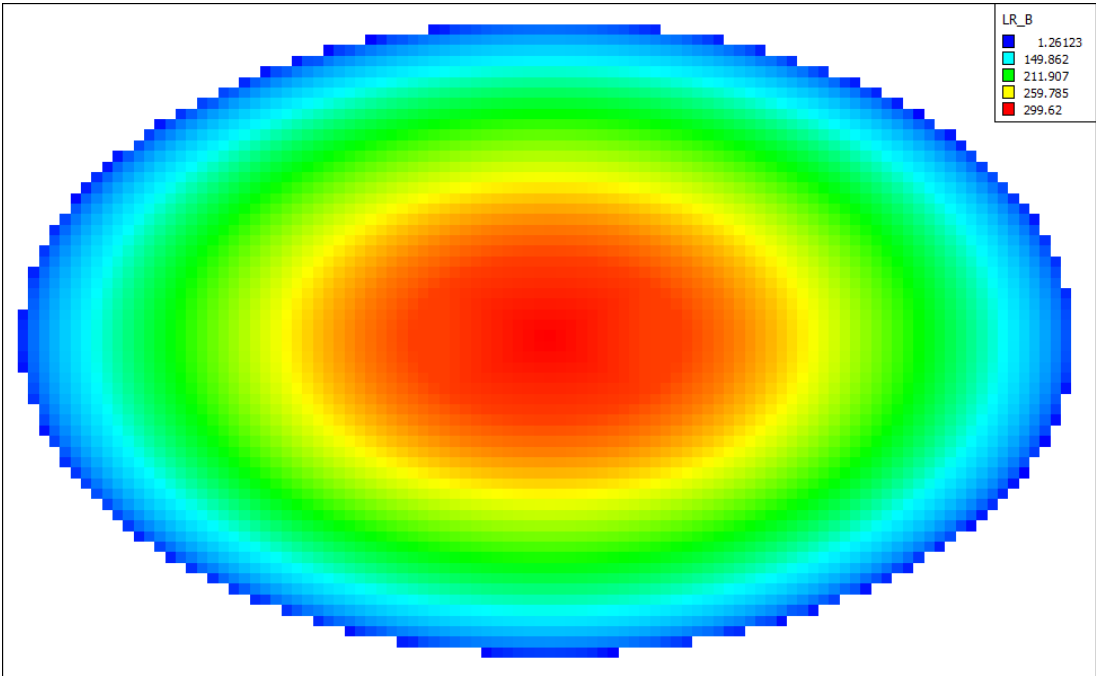
Figure 34 LR grid DEM B
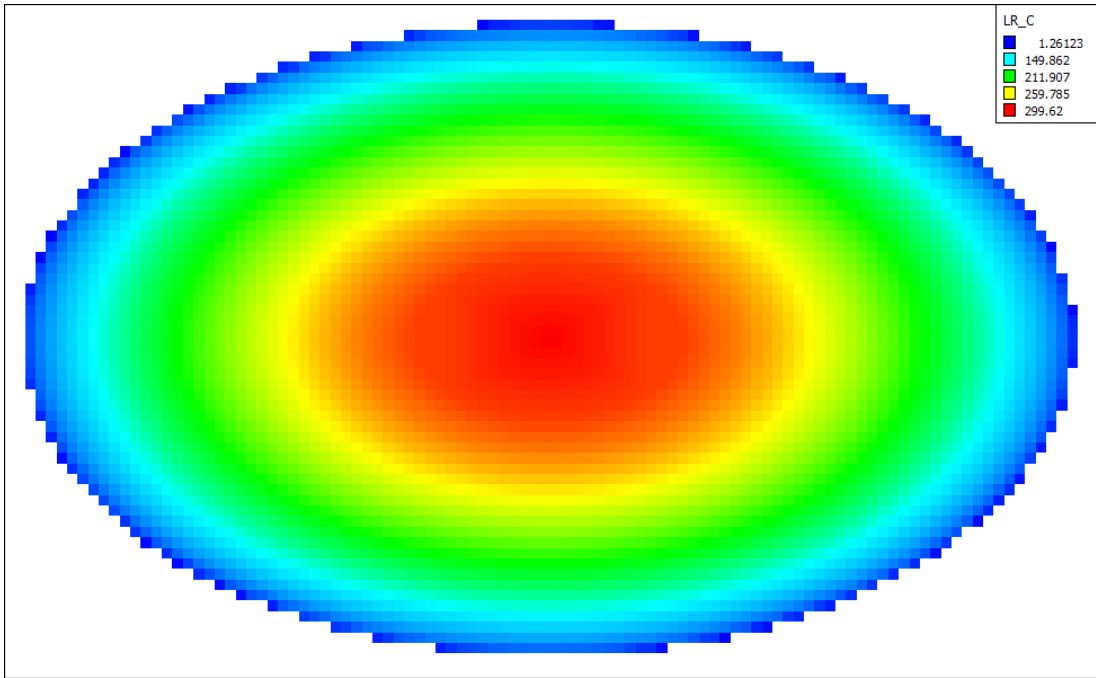
Figure 35 LR grid DEM C
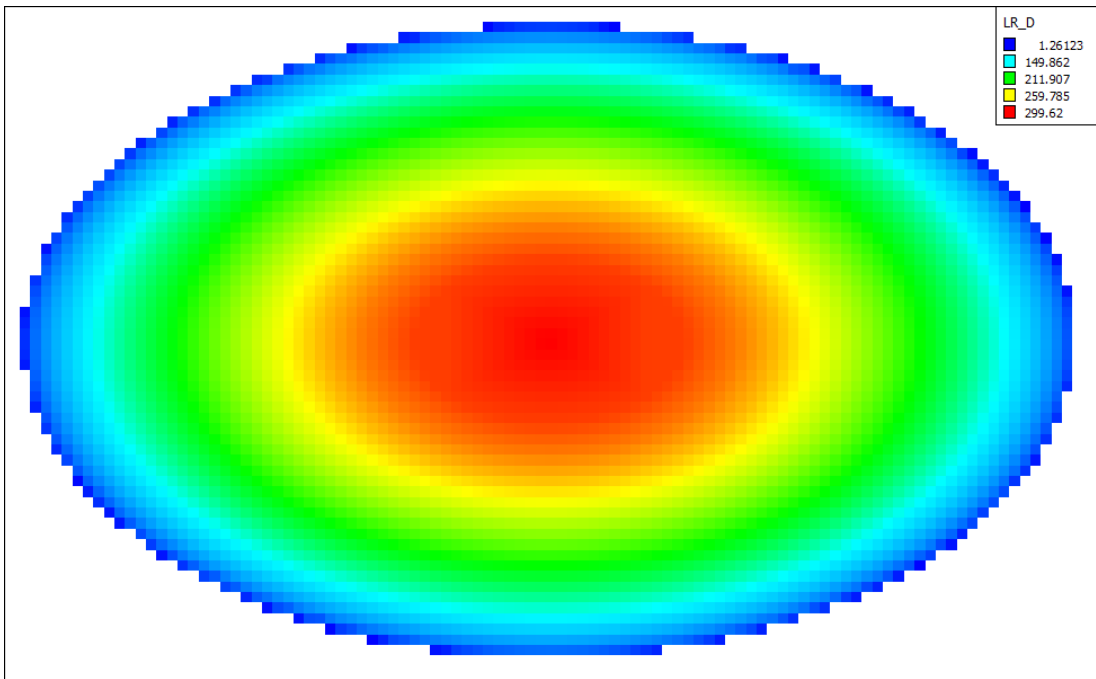
Figure 36 LR grid DEM D

As seen from the previous figures LR grid DEMs seem like they have no difference between them. However they are different and to show this, the difference DEMs are calculated and given in Figures 37 to 42.
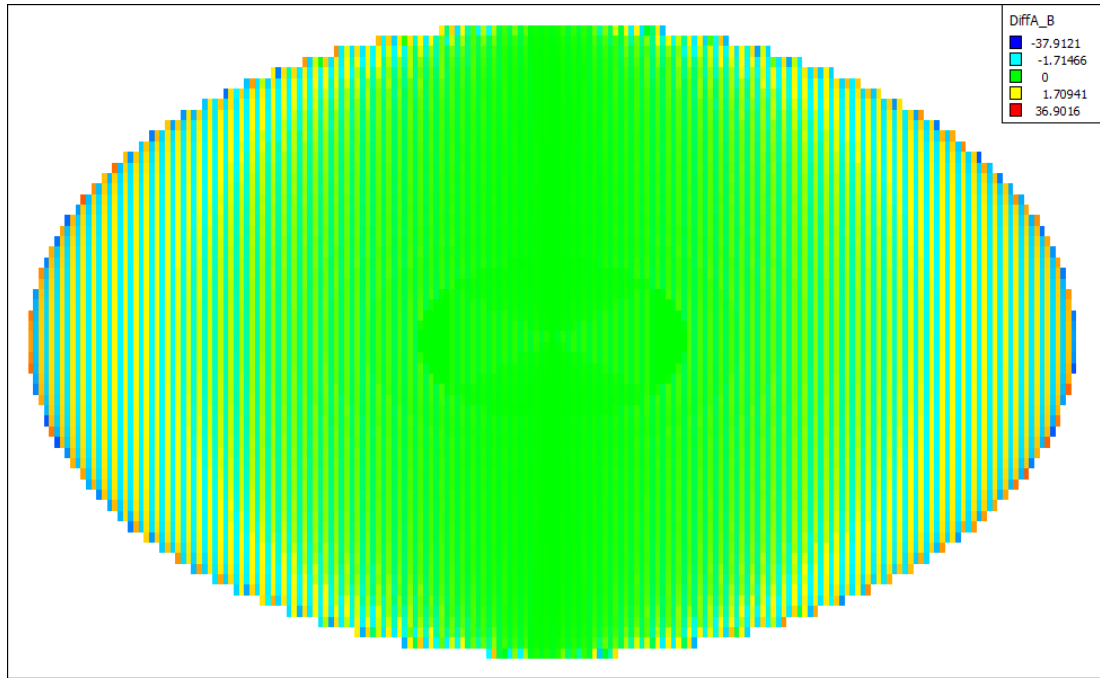
Figure 37 Difference between LR grid DEM A and LR grid DEM B
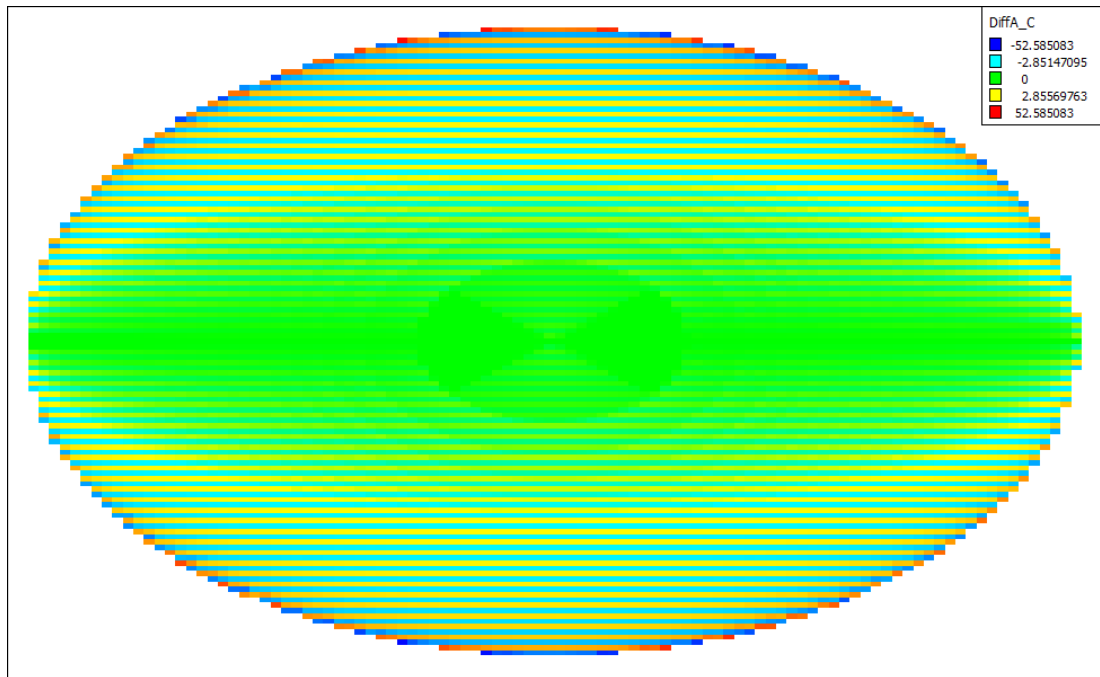
Figure 38 Difference between LR grid DEM A and LR grid DEM C
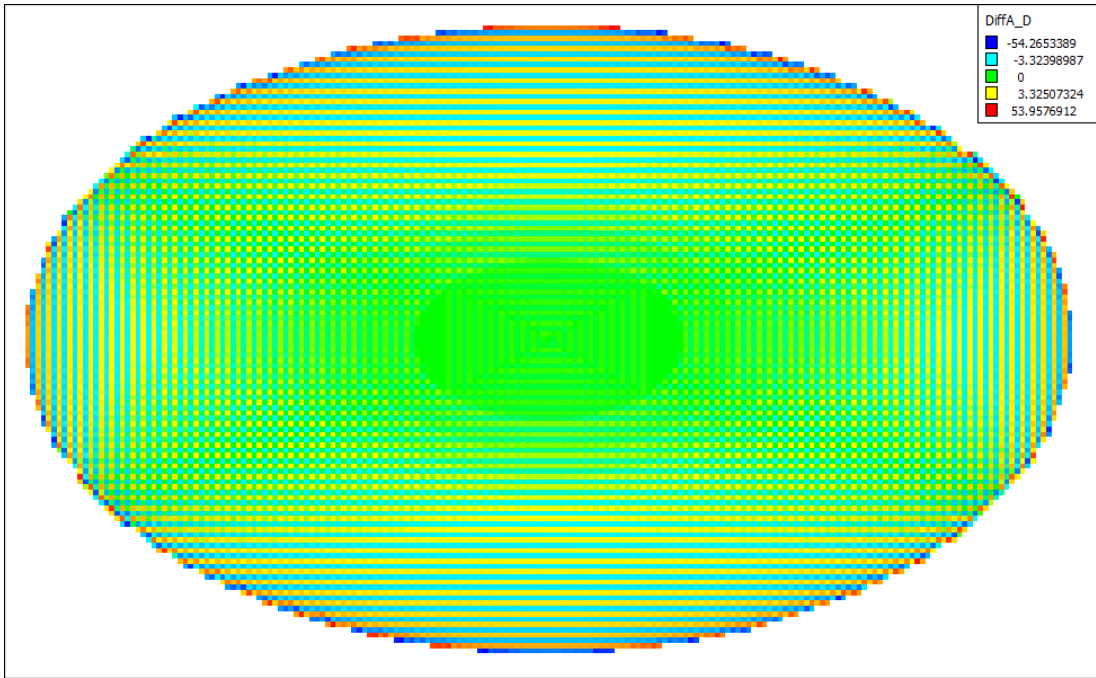
Figure 39 Difference between LR grid DEM A and LR grid DEM D
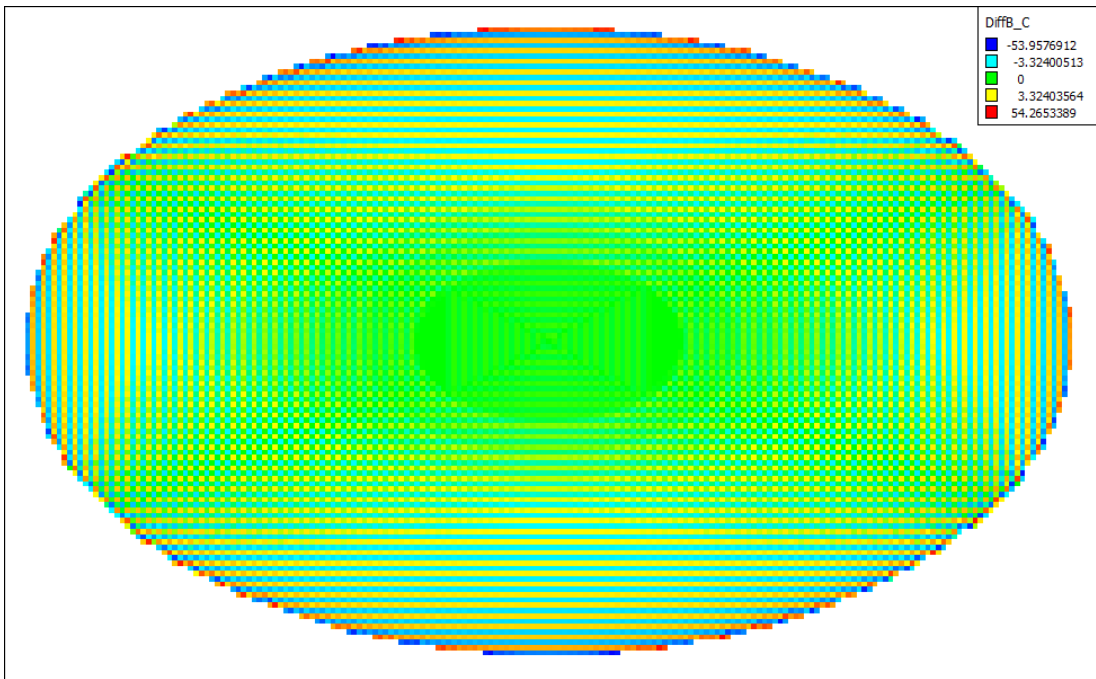
Figure 40 Difference between LR grid DEM B and LR grid DEM C
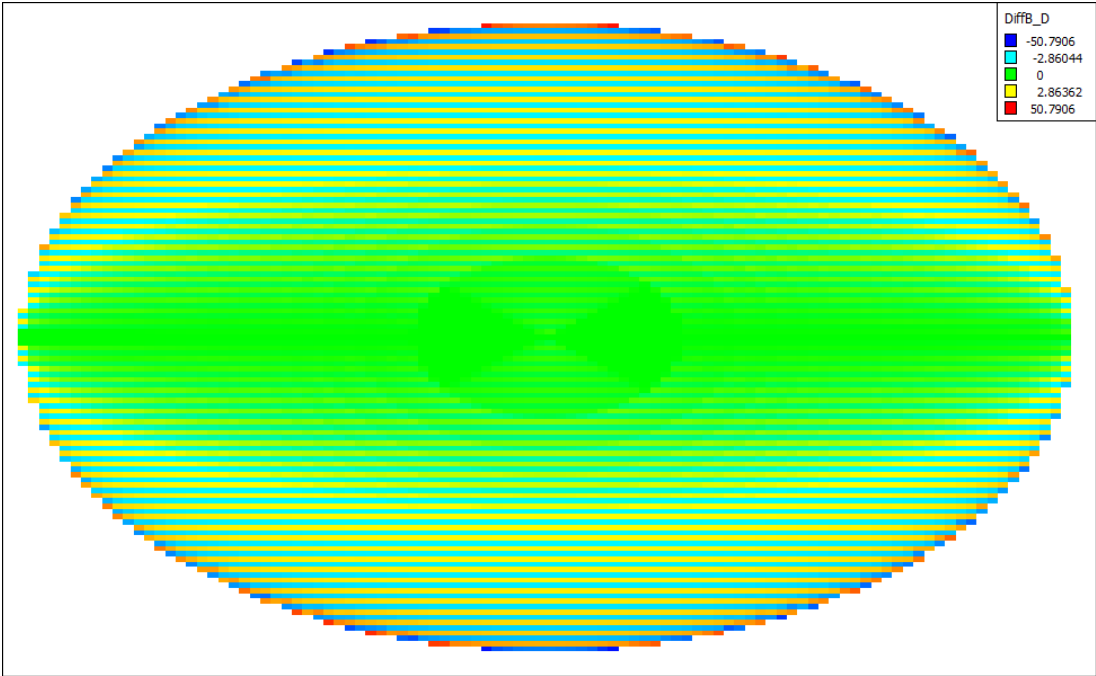
Figure 41 Difference between LR grid DEM B and LR grid DEM D
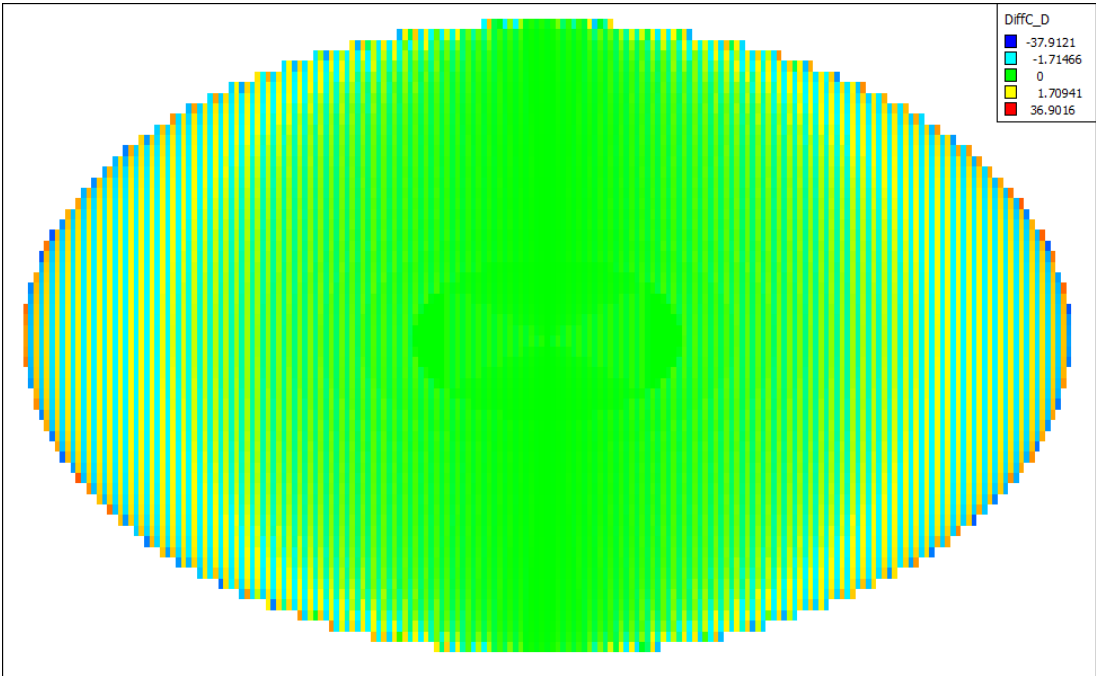
Figure 42 Difference between LR grid DEM C and LR grid DEM D

As seen from the last six figures, LR grid DEMs are not the same. However, these figures give only a visual implementation. Therefore; the similarity measures for these four LR grid DEMs are given below.

As seen from Tables 2 to 4, the difference has at least 4.5 m root mean square difference (RMSD), and 2.8 m mean absolute difference (MAD). If the LR grid DEMs were identical, the values of lower triangle of these tables would be all 0. As it is seen in the tables, they are not so.

Table 2 Squares of Intensity Differences for LR grid DEMs on ellipsoidal area

SSD	A	B	C	D
A	0			
B	20.68373	0		
C	50.24467	64.53812	0	
D	64.53802	49.36357	20.68381	0

Table 3 Root Mean Squares of Differences for LR grid DEMs on ellipsoidal area

RMSD	A	B	C	D
A	0			
B	4.547936	0		
C	7.088348	8.033562	0	
D	8.033556	7.025922	4.547946	0

Table 4 Mean Absolute Difference for LR grid DEMs on ellipsoidal area

MAD	A	B	C	D
A	0			
B	2.767929	0		
C	4.495399	5.174171	0	
D	5.174162	4.479199	2.767935	0

As stated earlier, difference over a neighborhood (DON) measure shows whether the second image is a shifted copy. As seen from Tables 5 to 7 the DEM pairs used for calculating this metric, are not shifted copies. The minimum metric values are 2.2, 3.1, and 3.9 for kernel sizes of 3x3, 5x5, and 7x7 respectively.

Table 5 Difference over a Neighborhood with Kernel 3x3 for LR grid DEMs on ellipsoidal area

DON 3	A	B	C	D
A	0			
B	2.226094	0		
C	2.235083	2.207495	0	
D	2.201498	2.234430	2.223771	0

Table 6 Difference over a Neighborhood with Kernel 5x5 for LR grid DEMs on ellipsoidal area

DON 5	A	B	C	D
A	0			
B	3.194854	0		
C	3.254507	3.126568	0	
D	3.123148	3.257988	3.193768	0

Table 7 Difference over a Neighborhood with Kernel 7x7 for LR grid DEMs on ellipsoidal area

DON 7	A	B	C	D
A	0			
B	4.155471	0		
C	4.051431	3.893235	0	
D	3.893532	4.059968	4.154681	0

The metrics based on the correlation does not give concrete results as the pixel-based difference based metrics do. According to the correlation coefficient (CC) metric results given in Table 8, all four LR grid DEMs seem to be identical, since their CC metric values are 1. However, structural content (SC) (Table 9), normalized cross-correlation (NCC) (Table 10) and Czenakowski distance (CD) (Table 11) metrics results indicate that there are minor differences among the LR grid DEMs. If the grid DEM pairs were identical then SC and NCC would result 1 and CD would results 0. The reason for the weak results in correlation based metrics is the usage of mean intensity value. The detailed explanation for these is given in discussion section.

Table 8 Correlation Coefficient for LR grid DEMs on ellipsoidal area

CC	A	B	C	D
A	0			
B	1.000002	0		
C	1	1.000002	0	
D	1.000002	1	1.000002	0

Table 9 Structural Content for LR grid DEMs on ellipsoidal area

SC	A	B	C	D
A	0			
B	0.999992	0		
C	0.999998	1.000006	0	
D	0.999991	0.999999	0.999993	0

Table 10 Normalized Cross-Correlation for LR grid DEMs on ellipsoidal area

NCC	A	B	C	D
A	0	1.006103	1.009976	1.011509
B	1.006111	0	1.011513	1.009971
C	1.009978	1.011507	0	1.006106
D	1.011518	1.009972	1.006113	0

Table 11 Czenakowski Distance for LR grid DEMs on ellipsoidal area

CD	A	B	C	D
A	0			
B	-0.0052	0		
C	-0.00869	-0.01006	0	
D	-0.01006	-0.00869	-0.00521	0

Table 12 shows the results of ratio image uniformity (RIU) measure for six LR grid DEM pairs. If the LR grid DEM pair is identical, then the measure results as 0. However, the minimum value in Table 12 is 1.01. This shows that the LR grid DEM pairs are not uniform as DEM ratio, which results that there is a difference in LR grid DEM pairs. Although there is no fixed value for totally different grid DEMs, these values state that there is a difference between the grid DEM pairs.

Table 12 Ratio Image Uniformity for LR grid DEMs on ellipsoidal area

RIU	A	B	C	D
A	0			
B	1.011704	0		
C	1.064333	1.064285	0	
D	1.021309	1.019418	1.011705	0

As can be recalled from the previous subsection, partitioned intensity uniformity (PIU) has not a fixed value for identical pairs. In order to see the difference, the identical values (i.e. LR grid DEM A – LR grid DEM A) are calculated and inserted on the diagonal of Table 13. The results show that the LR grid DEM pairs differ from each other. For example PIU_{CC} is 0.001816 and PIU_{CD} is 0.033439 and PIU_{DC} is 0.034380.

Table 13 Partitioned Intensity Uniformity for LR grid DEMs on ellipsoidal area

PIU	A	B	C	D
A	0.001816	0.034380	0.048344	0.056460
B	0.033438	0.001826	0.055845	0.048088
C	0.048344	0.056460	0.001816	0.034380
D	0.055845	0.048088	0.033439	0.001827

Joint probability distribution function (JPDF), joint entropy (JE), mutual information (MI), normalized mutual information (NMI), redundancy (RD), and symmetrical uncertainty (SU) are the measures that use histogram. As stated in section 0, the user is free to adjust the boundaries and the interval of the histogram. The mentioned measures are calculated on a histogram, whose minimum value is 0 and maximum value is 300 and the interval is 1 m.

As can be seen from Figure 43, there is dispersion at the upper left part and thickness in the middle part of the joint probability distribution function (JPDF). The identical pair has a solid thin line for JPDF as can be seen in Figure 29. Dispersion and thickness suggest that the LR grid DEM pairs used for calculating JDPF have differences.

Joint entropy, mutual information, normalized mutual information, redundancy and symmetrical uncertainty are the measures formulated based on the information theory. Table 14 is formed by the joint entropies in the lower triangle and the entropies on the diagonal. As seen from the table, joint entropies are slightly bigger than the entropies which suggest that the LR grid DEM pairs together carry more and different information than the single LR grid DEM. The difference between the joint entropy and the entropy shows the amount of different information carried by the other LR grid DEM. If the LR grid DEM pairs are identical, the values of joint entropy would be the same with single entropy value.

Table 14 Joint Entropy for LR grid DEMs on ellipsoidal area

JE	A	B	C	D
A	7.905663			
B	10.49127	7.906331		
C	10.95474	11.25755	7.905287	
D	11.25755	10.95519	10.49041	7.905955

Mutual information shows how much one random variable tells us about the other. Zero value of mutual information shows that two random variables are independent, as the number increases, the level of dependency (or similarity) increases. For identical pairs the value reaches to single entropy. As expected, the mutual information values are neither zero nor they reached to single entropy values; mutual information (Table 15) and the normalized form of mutual information (Table 16) suggest that, there are differences between the LR grid DEM pairs.

Table 15 Mutual Information for LR grid DEMs on ellipsoidal area

MI	A	B	C	D
A	7.905663			
B	5.286603	7.906331		
C	4.802906	4.493312	7.905287	
D	4.493312	4.801705	5.28670	7.905955
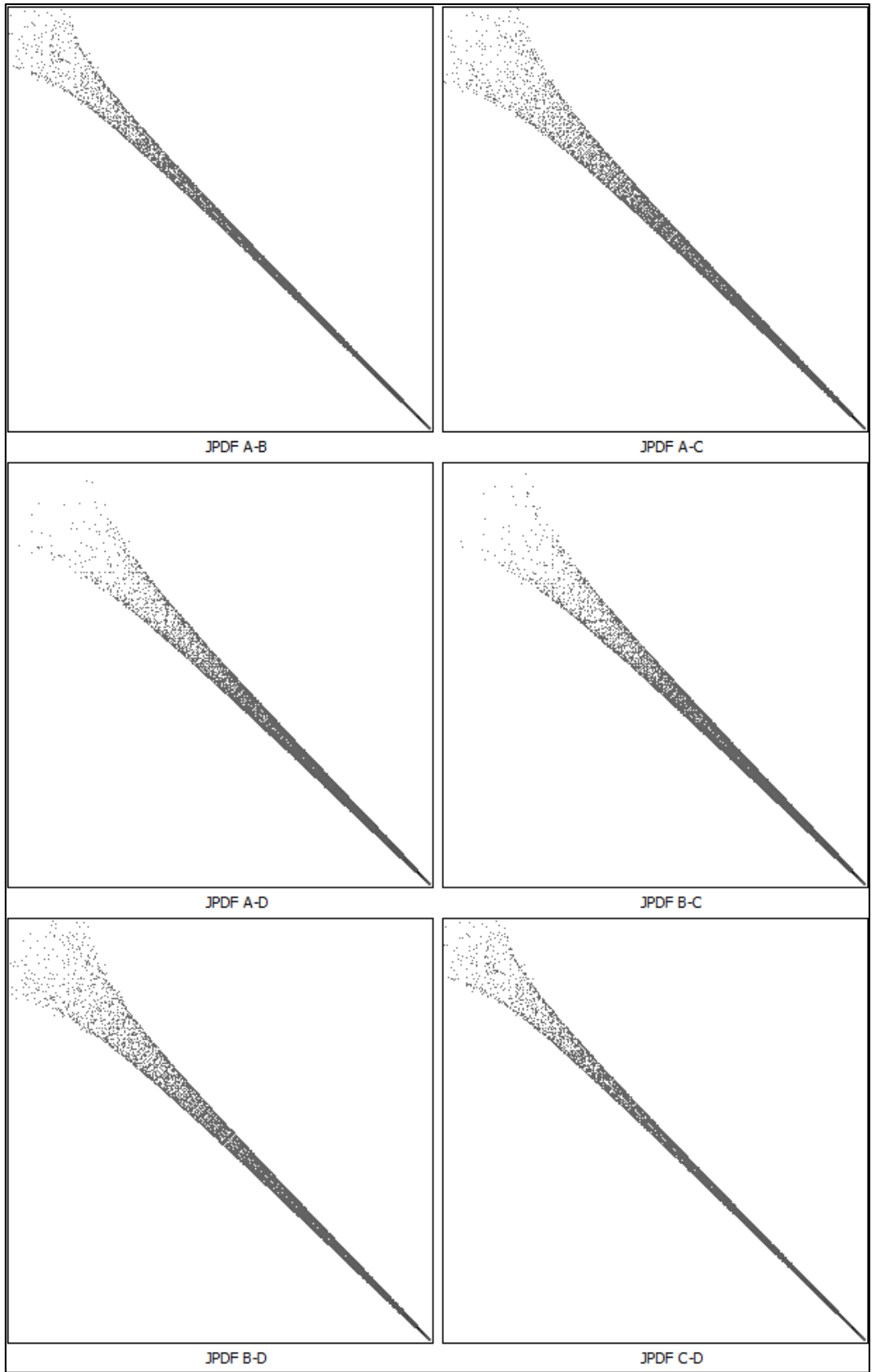
Figure 43 Joint Probability Distributions Function Graphs for LR grid DEMs on ellipsoidal area

NMI	A	B	C	D
A	0			
B	1.507094	0		
C	1.443332	1.404627	0	
D	1.404508	1.443395	1.507145	0

Definition of super resolution tells that high resolution (HR) image can be constructed from a set of low resolution (LR) images provided that the low resolution images contain non-redundant information of the same scene. Redundancy and symmetrical uncertainty measures show the redundancy level in LR grid DEM pairs. As can be remembered from the definition of the measures (Table 1), 0.5 value of redundancy measure and 1 value of symmetrical uncertainty show complete identical pairs. Deviation from these values shows that LR grid DEM pairs contain non-redundant information. Tables 17 and 18 declare that the LR grid DEM pairs which are used to create high resolution DEM, contains non-redundant information.

Table 17 Redundancy for LR grid DEMs on ellipsoidal area

RD	A	B	C	D
A	0			
B	0.334355	0		
C	0.303764	0.284159	0	
D	0.284183	0.303662	0.334377	0

Table 18 Symmetrical Uncertainty for LR grid DEMs on ellipsoidal area

SU	A	B	C	D
A	0			
B	0.668711	0		
C	0.607527	0.568318	0	
D	0.568366	0.607324	0.668755	0

In this section 16 measures are presented for four LR grid DEMs on synthetic surface. 15 of the measures result that these six pairs are different from each other and contain non-redundant information of the same surface.

4.4   Similarity Measures Application on METU area

Low resolution DEM for synthetic surface is constructed by forming four 10 m LR grid DEMs named LR_A, LR_B, LR_C, and LR_D. In order not to repeat the same things for the actual area, only one LR grid DEM (LR_A) is shown in Figure 44. Also the difference DEMs calculated by subtracting each grid DEM from each other are obtained and three of the difference DEMs are shown in Figures 45 to 47.

The measures on LR grid DEMs constructed on METU area are presented below. The first three difference-based measures suggest that there is a slight difference between the LR grid DEM pairs. The squares of intensity difference, root mean square of difference and mean absolute intensity difference results can be seen in Tables 19 to 21 respectively.
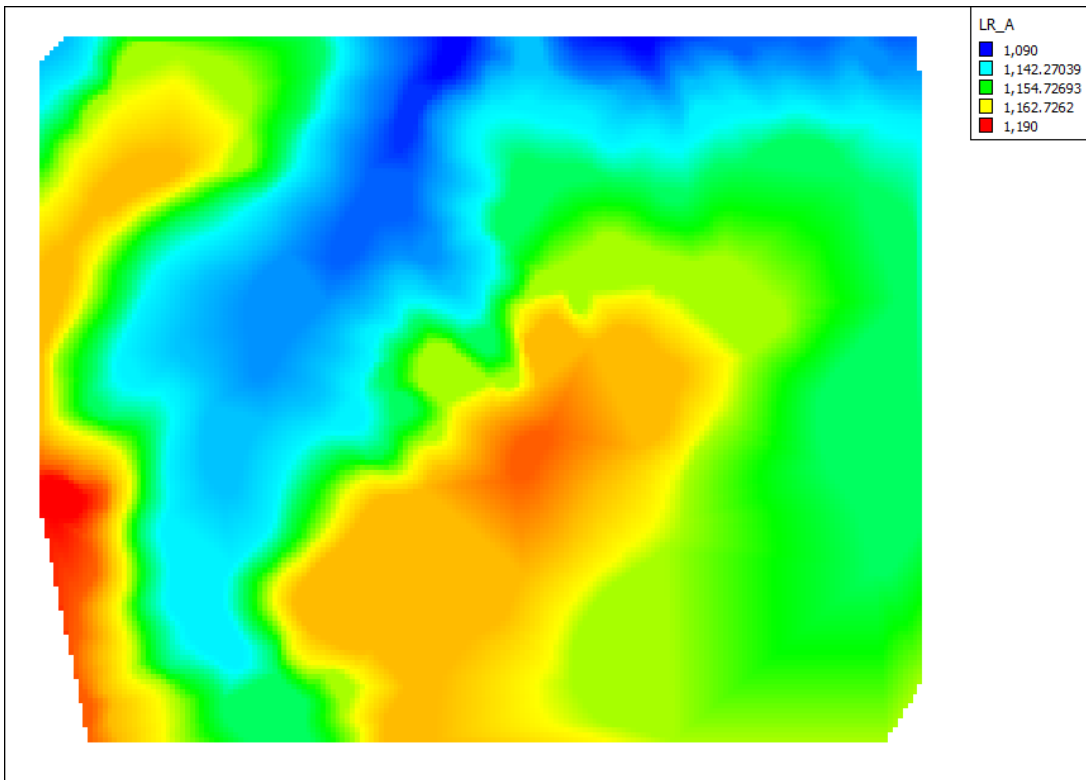
Figure 44 One of LR grid DEMs on METU Area (LR grid DEM A)
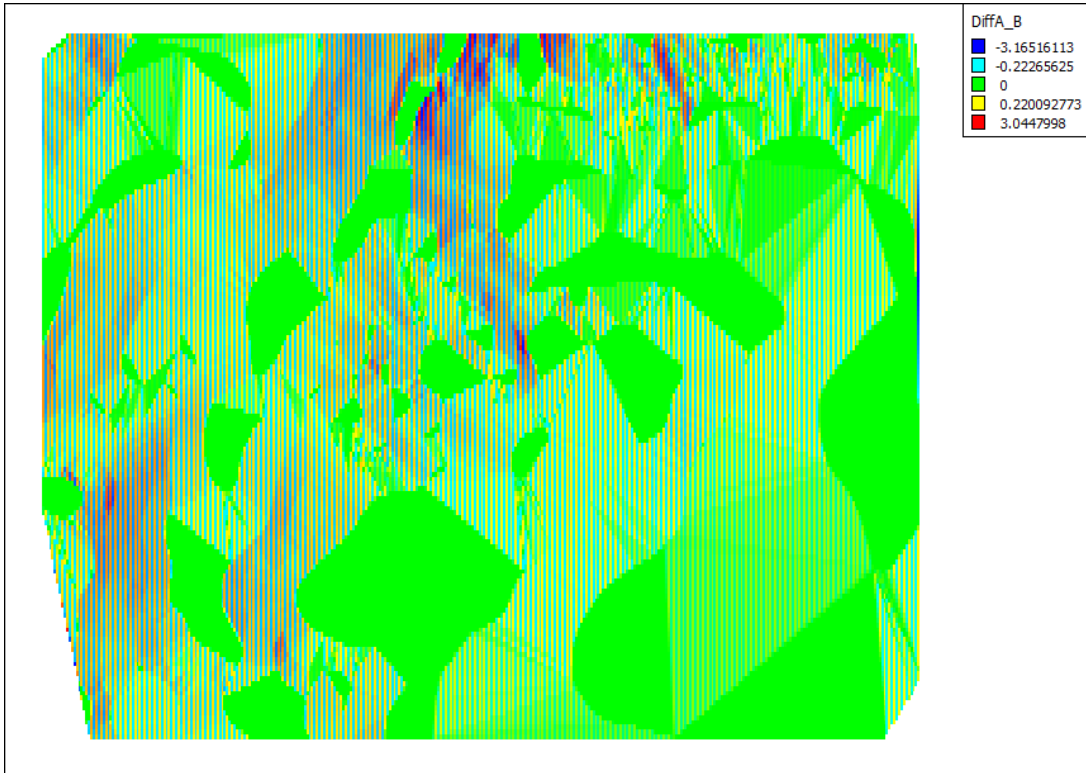
Figure 45 Difference between LR grid DEM A and LR grid DEM B for LR grid DEMs on METU area
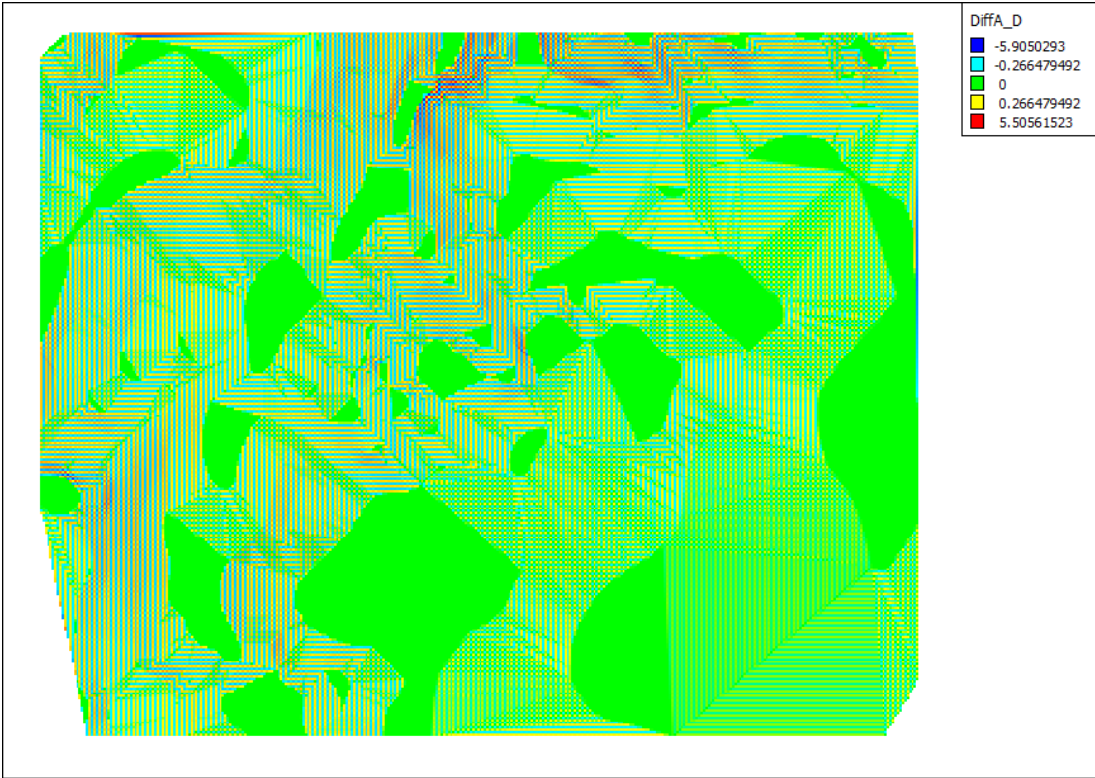
Figure 46 Difference between LR grid DEM A and LR grid DEM D for LR grid DEMs on METU area
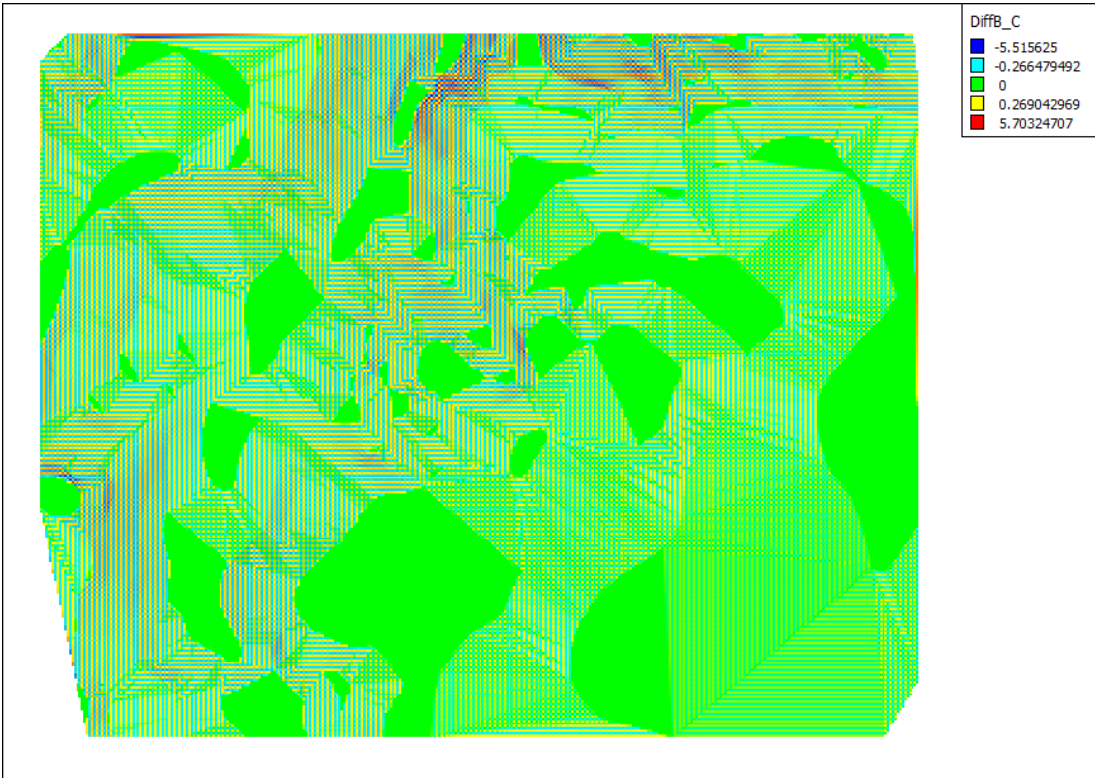
Figure 47 Difference between LR grid DEM B and LR grid DEM C for LR grid DEMs on METU area

55

Table 19 Squares of Intensity Difference for LR grid DEMs on METU area

SSD	A	B	C	D
A	0			
B	0.301158	0		
C	0.241716	0.538624	0	
D	0.538323	0.242006	0.303203	0

Table 20 Root Mean Squares of Difference for LR grid DEMs on METU area

RMSD	A	B	C	D
A	0			
B	0.548778	0		
C	0.491646	0.73391	0	
D	0.733705	0.491941	0.550639	0

Table 21 Mean Absolute Intensity Difference for LR grid DEMs on METU area

MAD	A	B	C	D
A	0			
B	0.359852	0		
C	0.307376	0.473178	0	
D	0.473017	0.307603	0.361055	0

Intensity difference over a neighborhood measure results can be seen in Tables 22, 23 and 24 for kernel sizes 3x3, 5x5 and 7x7 respectively. The results show that there is no case of shifted identical LR grid DEMs.

Table 22 Intensity Difference over a Neighborhood with Kernel Size 3 x 3 for LR grid DEMs on METU area

DON 3	A	B	C	D
A	0			
B	2.01658	0		
C	1.99569	1.916005	0	
D	1.91227	1.995883	2.019643	0

Table 23 Intensity Difference over a Neighborhood with Kernel Size 5 x 5 for LR grid DEMs on METU area

DON 5	A	B	C	D
A	0			
B	2.88579	0		
C	2.868895	2.782491	0	
D	2.780489	2.867882	2.883023	0

Table 24 Intensity Difference Over a Neighborhood with Kernel Size 7 x 7 for LR grid DEMs on METU area

DON 7	A	B	C	D
A	0			
B	3.746922	0		
C	3.626035	3.608697	0	
D	3.608240	3.627339	3.743581	0

Correlation-based measures; correlation coefficient (CC), structural content (SC), normalized cross-correlation (NCC), and Czenakowski distance (CD) results can be seen in Tables 25, 26, 27, and 28 respectively. Non-surprisingly they do not show the level of difference very explicitly, however NCC and CD suggest a little higher difference than the other two measures.

Table 25 Correlation Coefficient for LR grid DEMs on METU area

CC	A	B	C	D
A	0			
B	1	0		
C	1.000006	1.000006	0	
D	1.000006	0.999994	1	0

Table 26 Structural Content for LR grid DEMs on METU area

SC	A	B	C	D
A	0			
B	1.000018	0		
C	1.000229	1.000211	0	
D	1.000263	1.000245	1.000034	0

Table 27 Normalized Cross-Correlation for LR grid DEMs on METU area

NCC	A	B	C	D
A	0	0.999976	1.000164	1.000157
B	0.999958	0	1.000126	1.000173
C	0.999936	0.999916	0	0.999978
D	0.999895	0.999928	0.999944	0

Table 28 Czenakowski Distance for LR grid DEMs on METU area

CD	A	B	C	D
A	0			
B	-0.00261	0		
C	-0.00339	-0.00584	0	
D	-0.00585	-0.00338	-0.00261	0

Ratio image uniformity suggests very tiny difference between the LR grid DEM pairs as seen in Table 29. Surprisingly partitioned intensity uniformity declares that the differences between the LR grid DEM pairs are slightly higher as seen in Table 30.

Table 29 Ratio Image Uniformity for LR grid DEMs on METU area

RIU	A	B	C	D
A	0			
B	1.000002	0		
C	0.999998	0.999995	0	
D	1	0.999998	1.000001	0

Table 30 Partitioned Intensity Uniformity for LR grid DEMs on METU area

PIU	A	B	C	D
A	0.000115	0.000450	0.000397	0.000590
B	0.000449	0.000115	0.000588	0.000397
C	0.000397	0.000589	0.000115	0.000451
D	0.000588	0.000397	0.000450	0.000115

The highest elevation in METU area data set is 1190 m and the lowest is 1090 m. In order to see the histogram in detail, the interval was set to 0.5 m. Joint probability distribution function (JPDF), joint entropy (JE), mutual information (MI), normalized mutual information (NMI), redundancy (RD), and symmetrical uncertainty (SU) measures are calculated with these histogram parameters.

As seen from joint probability distribution function graphs (Figure 48); the lines are thicker in the middle, which suggest that there are differences between the LR grid DEM pairs.
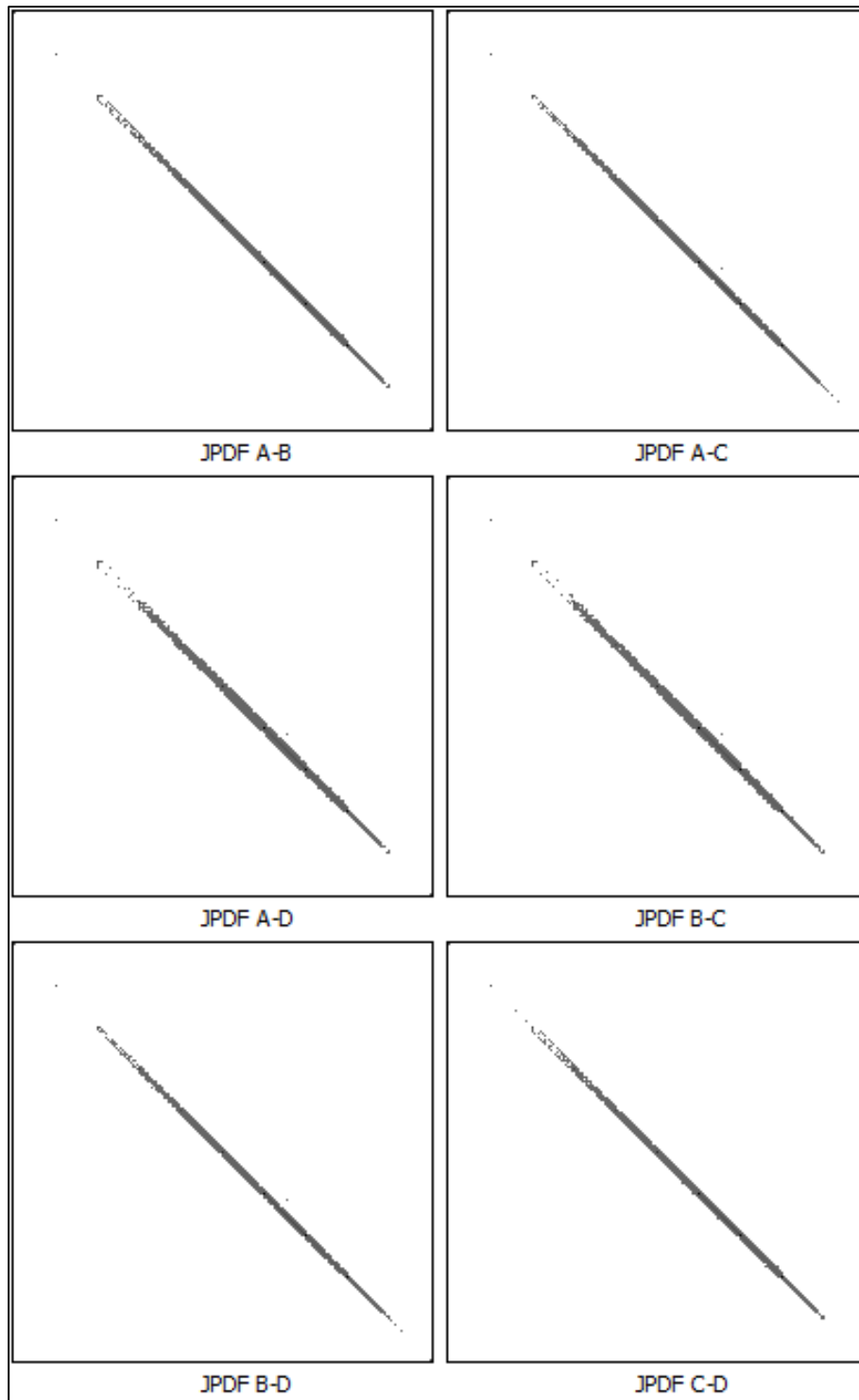
Figure 48 Joint Probability Distributions Function Graphs for LR grid DEMs on METU area

Information based measures, joint entropy (JE) and mutual information (MI) results can be seen in Tables 31 and 32 respectively. Joint entropy and mutual information measure results suggest that there are differences in LR grid DEM pairs. The difference between lower triangle values and the diagonal values in both tables confirm this statement.

Table 31 Joint Entropy for LR grid DEMs on METU area

JE	A	B	C	D
A	6.568402			
B	8.387125	6.568377		
C	8.219501	8.675389	6.577515	
D	8.674484	8.217096	8.397492	6.576802

Table 32 Mutual Information for LR grid DEMs on METU area

MI	A	B	C	D
A	6.568402			
B	4.745891	6.568377		
C	4.921193	4.462503	6.577515	
D	4.462416	4.92302	4.753247	6.576802

Normalized mutual information (NMI) measure results can be seen in Table 33. The lower triangle values of the table differ from the value for identical LR grid DEM pairs. This result helps to make the statement that NMI suggest that the LR grid DEM pairs are different from each other.

Table 33 Normalized Mutual Information for LR grid DEMs on METU area

NMI	A	B	C	D
A	0			
B	1.566306	0		
C	1.598248	1.514255	0	
D	1.514419	1.59871	1.566543	0

Redundancy (RD) and symmetrical uncertainty (SU) measure results can be seen in Tables 34 and 35 respectively. Both of them suggest that, LR grid DEMs are different from each other and they contain non-redundant information which is the preliminary condition for super resolution.

Table 34 Redundancy for LR grid DEMs on METU area

RD	A	B	C	D
A	0			
B	0.361267	0		
C	0.374611	0.339696	0	
D	0.339688	0.374752	0.361325	0

Table 35 Symmetrical Uncertainty for LR grid DEMs on METU area

SU	A	B	C	D
A	0			
B	0.722534	0		
C	0.749222	0.679392	0	
D	0.679376	0.749503	0.722651	0

On METU area, four low resolution DEMs are created which are used as inputs for 16 measures of similarity and redundancy. 14 of the measures result that these 6 pairs are different from each other and contain non-redundant information of the same surface.

CHAPTER 5

EFFECTS OF SUPER RESOLUTION ON DEM

In previous section, it is shown that, even the single source low resolution grid DEMs carry non-redundant information which is the preliminary condition of super resolution. In this section, it is explained that multi-frame super resolution (SR) helps to enhance spatial resolution of grid DEM. This explanation is made by using geometrical surfaces, METU area and SRTM and ASTER data sets as expressed in chapter 2. SRTM and ASTER dataset applications are also tested through real land data.

5.1 Effect of SR on Geometrical Surfaces

The effect of super resolution is investigated on geometrical surfaces from two different points of view. The first one is the level of enhancement on spatial resolution on the same source data set. The second one is the comparison of different scaled data sets. Both comparisons are made on two geometrical surfaces and the results are interpreted on the similarity measures as explained in previous chapter.

5.1.1 Effect of SR on Ellipsoid

Ellipsoid data set had been extracted from equation 1. Contour lines extracted for this equation have minimum value 1 m and maximum value 300 m. The first data set which represents 1/25000 scaled map, is the data set with 10 m contour interval (Figure 5). The second data set with 1 m contour intervals represents 1/5000 scaled map. Two comparisons are made on these data sets with 10 m grid size and 5 m grid size.

5.1.1.1 10 m grid size Ellipsoid

Low resolution grid DEMs which have a grid size of 20 m, are prepared using the first dataset. LR grid DEMs are arranged in such a way that, there is a distance of 10 m between grid centers for any of them. Then super resolution algorithm applied on these LR grid DEMs to obtain 10 m grid sized grid DEM. The control set also obtained from the first data set with 10 m grid sized grid DEM. In order to control the effect of multi-frame super resolution with single frame resolution, bi-cubic interpolation is applied on 20 m grid sized LR grid DEM. The algorithm of the data set creation is given in Figure 49. The control data is 10 m TIN grid DEM (TIN), the test subjects are SR 10 m grid DEM (SR), LR grid DEMs on HR grid projection (A, B, C, D) and Bi Cubic 10 m grid DEM (BC). The names given in parenthesis are the notations used in comparison reports. Boundaries of the control data and test grid DEMs are fixed and comparison program is applied.
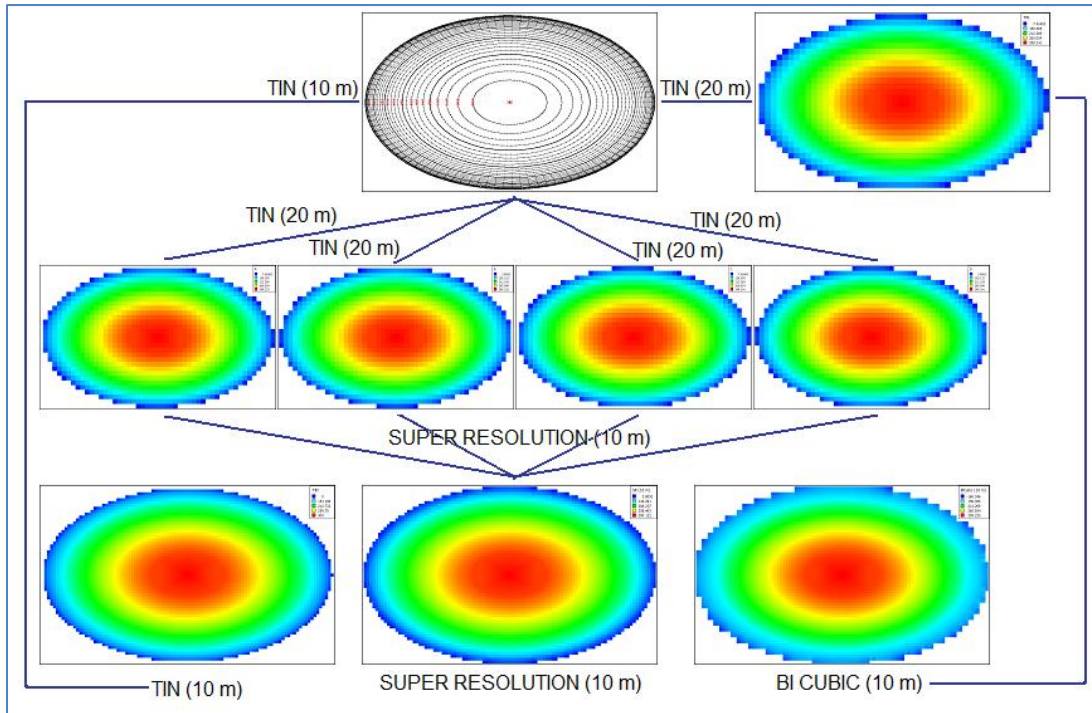
Figure 49 Super resolution test objects creation

Similarity reporting tool had been introduced in previous chapter. The same tool is applied on these grid DEMs and the comparison of test subjects with control data, give the level of enhancement in multi-frame super resolution. Example difference grid DEMs are presented in Figures 50, 51, and 52. The comparison results are given in Tables 36 and 37, the JPDF graphs are given in Figure 53.
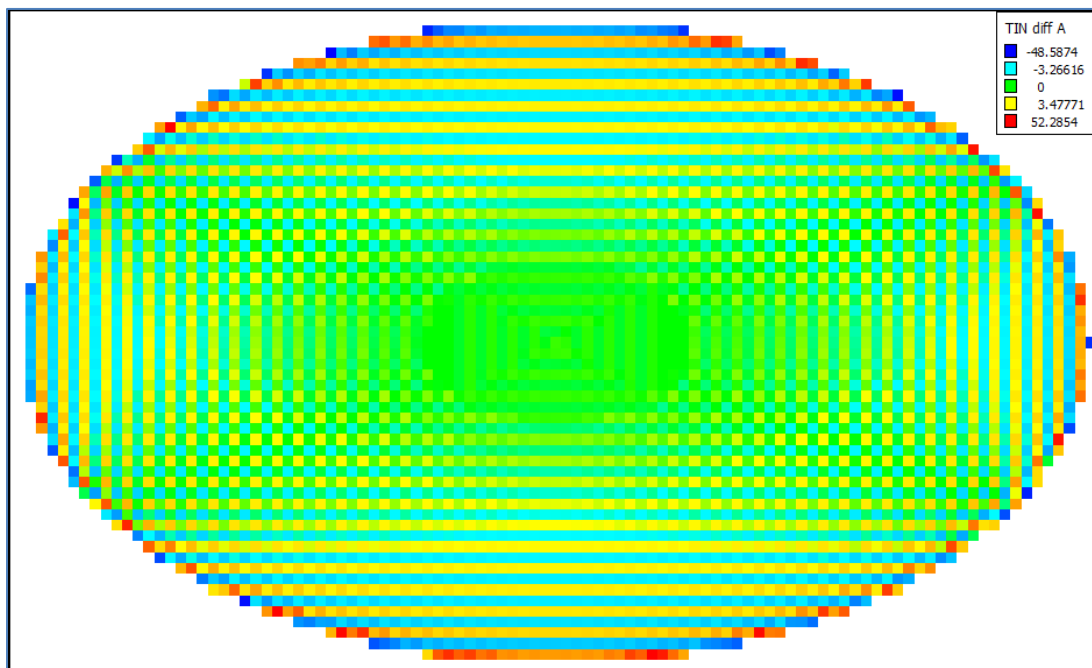
Figure 50 Difference between Ellipsoid TIN and A (10 m)

Figure 51 Difference between Ellipsoid TIN and BC (10 m)
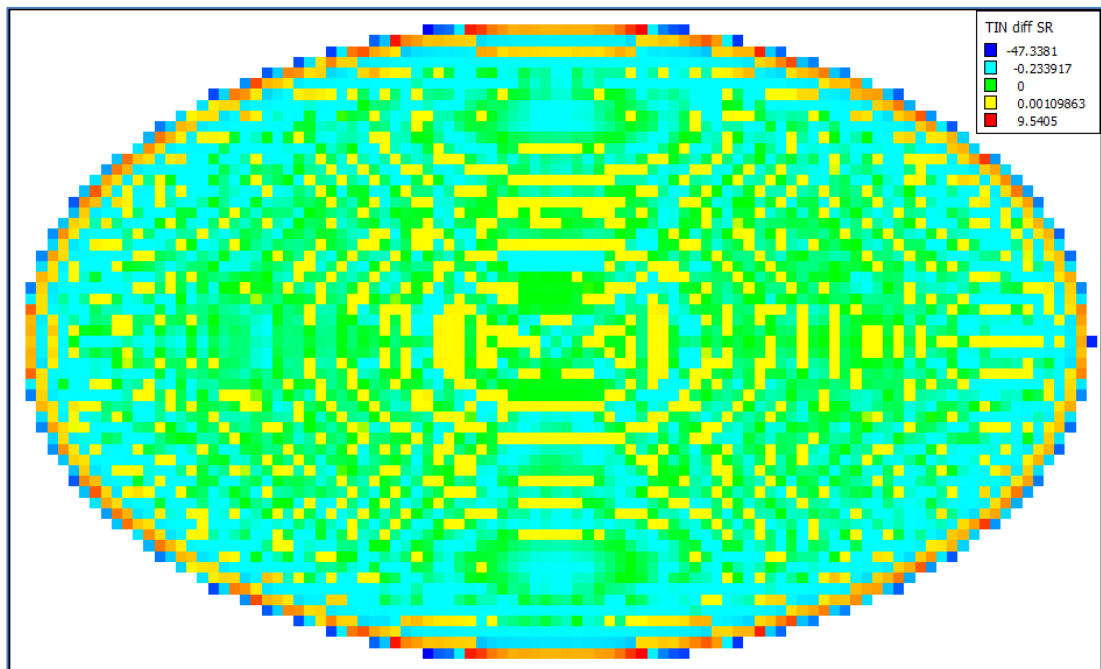
Figure 52 Difference between Ellipsoid TIN and SR (10 m)

Table 36 Comparison Result for Ellipsoid 10 m (Extends)

Grid Name	TIN	SR	A	B	C	D	BC
Grid Size	10	10	10	10	10	10	10
Dimensions	101 x 61	101 x 61	101 x 61	101 x 61	101 x 61	101 x 61	101 x 61
Min X	-500	-500	-500	-500	-500	-500	-500
Min Y	-300	-300	-300	-300	-300	-300	-300
Max X	500	500	500	500	500	500	500
Max Y	300	300	300	300	300	300	300
Min Z	0	3.809	7.455	3.809	7.455	3.809	-98.064
Max Z	300	300.122	299.232	299.232	299.240	299.240	299.234

Table 37 Comparison Result for Ellipsoid 10 m (Measures)

	SR	A	B	C	D	BC
SSD	13.445	60.389	60.977	60.390	60.977	16.071
RMSD	3.667	7.771	7.809	7.771	7.809	4.009
MAD	0.989	5.092	5.076	5.092	5.076	0.946
CC	1.000	1.000	1.000	1.000	1.000	1.000
MI	7.066	4.828	4.832	4.828	4.832	7.157
NMI	1.826	1.458	1.458	1.458	1.458	1.842
RD	0.453	0.309	0.310	0.309	0.310	0.459
SU	0.906	0.619	0.619	0.619	0.619	0.918
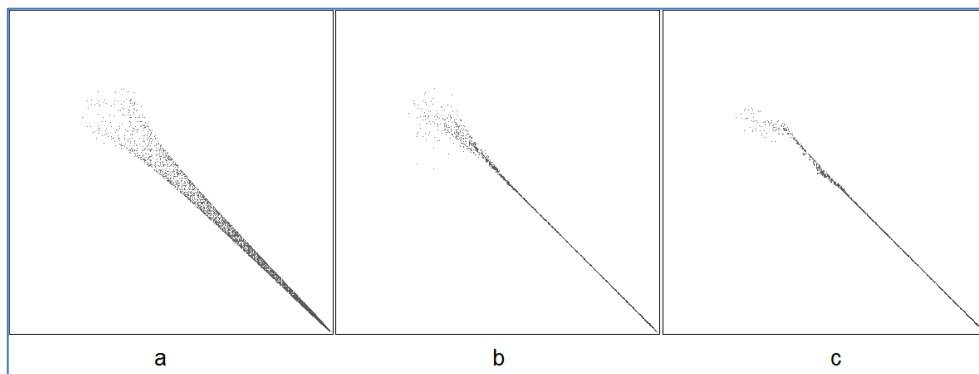
Figure 53 JPDF Graphs for Ellipsoid (10 m) a) TIN vs. A b) TIN vs. BC c) TIN vs. SR

Tables and figures show that multi-frame super resolution resulted in spatial resolution enhancement although LR grid DEMs have same source. It also shows good performance in finding the extreme values. RMSD value is only 3.7 m and symmetrical uncertainty is 0.9 which suggest that there is only a tiny difference between the 10 m super resolution grid DEM and the directly obtained 10 m grid DEM.

5.1.1.2 5 m grid size Ellipsoid

The above case is repeated with LR grid DEMs having a grid size of 10 m. The SR grid DEM has 5 m grid size. This time, control set which has 5 m grid size, obtained from the second data set which has contour interval of 5 m. The control data is 5 m TIN grid DEM (TIN), the test subjects are SR 5 m grid DEM (SR), LR grid DEMs on HR grid projection (A, B, C, D) and bi cubic 5 m grid DEM (BC). The difference grid DEMs are presented in Figures 54, 55, and 56. The comparison results are given in Tables 38 and 39, the JPDF graphs are given in Figure 57.

Table 38 Comparison Result for Ellipsoid 5 m (Extends)

Grid Name	TIN	SR	A	B	C	D	BC
Grid Size	5	5	5	5	5	5	5
Dimensions	201 x 121	201 x 121	201 x 121	201 x 121	201 x 121	201 x 121	201 x 121
Min X	-500	-500	-500	-500	-500	-500	-500
Min Y	300	300	300	300	300	300	300
Max X	500	500	500	500	500	500	500
Max Y	-300	-300	-300	-300	-300	-300	-300
Min Z	0.000	0.119	0.119	1.261	0.119	1.261	-81.596
Max Z	295.000	300.058	299.612	299.612	299.620	299.620	299.620
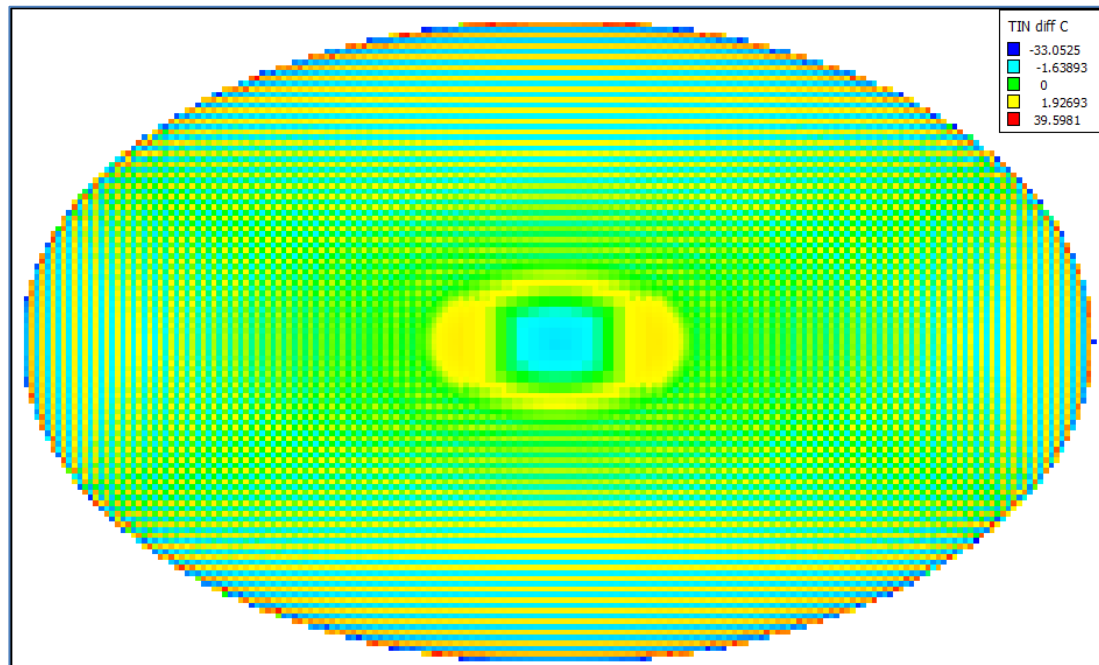
Figure 54 Difference between TIN and C (5 m)

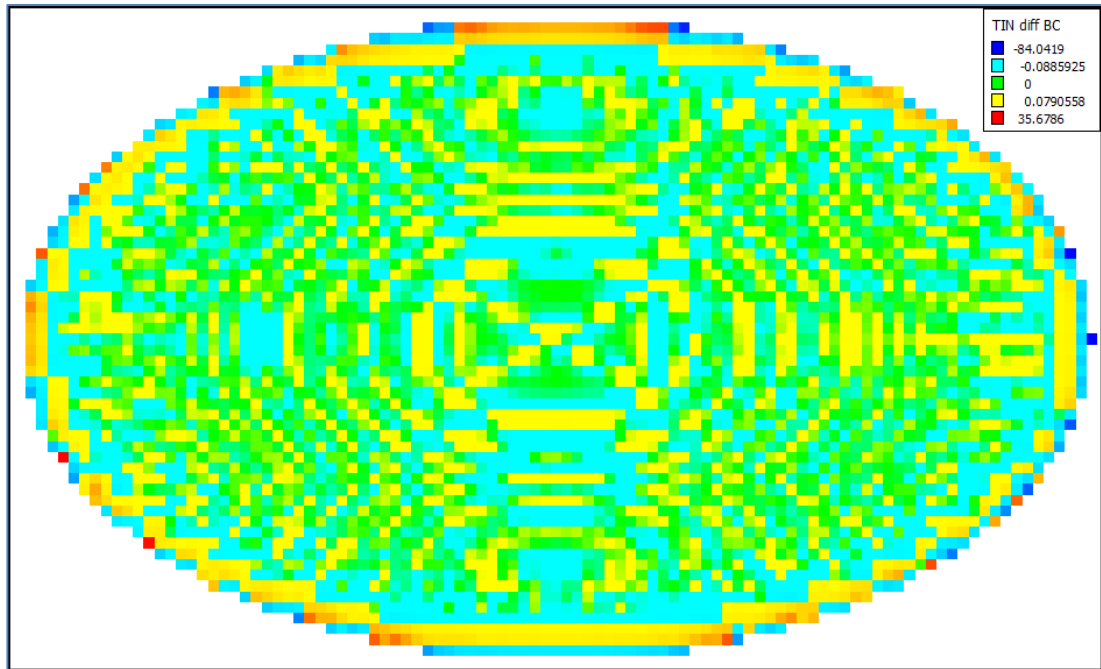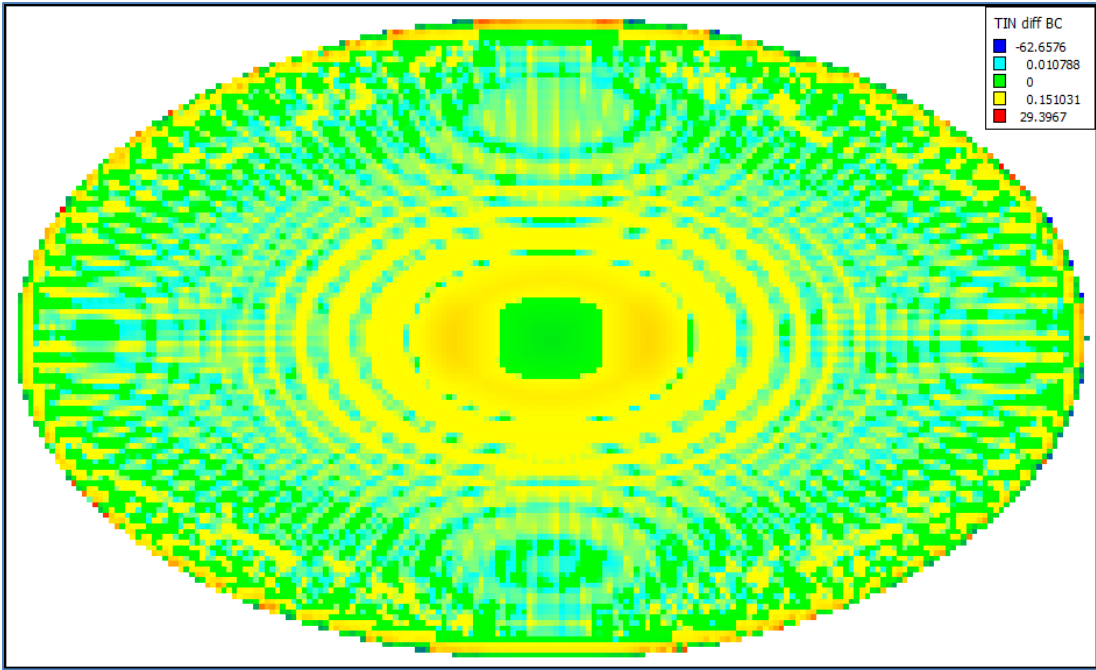**Figure 55 Difference between TIN and BC (5 m)**
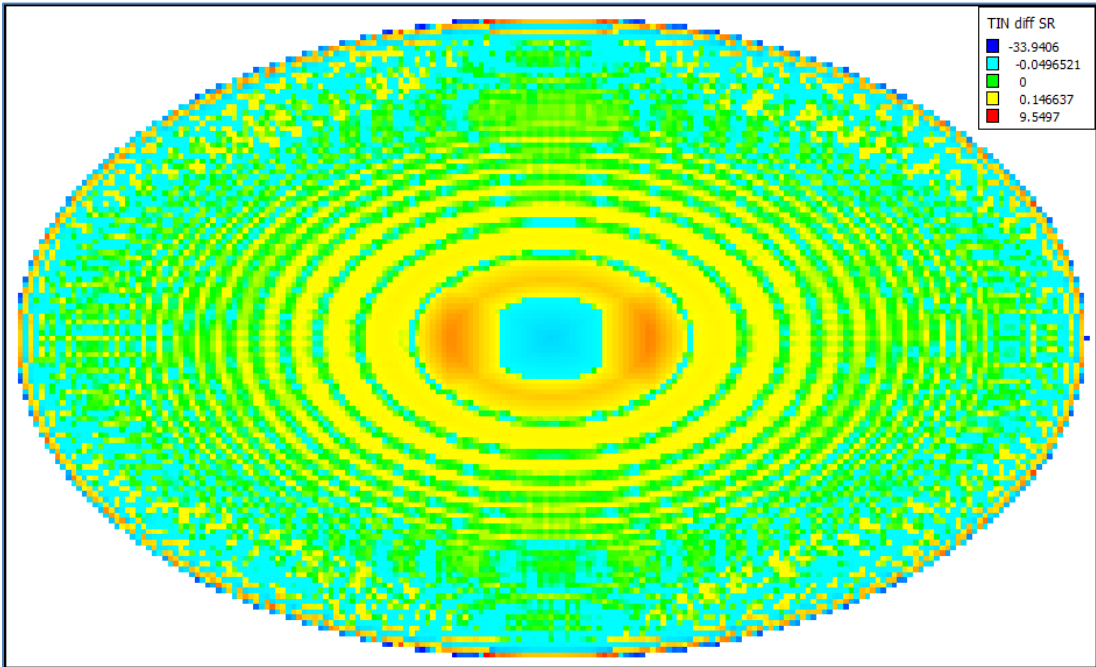
Figure 56 Difference between TIN and SR (5 m)

Table 39 Comparison Result for Ellipsoid 5 m (Measures)

	SR	A	B	C	D	BC
SSD	3.498	19.189	19.083	19.189	19.083	4.346
RMSD	1.870	4.381	4.368	4.381	4.368	2.085
MAD	0.511	2.774	2.774	2.774	2.774	0.514
CC	1.000	1.000	1.000	1.000	1.000	1.000
MI	7.321	5.280	5.276	5.280	5.276	7.338
NMI	1.821	1.477	1.475	1.477	1.475	1.825
RD	0.467	0.337	0.336	0.337	0.336	0.468
SU	0.934	0.673	0.673	0.673	0.673	0.936
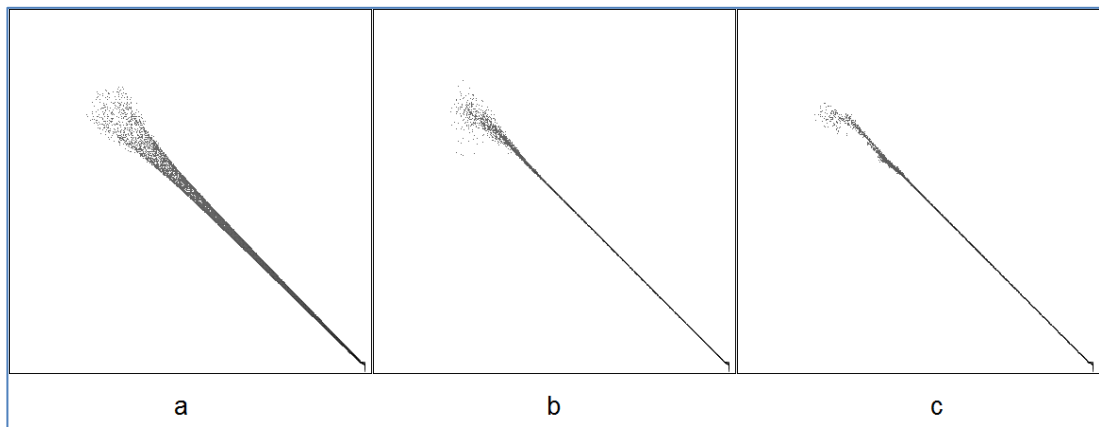
Figure 57 JPDF Graphs for Ellipsoid (5 m) a) TIN vs. C b) TIN vs. BC c) TIN vs. SR

In this case the control data is 5 m grid sized DEM obtained from contour values having a 5 m interval, which is denser than the previous one. Multi-frame super resolution 5 m grid sized DEM again showed a good performance in similarity measures and catching the extreme values. In most of the measures it exceeds the bi-cubic interpolation.

5.1.2 Effect of SR on Gaussian Surface

In ellipsoid surface, the slopes are in one direction. They are all convex. However, the effect of multi-frame super resolution must be tested through complex areas having different slope types. In order to employ complex slope types, Gaussian surface is used. Gaussian surfaces data set had been extracted from equation 2. Contour lines extracted for this equation have minimum value -30 m and maximum value 40 m. The first data set which represents 1/5000 scaled map, is the data set with 5 m contour intervals (Figure 7). The second data set with 1 m contour intervals represents 1/1000 scaled map. Two comparisons are made on these data sets with 5 m grid size and 2.5 m grid size.

5.1.2.1 5 m grid size Gaussian Surface

10 m grid sized LR grid DEMs, are prepared using the first dataset. Their grid centers have a distance of 5 m between each of them. Super resolution algorithm is applied on these LR grid DEMs to obtain 5 m grid sized grid DEM. 5 m grid sized control grid DEM is obtained from the first data set. Bi-cubic interpolation is applied on 10 m grid sized low resolution grid sized grid DEM. The comparison test is applied on the grid DEMs:

1. Control data: TIN grid DEM (TIN) 5m,

2. SR grid DEM (SR) 5 m,

3. Bi Cubic grid DEM (BC) 5 m,

4. -7. LR grid DEMs projected on high resolution grid (A, B, C, D) 5 m.

Boundaries of the control data and test grid DEMs are fixed and comparison program is applied. The comparison results are given in Tables 40 and 41. The difference grid DEMs are presented in Figures 58, 59, 60 and the JPDF graphs are given in Figure 61.

Table 40 Comparison Result for Gaussian Surface 5 m (Extends)

Grid Name	TIN	SR	A	B	C	D	BC
Grid Size	5	5	5	5	5	5	5
Dimensions	201 x 201	201 x 201	201 x 201	201 x 201	201 x 201	201 x 201	201 x 201
Min X	-500	-500	-500	-500	-500	-500	-500
Min Y	500	500	500	500	500	500	500
Max X	500	500	500	500	500	500	500
Max Y	-500	-500	-500	-500	-500	-500	-500
Min Z	-30	-30.511	-30	-30	-30	-30	-30.183
Max Z	40.274	40.395	40.186	40.170	40.193	40.187	40.241

Table 41 Comparison Result for Gaussian Surface 5 m (Measures)

	SR	A	B	C	D	BC
SSD	0.010	0.095	0.095	0.095	0.095	0.002
RMSD	0.098	0.308	0.308	0.308	0.309	0.046
MAD	0.064	0.220	0.220	0.221	0.221	0.019
CC	1.001	1.000	1.000	1.000	1.000	1.001
MI	6.157	5.171	5.165	5.159	5.160	6.796
NMI	1.741	1.556	1.552	1.554	1.553	1.888
RD	0.428	0.359	0.359	0.359	0.359	0.472
SU	0.856	0.719	0.718	0.717	0.717	0.945
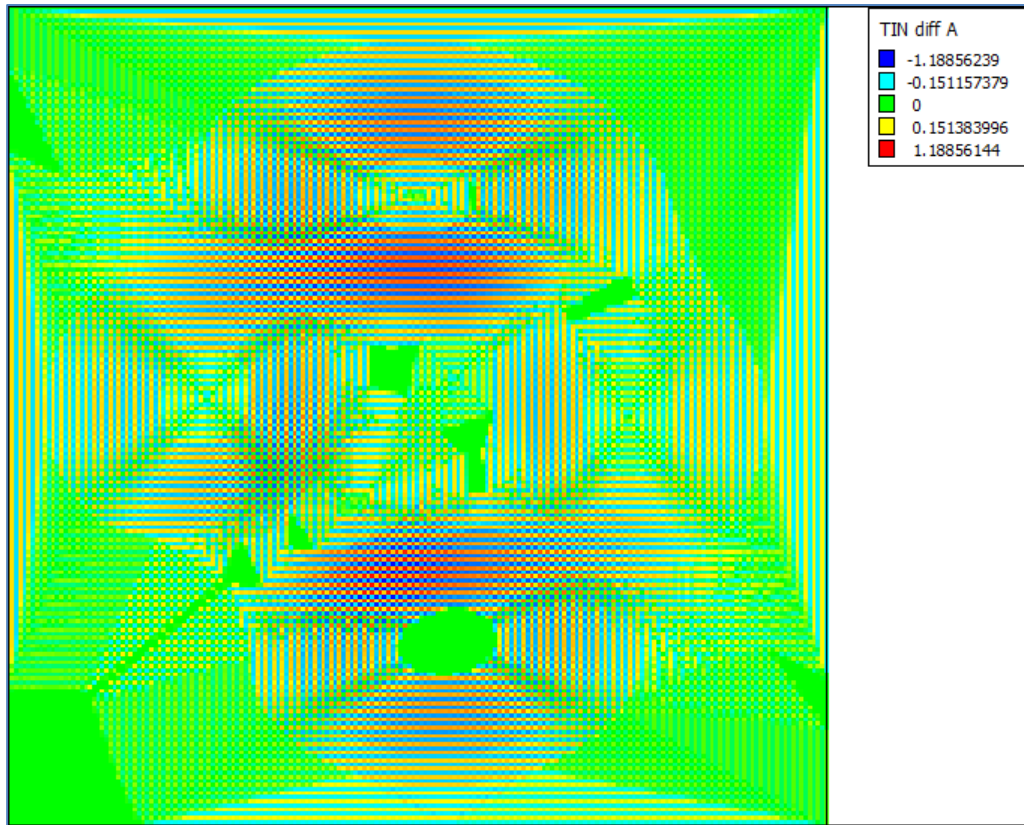
Figure 58 Difference between Gaussian TIN and A (5 m)
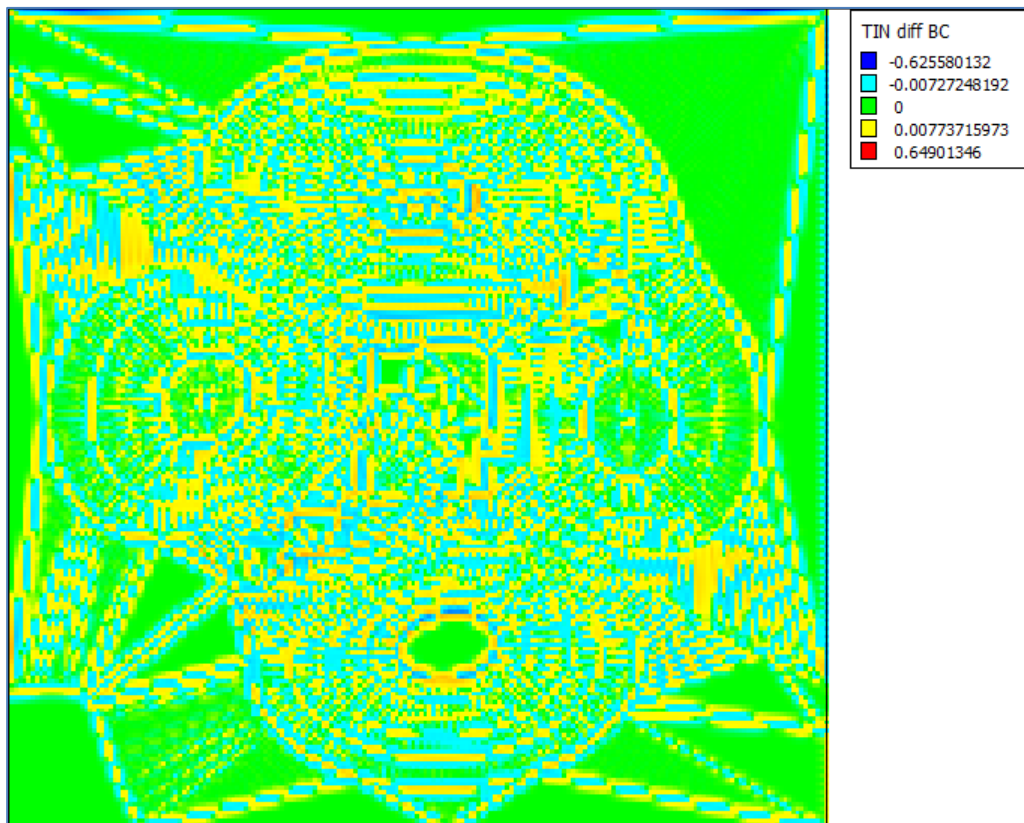
Figure 59 Difference between Gaussian TIN and BC (5 m)
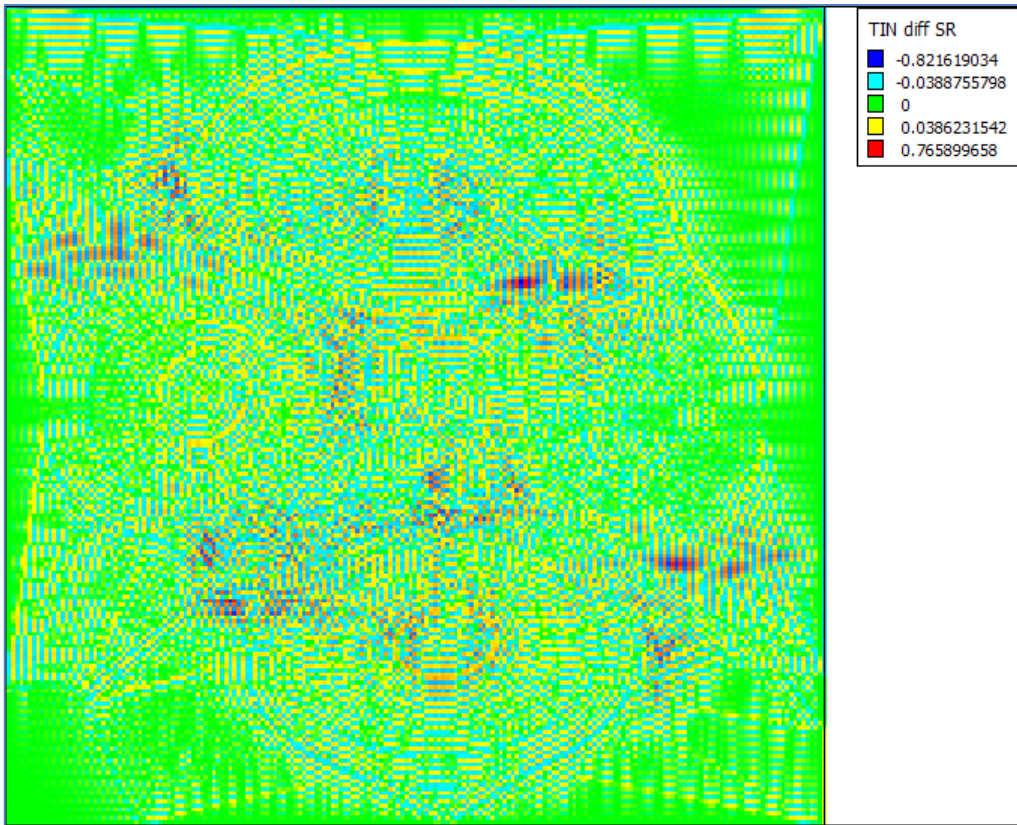
Figure 60 Difference between Gaussian TIN and SR (5 m)

The reason for selection of Gaussian surface is that it has complex slopes. The results on this surface, strengthens our idea about the enhancement by multi-frame super resolution. SR resulted 9.5 times smaller SSD than its parent LR grid DEMs, although they have the same source. Some of the similarity measures between the low resolution grid DEMs can be seen in Table 42. The histogram interval used in information based measures is 1 m. The minimum value is -30 and the maximum value is 40. As can be seen from the similarity measures that there is a difference between the low resolution grid DEMs, however the non-redundant information level is low.
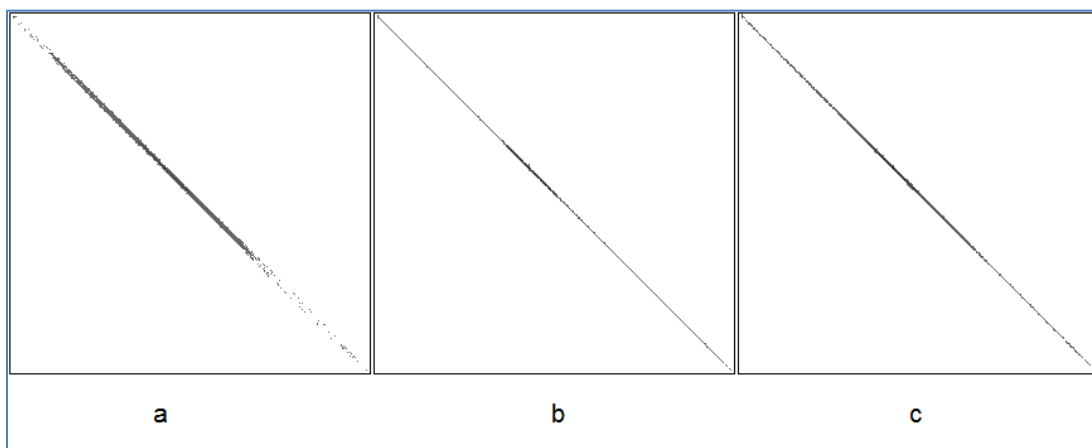
Figure 61 JPDF Graphs for Gaussian Surfaces (5 m) a) TIN vs. A b) TIN vs. BC c) TIN vs. SR

Table 42 Similarity measures of low resolution Gaussian Grid DEMs

SSD	A	B	C	D
A	0.000			
B	0.127	0.000		
C	0.252	0.385	0.000	
D	0.380	0.252	0.127	0.000

RMSD	A	B	C	D
A	0.000			
B	0.357	0.000		
C	0.502	0.621	0.000	
D	0.616	0.502	0.357	0.000

JE	A	B	C	D
A	5.263			
B	6.313	5.268		
C	6.458	6.714	5.265	
D	6.695	6.468	6.311	5.270

MI	A	B	C	D
A	5.263			
B	4.249	5.268		
C	4.101	3.880	5.265	
D	3.899	4.099	4.254	5.270

NMI	A	B	C	D
A	0.000			
B	1.667	0.000		
C	1.630	1.569	0.000	
D	1.572	1.629	1.668	0.000

RD	A	B	C	D
A	0.000			
B	0.404	0.000		
C	0.390	0.368	0.000	
D	0.370	0.389	0.404	0.000

Bi-cubic interpolation enhances more than multi-frame super resolution. Also bi-cubic interpolation predicted the extreme values better than multi-frame super resolution. This result was not expected. In previous comparisons, multi-frame super resolution enhanced as the same or better than bi-cubic interpolation. This result needs detailed investigation. In order to perform this investigation, a special case of bi-cubic interpolation is employed. Bi-cubic interpolation algorithm is applied to all LR grid DEMs simultaneously. Application of this algorithm is sketched in Figure 62. In bi-cubic interpolation algorithm, nearest 16 samples are used for finding the required data. 16 LR grid DEM cells (notated in red circles) are the inputs to bi-cubic interpolation algorithm to found put the value of bi-cubic grid DEM (LRall_BC) cell (named as HR Grid, black cross in red circle). In the analysis averaging is also employed. The average of LR grid DEMs (LRall_AVE) is found by averaging the four grid cells that are the nearest LR grid DEM cells near HR grid cell (cross in red circle). The difference grid DEM presented in Figure 60 states that there may be a ringing effect problem. In part 3.3.2 it is stated that the ringing problem is solved by employing "boundary adjustment". In boundary adjustment; a number of cells on the boundary are calculated by using bi-cubic interpolation. The values for these cells are fixed and they do not change during iterations. However, even boundary adjustment applied on multi-frame super resolution algorithm, the repeated high and low peaks in the middle parts of the grid DEM suggest that there is another ringing effect problem.
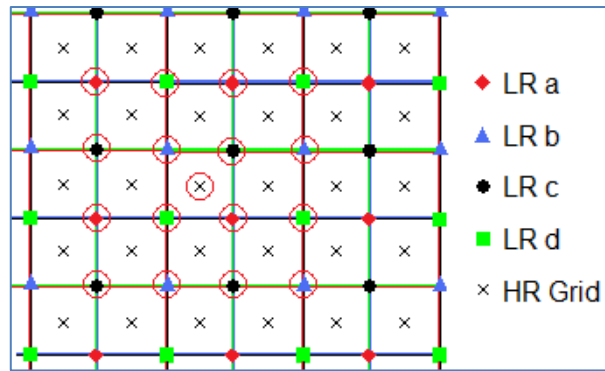
Figure 62 Simultaneous application of bi-cubic interpolation to all LR Grid DEMs

Particularly, in this case the range of grid values is very narrow and this results in ringing effects. In multi-frame super resolution application, boundary adjustment is employed. The narrow range inserts the ringing effect. In order to solve this problem, the number of iteration in IBP is adjusted to 1 and the result (SR_It1) is also included in comparison test. The revised comparison test results are given in Tables 43 and 44. The difference grid DEMs are presented in Figures 63, 64, and 65. The JPDF graphs are given in Figure 66.

Table 43 2nd Comparison Test Result for Gaussian Surface 5 m (Extends)

Grid Name	TIN	SR	SR_It1	BC	LRall_AVE	LRall_BC
Grid Size	5	5	5	5	5	5
Dimensions	201 x 201	201 x 201	201 x 201	201 x 201	201 x 201	201 x 201
Min X	-500	-500	-500	-500	-500	-500
Min Y	500	500	500	500	500	500
Max X	500	500	500	500	500	500
Max Y	-500	-500	-500	-500	-500	-500
Min Z	-30	-30.511	-30.284	-30.183	-30	-30.062
Max Z	40.274	40.395	40.23603	40.241	40.193	40.209

Table 44 2nd Comparison Test Result for Gaussian Surface 5 m (Measures)

	SR	SR_It1	BC	LRall_AVE	LRall_BC
SSD	0.010	0.002	0.002	0.001	0.001
RMSD	0.098	0.041	0.046	0.035	0.017
MAD	0.064	0.020	0.019	0.013	0.008
CC	1.001	1.001	1.001	1.000	1.000
MI	6.157	6.785	6.811	6.924	6.992
NMI	1.741	1.888	1.894	1.922	1.944
RD	0.428	0.472	0.474	0.481	0.486
SU	0.856	0.944	0.947	0.963	0.972
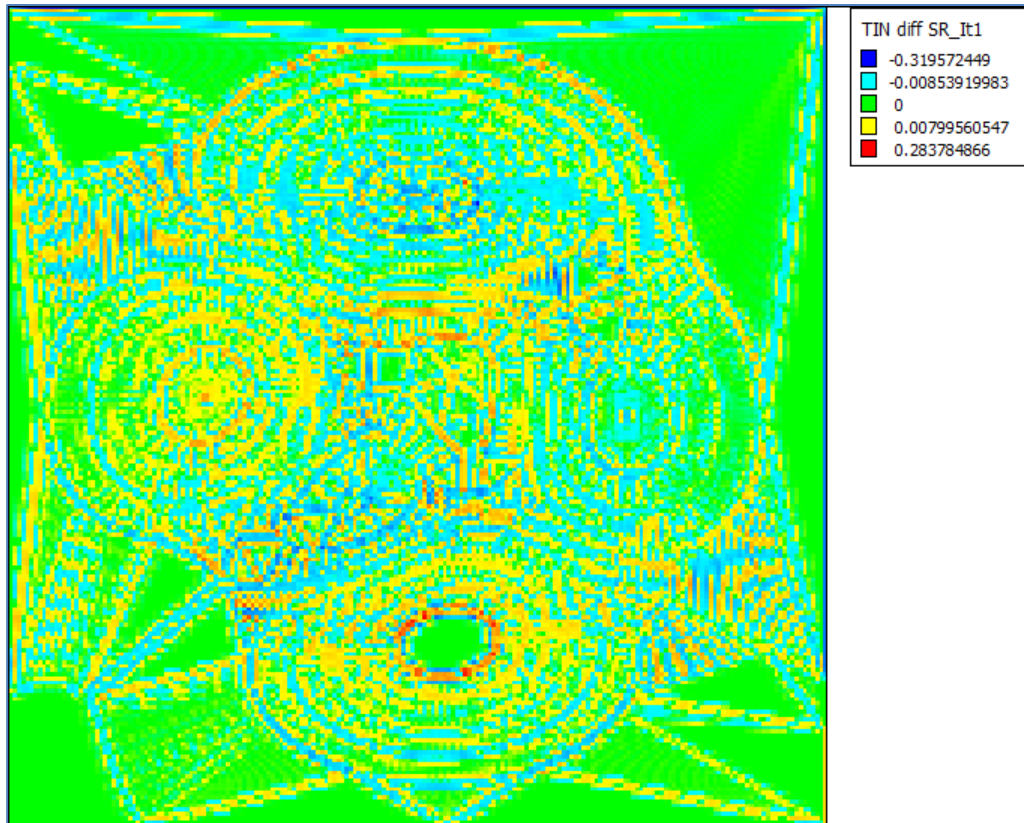
Figure 63 Difference between Gaussian TIN and SR_It1 (5 m)
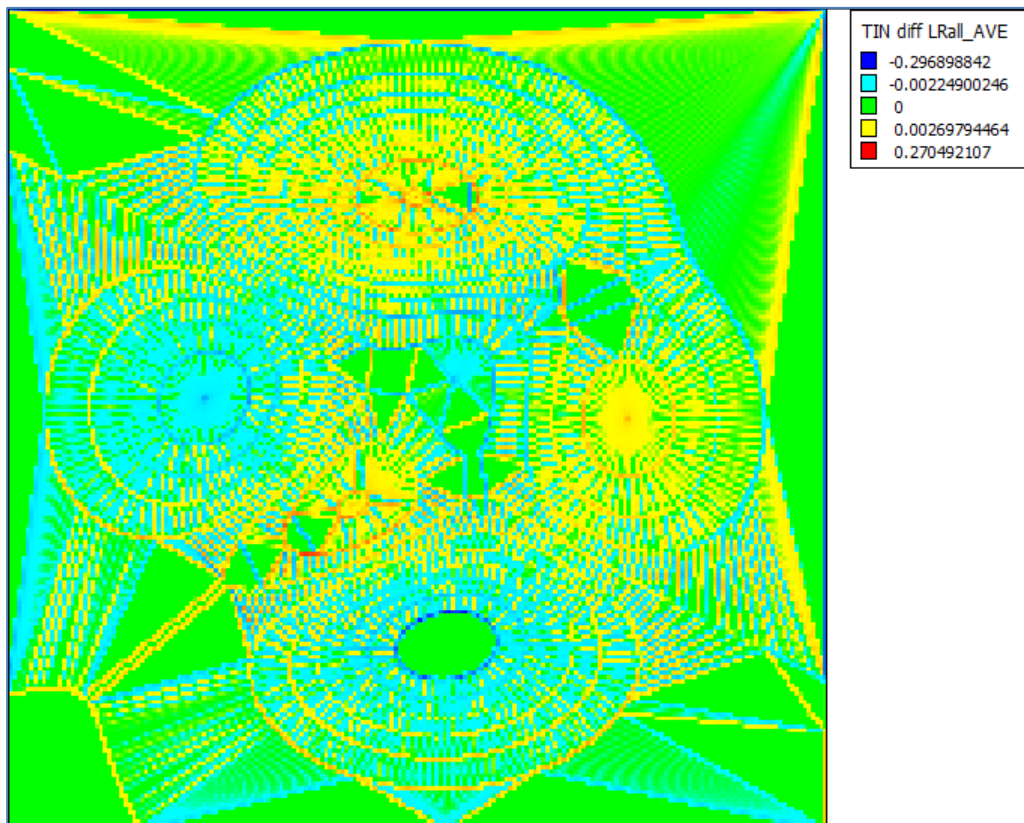
Figure 64 Difference between Gaussian TIN and LR_All_Ave (5 m)
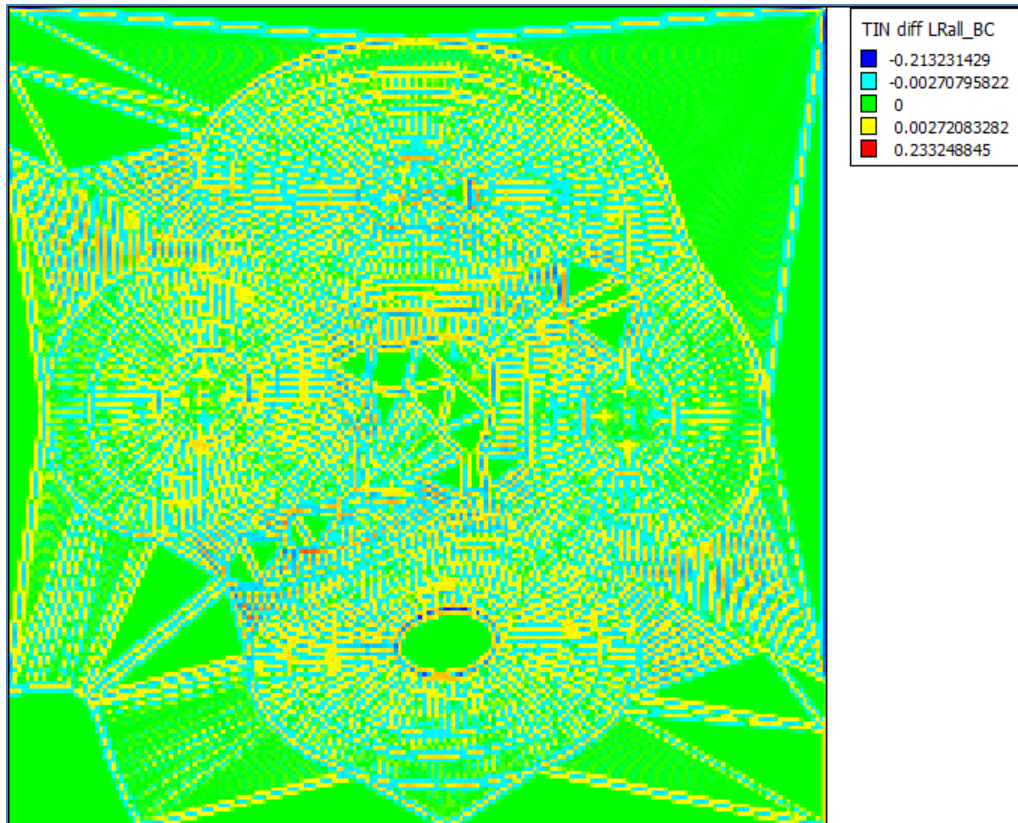
Figure 65 Difference between Gaussian TIN and LR_All_BC (5 m)
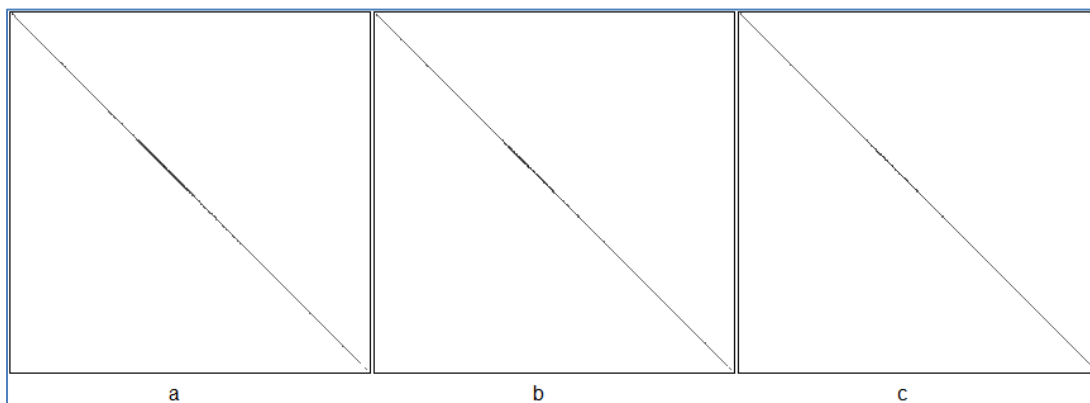
Figure 66 JPDF Graphs for Gaussian Surfaces (5 m) a) TIN vs. SR_It1 b) TIN vs. LR_All_Ave c) TIN vs. LR_All_BC

As can be seen from the above tables and figures, in this test case standard multi-frame super resolution did not give good result for extends and grid cell values. Only one time iterated multi-frame super resolution gives better than standard multi-frame super resolution however its results are not as good as average or bi-cubic interpolation results. Detailed discussion is left for the conclusion chapter.

5.1.2.2 2.5 m grid size Gaussian Surface

The second data set obtained from Gaussian surface has 1 m contour interval. As can be seen from Figure 7, in the second data set local hills and lowest pits have more contour lines

than the first data set. Only peak and pit points are included in the first data set. In this case, the control data is 2.5 m TIN grid DEM (TIN), the test subjects are SR 2.5 m grid DEM (SR), LR grid DEMs on HR grid projection (A, B, C, D) and Bi Cubic 2.5 m grid DEM (BC). The difference grid DEMs are presented in Figures 67, 68, and 69. The comparison results are given in Tables 45 and 46, the JPDF graphs are given in Figure 70.

Table 45 Comparison Result for Gaussian Surface 2.5 m (Extends)

| Grid Name	TIN	SR	A	B	C	D	BC
Grid Size	2.5	2.5	2.5	2.5	2.5	2.5	2.5
Dimensions	409 x 409	409 x 409	409 x 409	409 x 409	409 x 409	409 x 409	409 x 409
Min X	-510	-510	-510	-510	-510	-510	-510
Min Y	510	510	510	510	510	510	510
Max X	510	510	510	510	510	510	510
Max Y	-510	-510	-510	-510	-510	-510	-510
Min Z	-34	-30.232	-30	-30	-30	-30	-30.097
Max Z	40	40.320	40.230	40.222	40.233	40.230	40.233

Figure 67 Difference between Gaussian TIN and A (2.5 m)

77
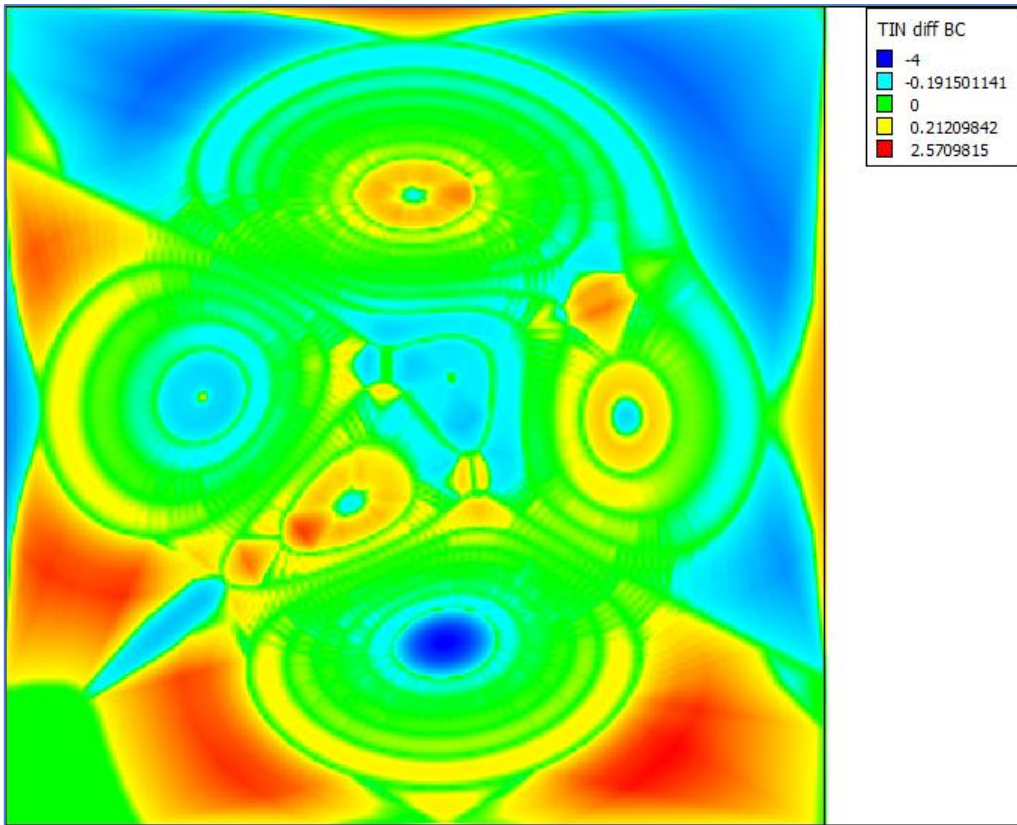
Figure 68 Difference between Gaussian TIN and BC (2.5 m)
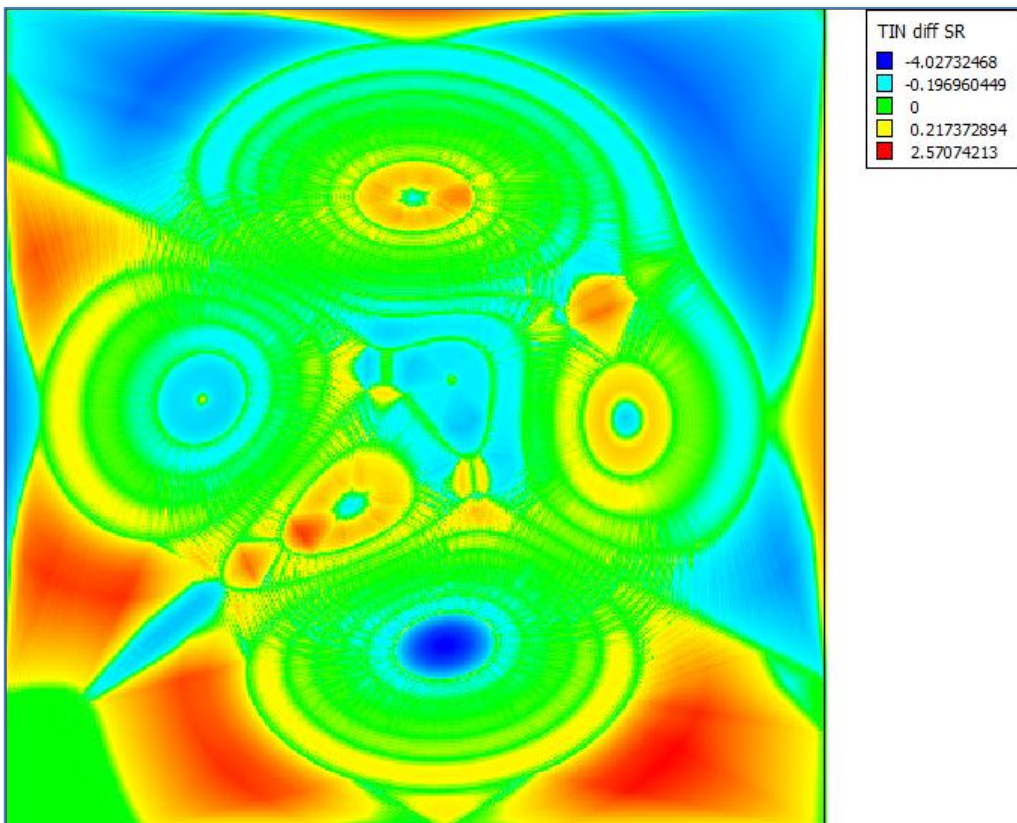
Figure 69 Difference between Gaussian TIN and SR (5 m)

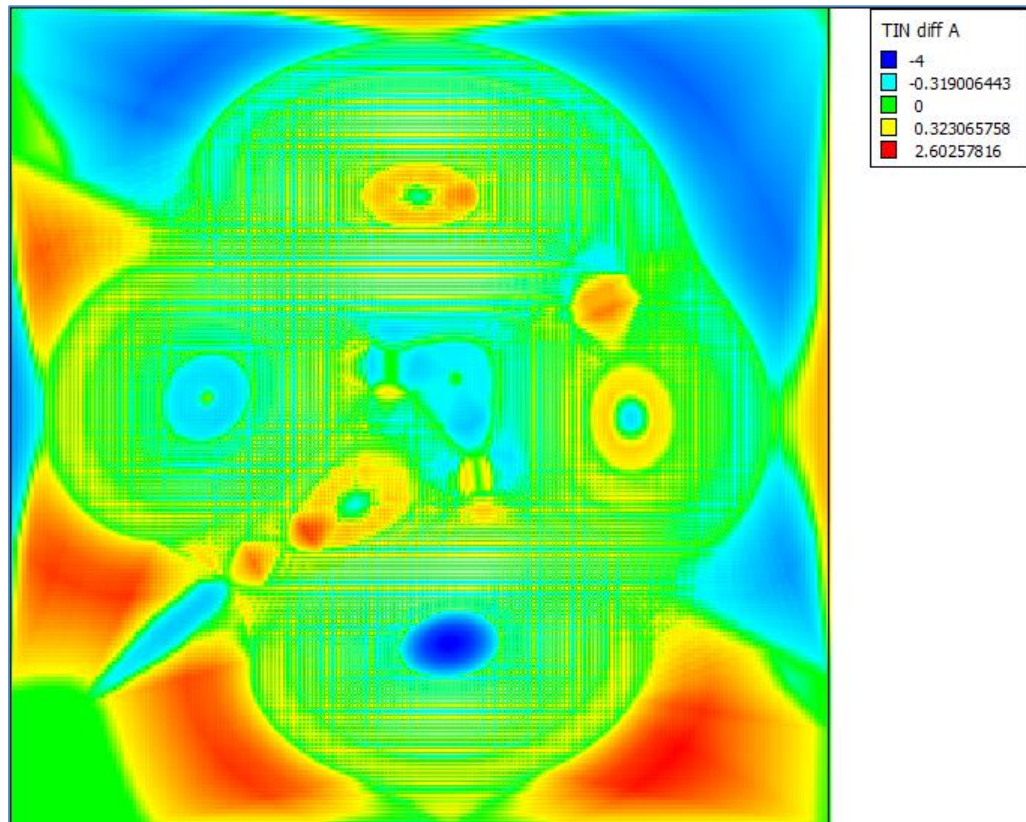**Table 46 Comparison Result for Gaussian Surface 2.5 m (Measures)**

	SR	A	B	C	D	BC
SSD	0.689	0.710	0.712	0.712	0.713	0.688
RMSD	0.829	0.843	0.844	0.844	0.844	0.829
MAD	0.520	0.570	0.571	0.571	0.572	0.518
CC	1.001	0.998	0.998	0.998	0.998	1.000
MI	5.014	4.668	4.669	4.659	4.661	5.058
NMI	1.523	1.469	1.468	1.469	1.469	1.531
RD	0.353	0.328	0.328	0.328	0.328	0.356
SU	0.705	0.657	0.657	0.655	0.656	0.712

As seen on the geometrical surfaces, multi-frame super resolution enhances spatial resolution over the low resolution grid DEMs. In most of the cases, it enhances more than bi-cubic interpolation. However in some cases, bi-cubic interpolation results are better than those of multi-frame super resolution. Discussion on this issue is presented in the next chapter.
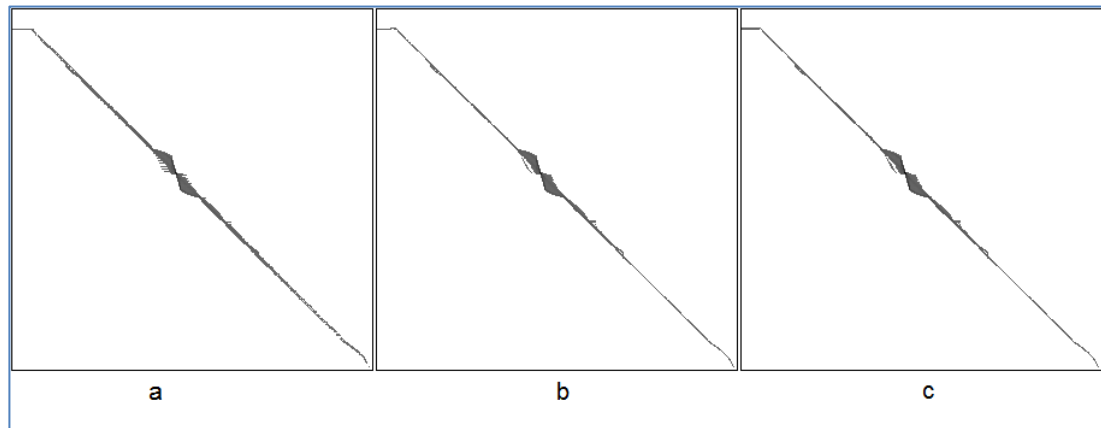
Figure 70 JPDF Graphs for Gaussian Surfaces (2.5 m) a) TIN vs. A b) TIN vs. BC c) TIN vs. SR

5.2 Effect of SR on Real Land Surface

Investigation on the effect of super resolution for only geometrical surfaces would be incomplete. Real land application would enrich the idea about the performance of multi-frame super resolution on spatial enhancement. Selected land is part of the Middle East Technical University campus area (Figures 8 and 9). Two tests are made on real land data. The first one is the effect of multi-frame super resolution on the same source data. The second test is about the level of enhancement. As explained before, grid size depends on the scale. If super resolution shows good level of spatial enhancement, it may break the dependency caused by scale. There are two data sets, one is originated from 1/25000 scale map having 10 m contour interval and the other from 1/5000 scaled map, which has 5 m contour interval. In some places 1/5000 scaled map has mid contours also.

5.2.1 10 m grid size METU area

Four 20 m low resolution grid DEMs are obtained from the first data set. The grid centers of LR grid DEMs have 10 m distance from each other. Multi-frame super resolution had been applied on these low resolution grid DEMs. Resulting grid DEM is tested with original 10 m grid DEM and bi-cubic interpolation 10 m grid DEM. The difference grid DEMs can be seen in Figures 71, 72 and 73 . The comparison report can be seen in Tables 47 and 48, and the resulting JPDF graphs are given in Figure 74.

Figure 71 METU Area difference grid DEM between TIN and A (10 m)

Table 47 Comparison Result for METU Area 10 m (Extends)

Grid Name	TIN	SR	A	B	C	D	BC
Grid Size	10	10	10	10	10	10	10
Dimensions	184 x 146	184 x 146	184 x 146	184 x 146	184 x 146	184 x 146	184 x 146
Min X	472450	472450	472450	472450	472450	472450	472450
Min Y	4407150	4407150	4407150	4407150	4407150	4407150	4407150
Max X	474280	474280	474280	474280	474280	474280	474280
Max Y	4405700	4405700	4405700	4405700	4405700	4405700	4405700
Min Z	1090	1088.31	1090	1090	1089.24	1090	1084.49
Max Z	1190	1191.11	1190	1190	1190.90	1190	1190.81

Figure 72 METU Area difference grid DEM between TIN and BC (10 m)

Figure 73 METU Area difference grid DEM between TIN and SR (10 m)

Table 48 Comparison Result for METU Area 10 m (Measures)

	SR	A	B	C	D	BC
SSD	0.035	0.528	0.538	0.539	0.547	0.039
RMSD	0.187	0.727	0.733	0.734	0.740	0.197
MAD	0.099	0.470	0.473	0.473	0.476	0.095
CC	1.000	1.000	1.000	1.000	1.000	1.000
MI	5.766	4.500	4.504	4.507	4.509	5.827
NMI	1.757	1.525	1.524	1.525	1.524	1.768
RD	0.439	0.343	0.343	0.343	0.343	0.444
SU	0.878	0.685	0.686	0.686	0.686	0.887
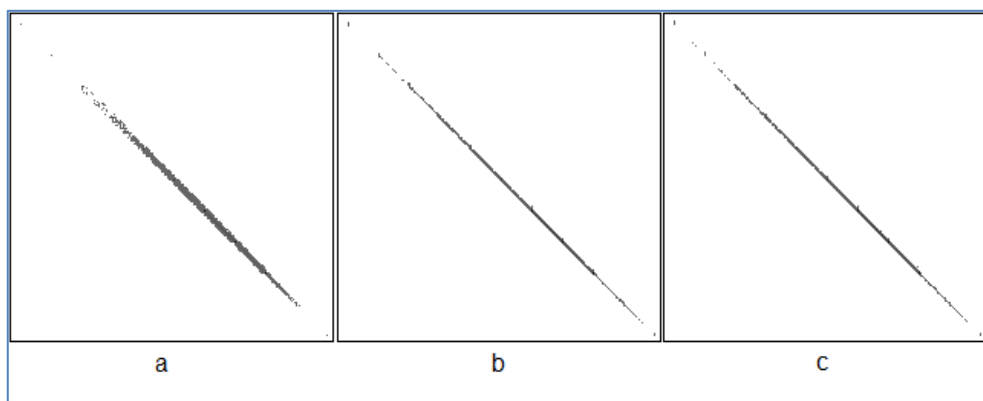
Figure 74 JPDF Graphs for part of METU Area (10 m) a) TIN vs. A b) TIN vs. BC c) TIN vs. SR

Multi-frame grid DEM super resolution on 10 m grid size enhanced spatially over low resolution grid DEMs. Its level of enhancement is a little higher than bi-cubic interpolation. RMSD is around 0.19 m which is very low. The reason for this low RMSD is the existence of flat TINs (Figure 75) in the area. Flat TINs do not carry additional information, but these grid cells are counted in RMSD calculations. 8 out of 16 similarity measures states that the low resolution grid DEMs and multi-frame SR grid DEMs are almost similar. However, SSD, RMSD, MAD, JE, MI, NMI, and RD (SU) find out that LR grid DEMs and SR grid DEMs are different. This result shows the measures which are sensitive to the whole area even the source of TIN surface has a large number of flat TINs.

5.2.2   5 m grid size METU area

The second test on real land is whether the enhancement level exceeds the scale dependency level. In order to realize this goal; four 10 m low resolution grid DEMs are obtained from the first data set by moving their grid centers 5 m away from each other. Then multi-frame super resolution is applied on these grid DEMs. Bi-cubic interpolation grid DEM is also obtained from the same data set. These grid DEMs are tested with 5 m grid sized grid DEM obtained from second data set. Examples from resulting difference grid DEMs can be seen in Figures 76, 77, and 78. The comparison results can be seen in Tables 49 and 50. Examples from JPDF graphs are shown in Figure 79.
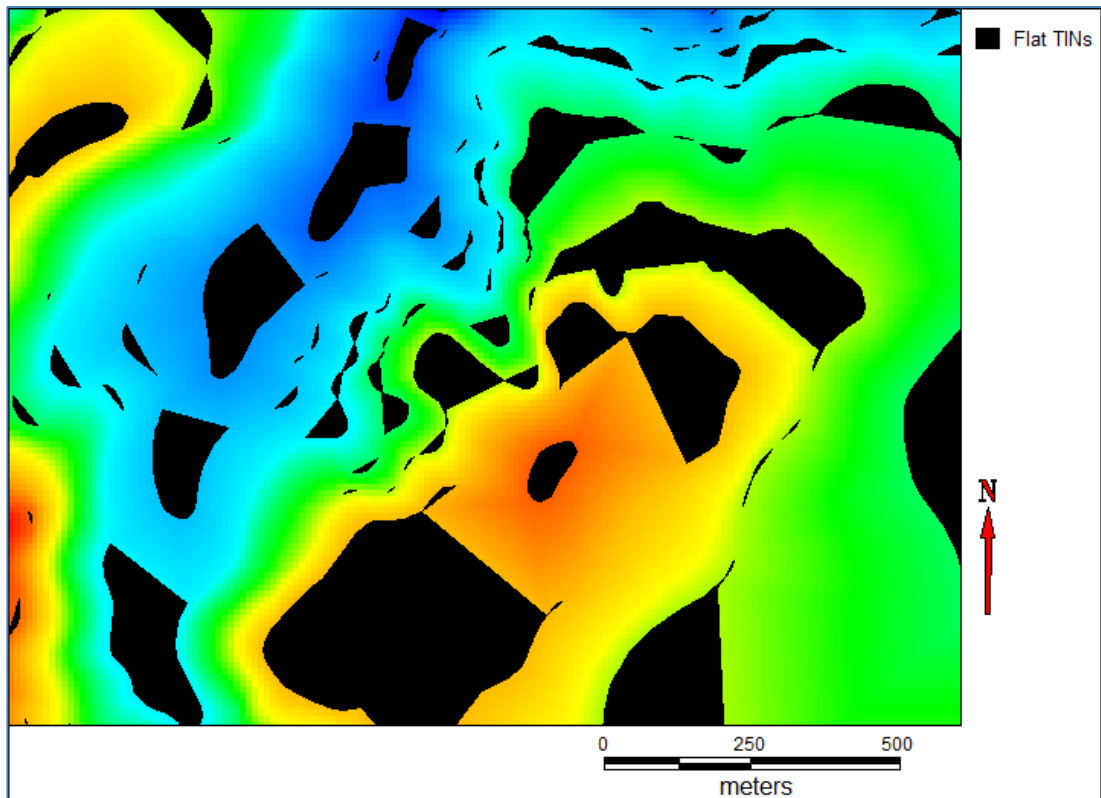
Figure 75 Flat TINs on METU area are colored as black
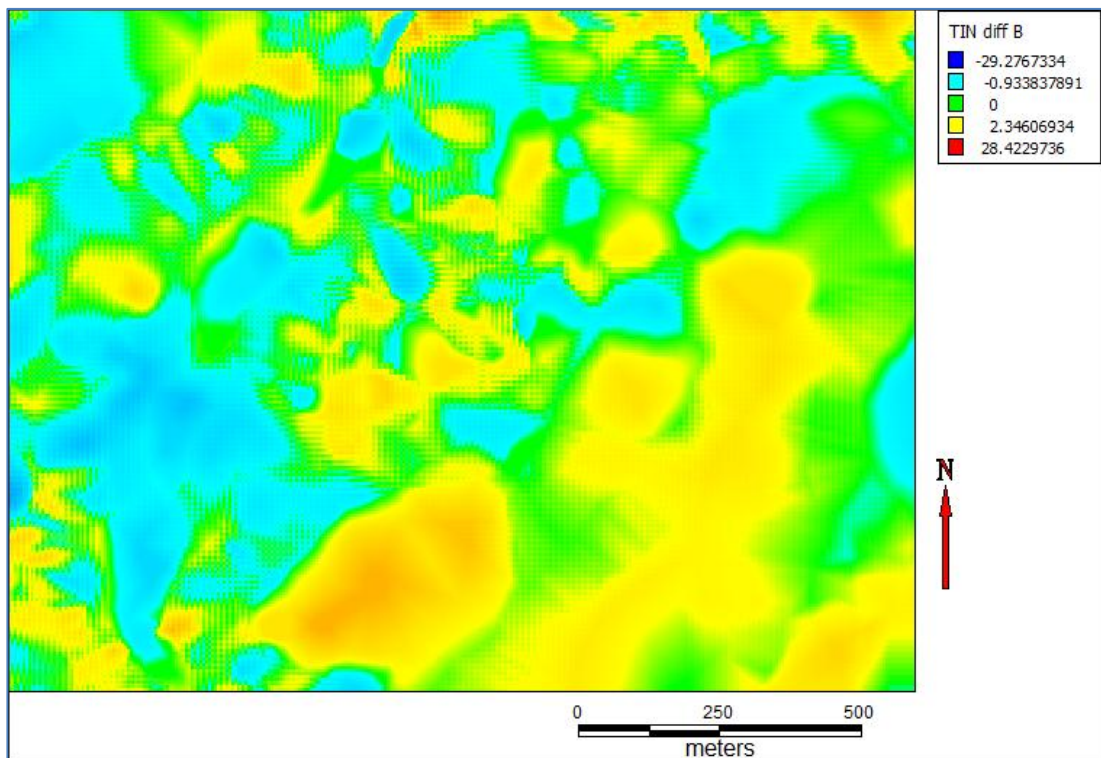
Figure 76 METU Area difference grid DEM between TIN and B (5 m)
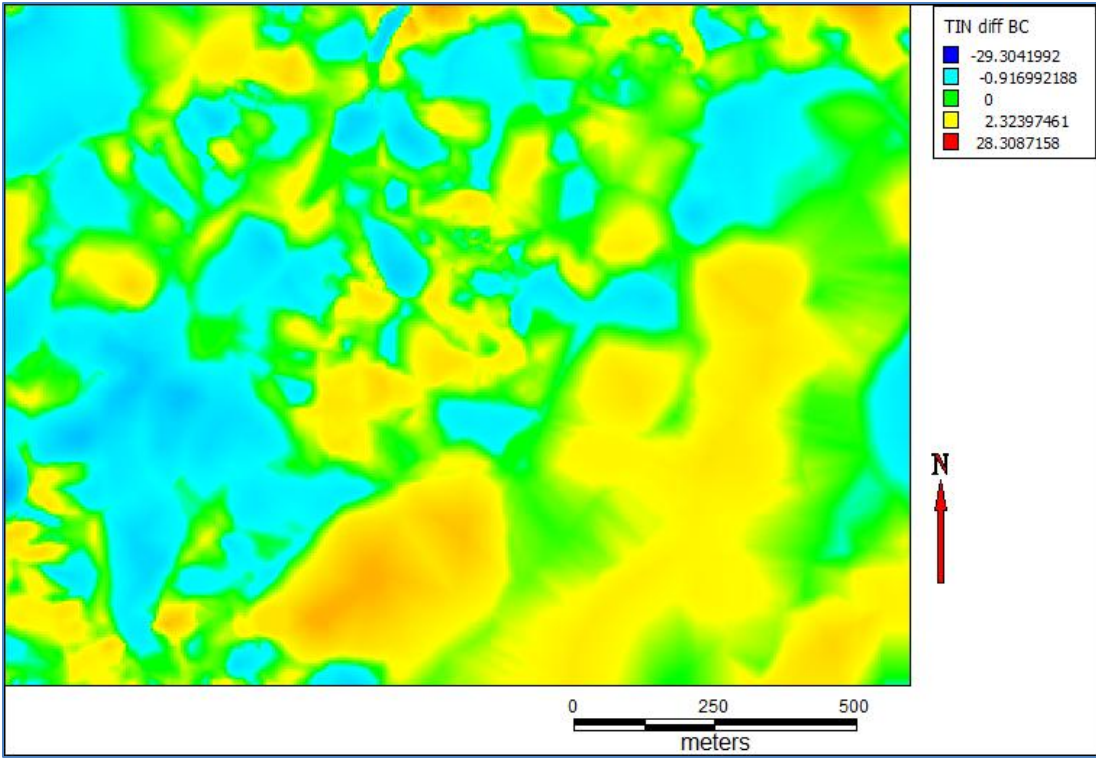
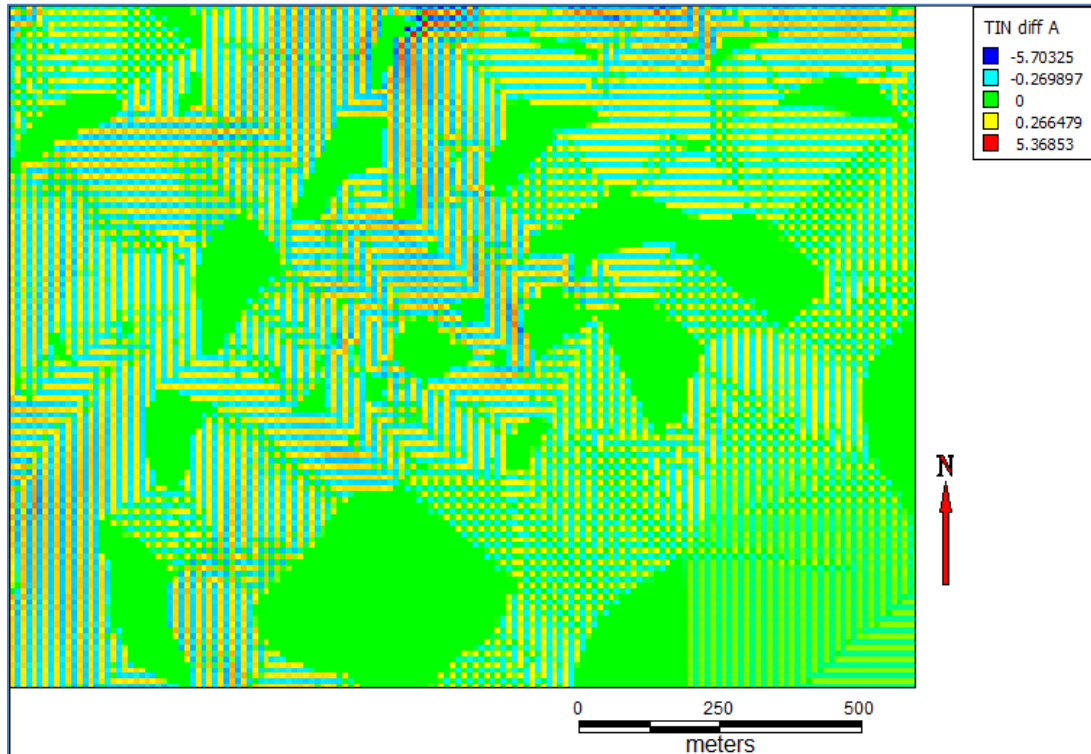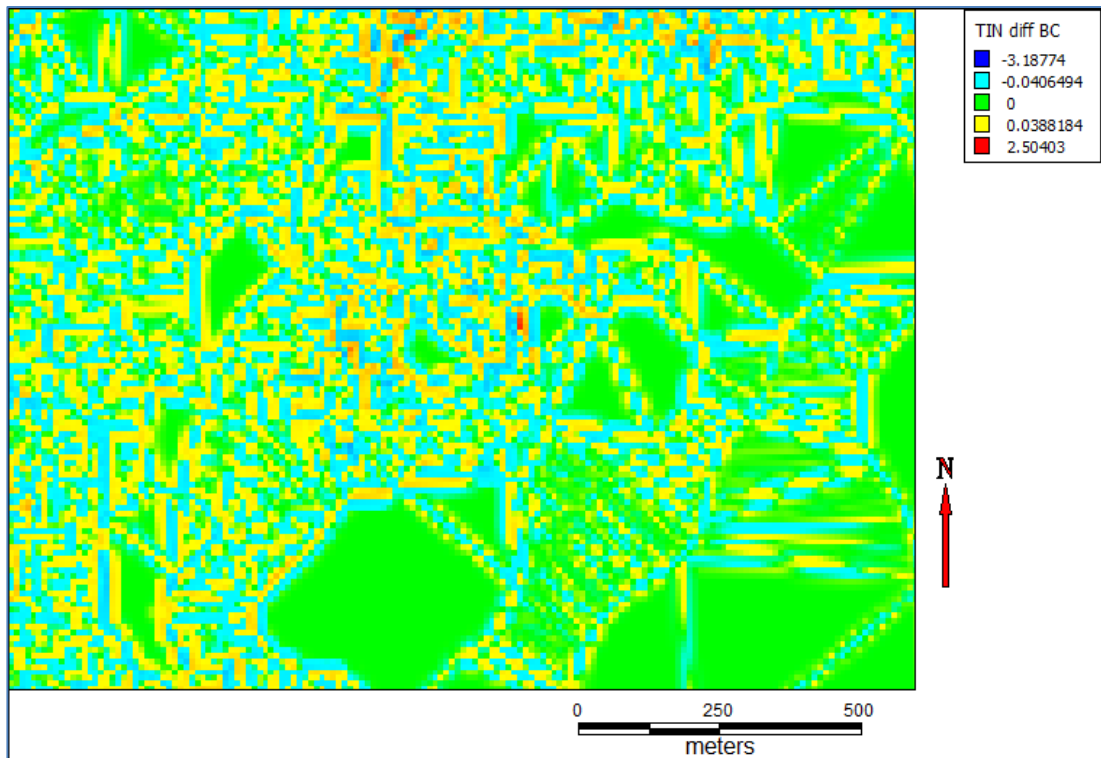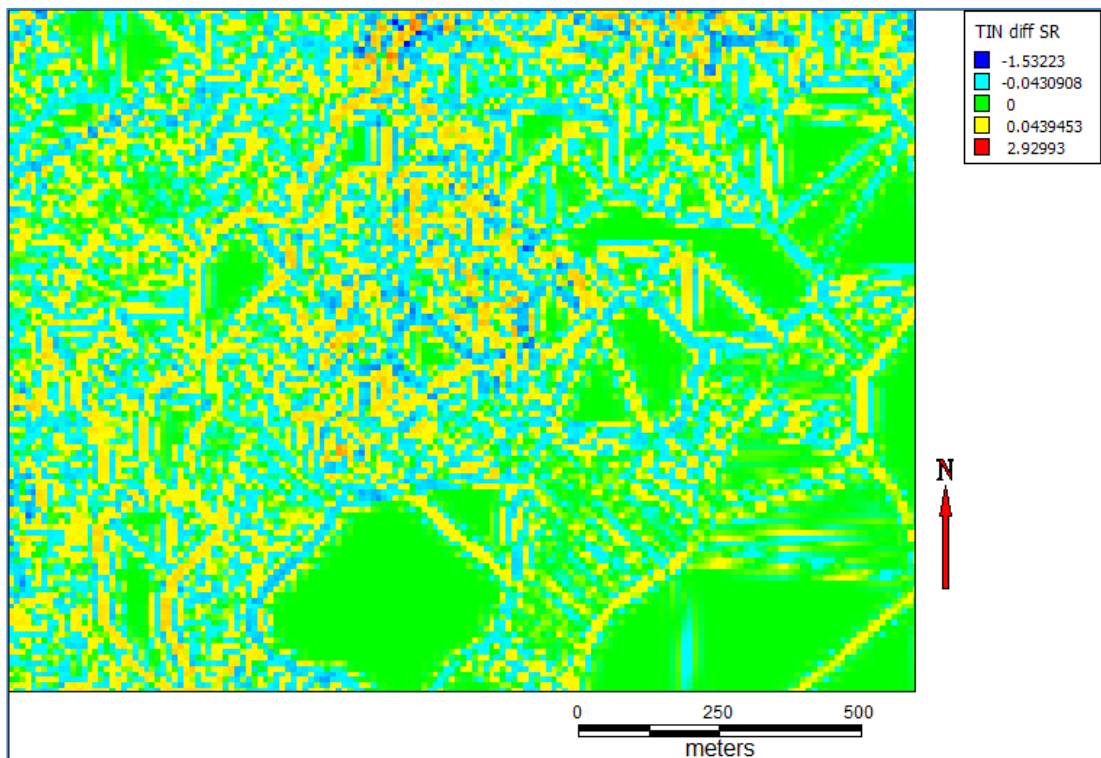**Figure 77 METU Area difference grid DEM between TIN and SR (5 m)**
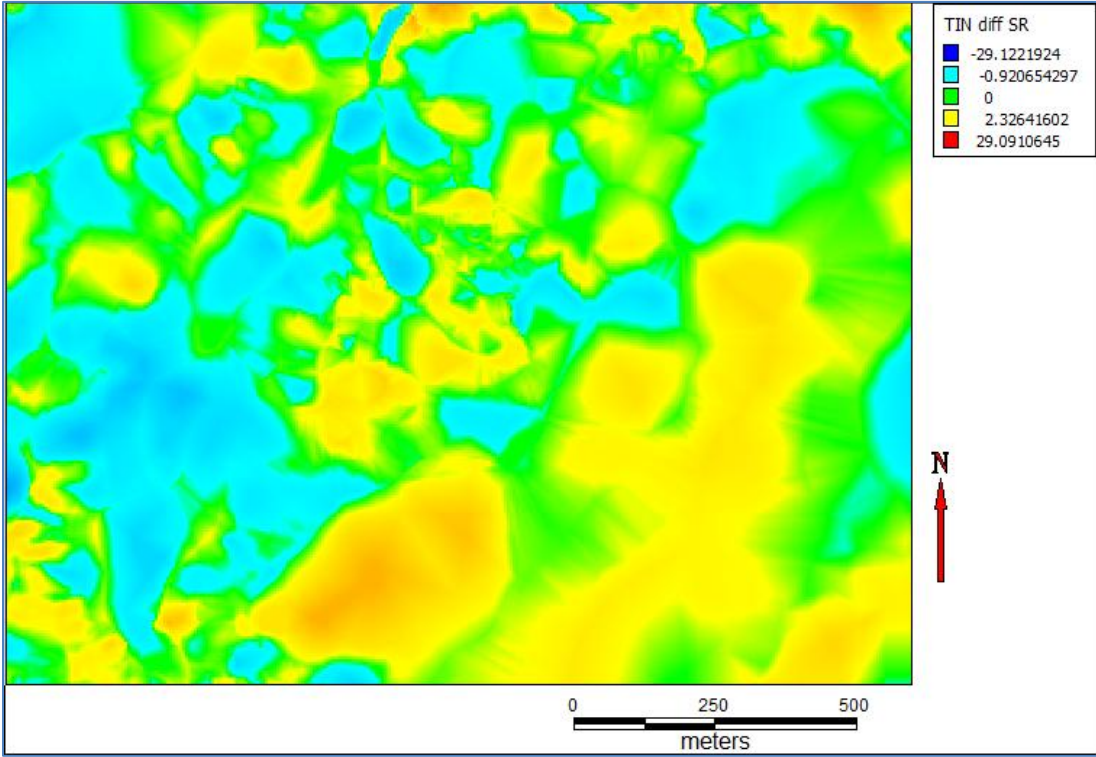
Figure 78 METU Area difference grid DEM between TIN and SR (5 m)

84

Table 49 Comparison Result for METU Area 5 m (Extends)

Grid Name	TIN	SR	A	B	C	D	BC
Grid Size	5	5	5	5	5	5	5
Dimensions	367 x 291	367 x 291	367 x 291	367 x 291	367 x 291	367 x 291	367 x 291
Min X	472450	472450	472450	472450	472450	472450	472450
Min Y	4407150	4407150	4407150	4407150	4407150	4407150	4407150
Max X	474280	474280	474280	474280	474280	474280	474280
Max Y	4405700	4405700	4405700	4405700	4405700	4405700	4405700
Min Z	1090	1089.34	1090	1087.14	1090	1090	1087.14
Max Z	1190	1190.70	1190	1190.46	1190	1190	1190.46

Table 50 Comparison Result for METU Area 5 m (Measures)

|	SR	A	B	C	D	BC
SSD	9.545	9.618	9.611	9.630	9.626	9.499
RMSD	3.089	3.101	3.100	3.103	3.103	3.082
MAD	2.204	2.217	2.216	2.219	2.219	2.198
CC	1.000	1.000	1.000	1.000	1.000	1.000
MI	2.931	2.929	2.926	2.924	2.924	2.942
NMI	1.319	1.320	1.319	1.319	1.318	1.317
RD	0.208	0.208	0.208	0.208	0.208	0.209
SU	0.416	0.416	0.416	0.415	0.415	0.418
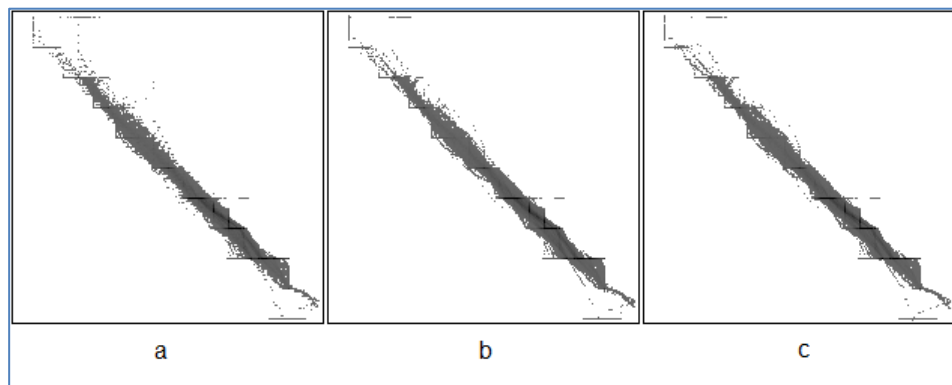
Figure 79 JPDF Graphs for part of METU Area (5 m) a) TIN vs. B b) TIN vs. BC c) TIN vs. SR

The tests on the real land show the same results as geometrical surfaces. That is: multi-frame super resolution enhances spatial resolution over the low resolution grid DEMs. Its level of enhancement is more or less as bi-cubic interpolation enhancement. However in some cases, bi-cubic interpolation results are better than multi-frame super resolution. RMSD of multi-frame super resolution and bi-cubic interpolation is about 3 m. Detailed discussion is left for the next chapter.

Multi-frame super resolution enhances over the low resolution grid DEMs, and its level of enhancement competes with bi-cubic interpolation. The multi-frame super resolution is one step ahead in predicting the extreme values of the scene. The level of enhancement is directly related to non-redundant information carrying capacity of low resolution grid DEMs.

5.3   Effect of SR on space-borne DEMs

The effect of multi-frame super resolution is investigated through space-borne DEMs. Space-borne DEMs can be an answer to "single source of data" objections. Most common space-borne DEMs, which are SRTM and ASTER data sets, are used in investigation. These data sets are introduced in section 2.3.3. The test is to find the level of enhancement of super resolution of SRTM and ASTER together. The result is compared with the grid DEMs of real land.

5.3.1   SRTM + ASTER vs. Real Land

The second test is on super resolution with SRTM and ASTER data sets. The result will be tested with real land data. However; as seen in Figures 8 and 9, there is a shift between SRTM and ASTER data and contour lines of METU area. This shift would have an enormous effect on the results. Therefore the test area is changed. The position of the new test area on Turkey map can be seen in Figure 80. SRTM data set for this test area is N37E31. The contour lines and extracted part of N37E31 SRTM data set can be seen in Figure 81. The same configuration for ASTER data set is shown in Figure 82.
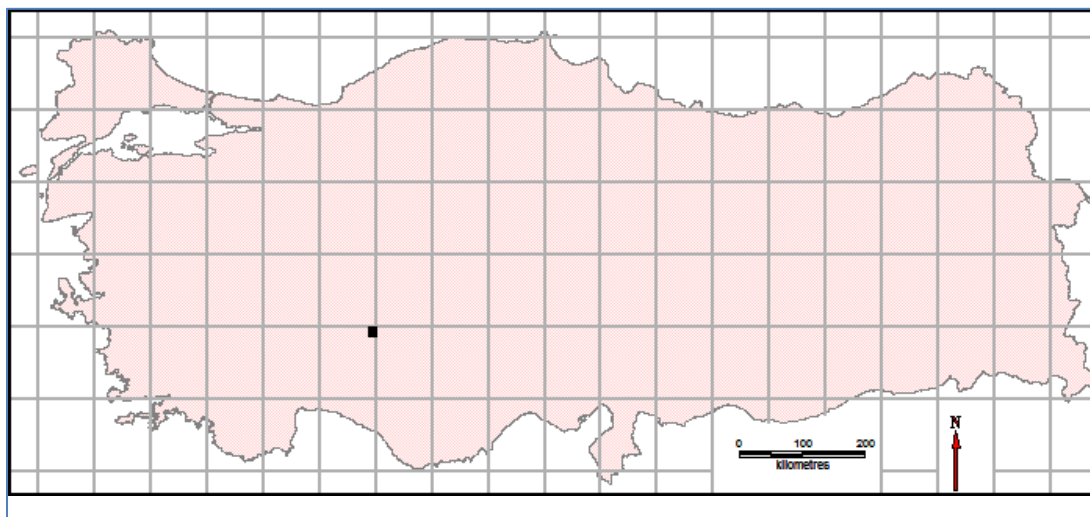
Figure 80 The new test area position on Turkey Map

Multi-frame super resolution is applied on SRTM and ASTER grid DEMs. SRTM has 3 arc-second grid size and ASTER has 1 arc-second grid size. The resulting grid (SR) (Figure 83) DEM's grid size is 0.5 arc-second and it is tested with grid DEM (TIN) obtained from contour lines via TIN algorithm. Level of enhancement is investigated through the low resolution couples (SRTM_HR, ASTER_HR). In order to check super resolution performance, bi-cubic interpolation applied on SRTM (SRTM_BC) and ASTER (ASTER_BC) and they are also included in the test. The comparison results are given in Tables 51 and 52. The difference grid DEM (TIN-SR) can be seen in Figure 84. The JPDF graphs are shown in Figure 85.
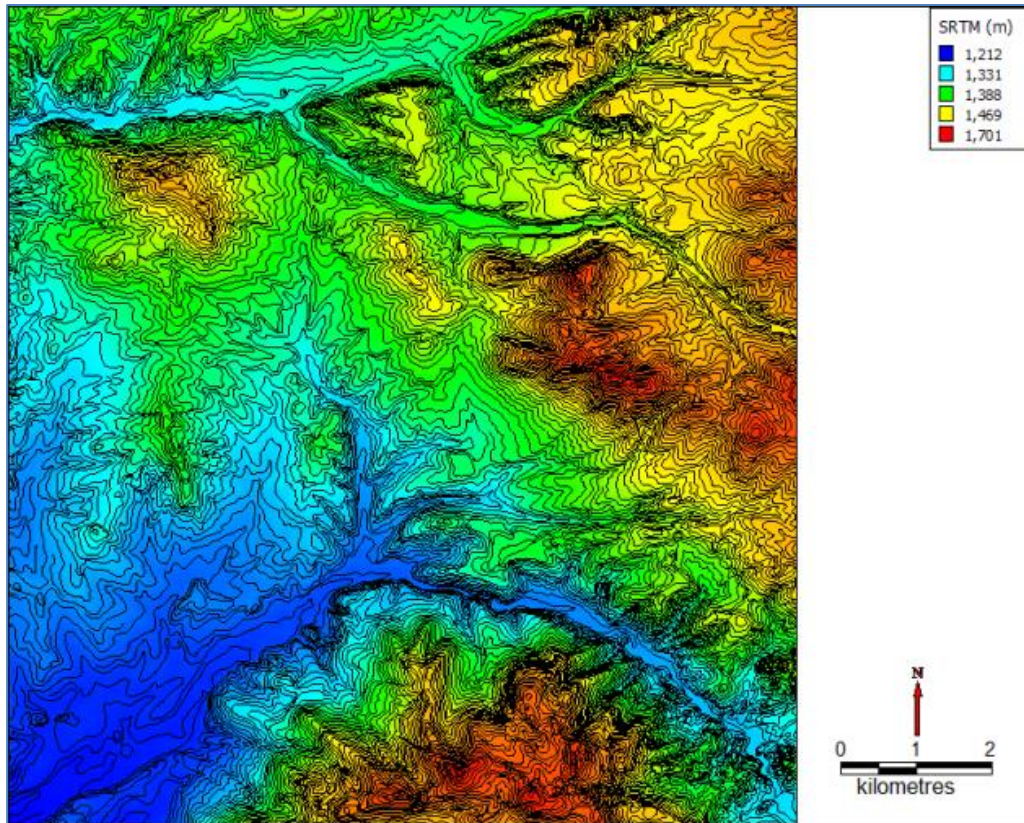
Figure 81 Part of SRTM and contour lines for N37E31
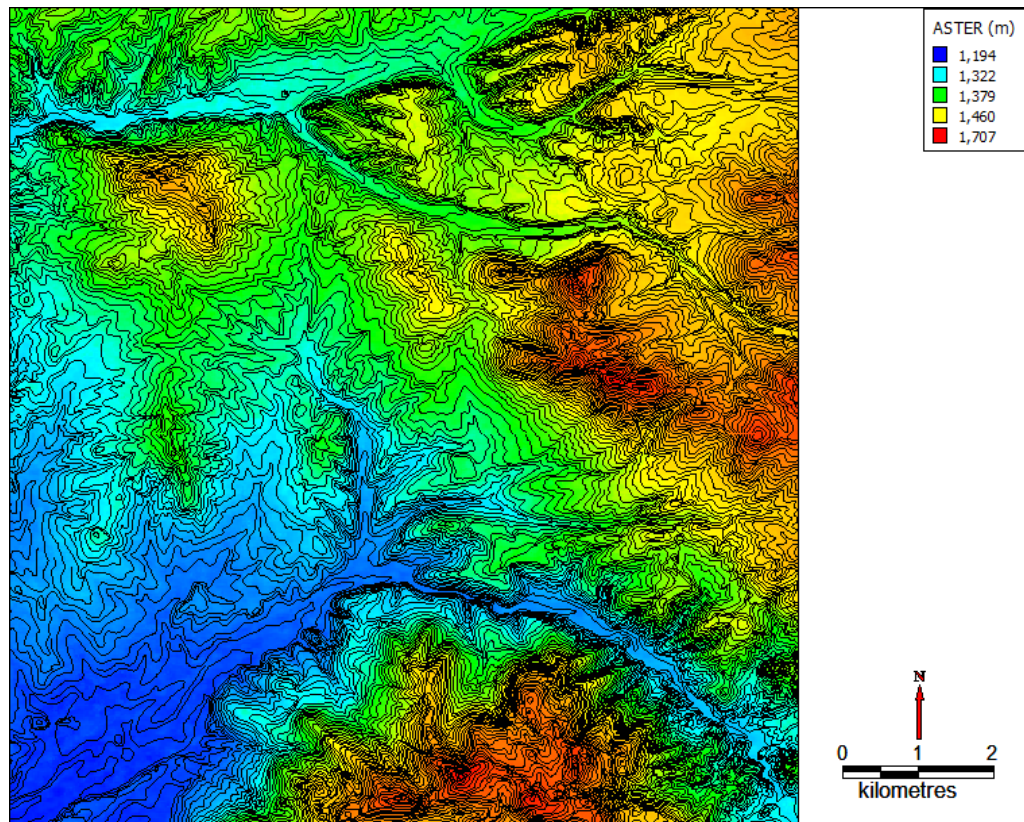
Figure 82 Part of ASTER and contour lines for N37E31
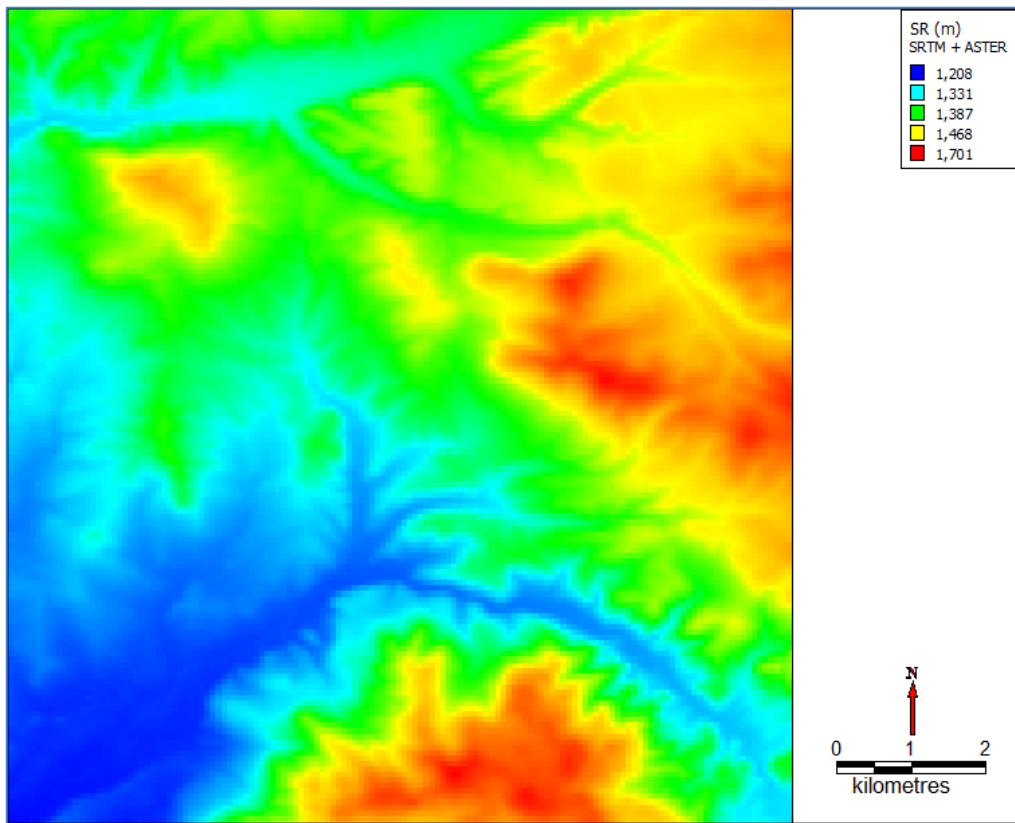
Figure 83 SR result after application of multi-frame super resolution to SRTM and ASTER

Table 51 Comparison Result for ASTER + SRTM vs. TIN (Extends)

Grid Name	TIN	SR	ASTER_BC	SRTM_BC	SRTM_HR	ASTER_HR
Grid Size (arc-second)	0.5	0.5	0.5	0.5	0.5	0.5
Dimensions	859 x 895	859 x 895	859 x 895	859 x 895	859 x 895	859 x 895
Min X	31.88076	31.88076	31.88076	31.88076	31.88076	31.88076
Min Y	37.9991	37.9991	37.9991	37.9991	37.9991	37.9991
Max X	31.99993	31.99993	31.99993	31.99993	31.99993	31.99993
Max Y	37.87493	37.87493	37.87493	37.87493	37.87493	37.87493
Min Z	1210	1194	1199.592	1211.578	1212	1194
Max Z	1710	1707	1707.235	1703.335	1701	1707

Table 52 Comparison Result for ASTER + SRTM vs. TIN (Measures)

	SR	ASTER_BC	SRTM_BC	SRTM_HR	ASTER_HR
SSD	38.275	63.720	33.456	38.245	65.977
RMSD	6.187	7.982	5.784	6.184	8.123
MAD	4.365	6.296	4.087	4.362	6.392
CC	1.000	1.001	1.000	1.000	1.001
MI	4.133	3.969	4.221	4.135	3.931
NMI	1.372	1.349	1.382	1.372	1.344
RD	0.274	0.263	0.280	0.274	0.261
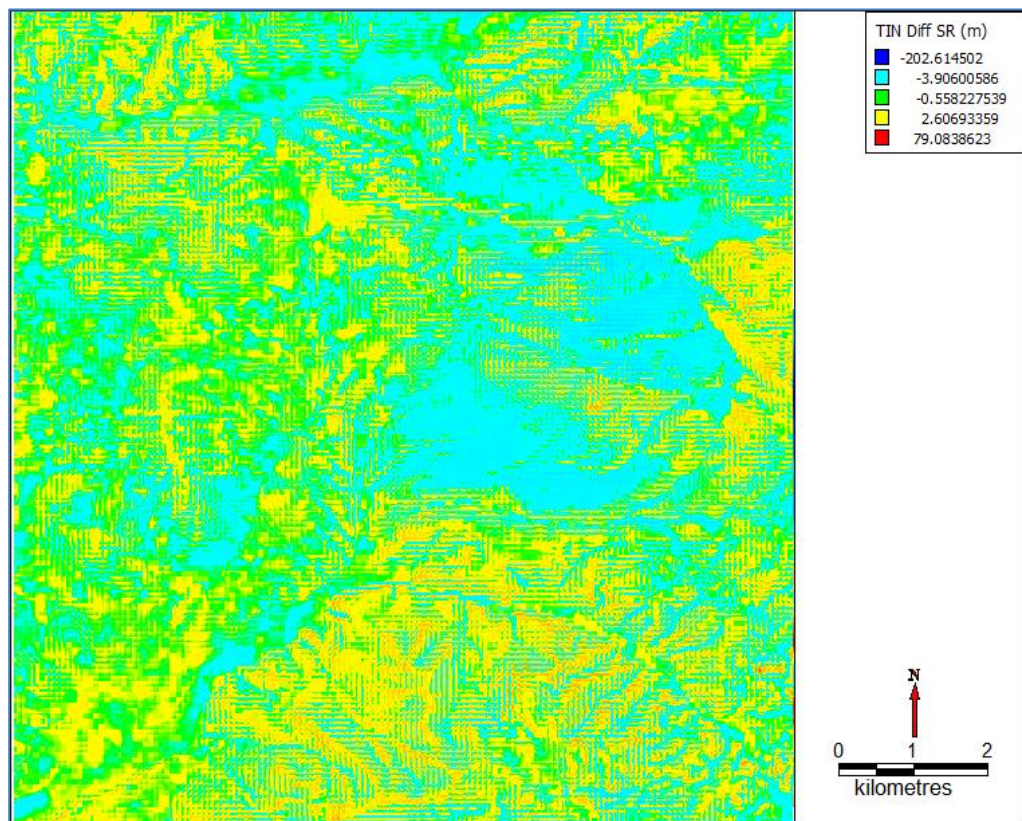
Figure 84 Difference grid DEM between TIN and SR (0.5 arc second)
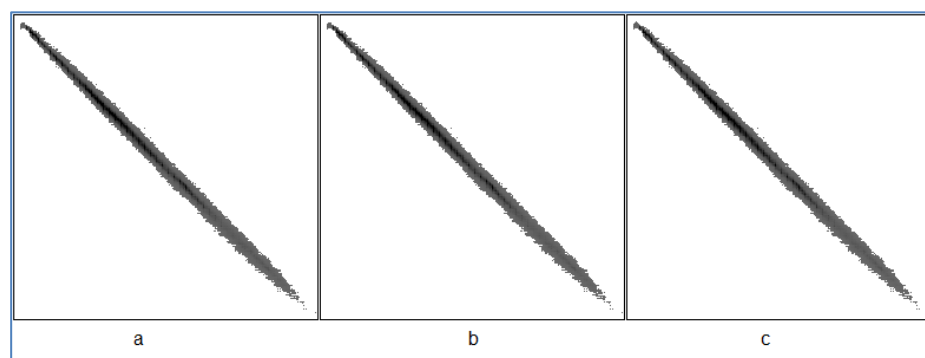
Figure 85 JPDF Graphs for N37E31 a) TIN vs. SRTM_HR b) TIN vs ASTER_BC c) TIN vs. SR

As can be seen from results, the best enhancement is achieved with SRTM bi-cubic interpolation grid DEMs. Even SRTM_HR resulted better than multi-frame super resolution. ASTER_BC and ASTER_HR resulted nearly 8 m RMSD compared to TIN. This result again reminds that there is a shift in ASTER data set. In order to prove this conclusion further investigation is done on ASTER data set.

5.3.2 ASTER Data set investigation

In the last test, ASTER data set altered super resolution in a negative way that is it resulted worse than bi-cubic interpolation, even worse than low resolution grid DEMs. In order to find out the problem with ASTER data set, it is controlled with 1 arc second grid DEM obtained from contour lines via TIN algorithm. The first step is to compare the ASTER data set with Grid DEM 1 arc-second via similarity measures. In order to control the comparison test, SRTM data is also included. The results of similarity measures are presented in Table 53. The results are highly compatible with the ones that had represented by Sefercik et al. (2007). They find the standard deviation of the heights based on SRTM 3.97 m for open and 4.49 m for forest areas. The values they found for ASTER is 7.29 m for open and 8.08 m for forest areas. The problem that comes from ASTER is not because of the shift, it is because of the original values of ASTER. The second item on ASTER is the histogram test.

Table 53 Similarity Measures of ASTER and SRTM controlled with 1 arc-second Grid DEM

Similarity Measure	ASTER	SRTM
SSD	61.0114	18.2563
RMSD	7.8110	4.2727
MAD	6.2962	3.2441
CC	1.0012	0.9998
MI	4.0533	4.9308
NMI	1.3010	1.3980
RD	0.2393	0.2914
SU	0.4785	0.5828

In order to check the values for the whole area of ASTER data set, the histograms for ASTER and 1 arc-second grid DEM are plotted. Grid DEM 1 Histograms can be seen in Figure 86. ASTER histogram is shown in Figure 87 and they can be viewed both in Figure 88. The three figures state that if there is a shift in the ASTER for this study area, it is very hard to find out. The grid cell values may differ however the overall ratio of the grid cell values shows similar pattern. This suggests that the differences in the grid cell values are not bringing new information. They only enlarge the RMSD values in multi-frame super resolution. The resulting multi-frame super resolution of ASTER and SRTM showed 6.2 m RMSD which is smaller than ASTER HR and ASTER BC. The results obtained from similarity measures and the histogram suggest that ASTER and SRTM multi-frame super resolution enhanced ASTER. However STRM bi-cubic interpolation resulted better than multi-frame super resolution.
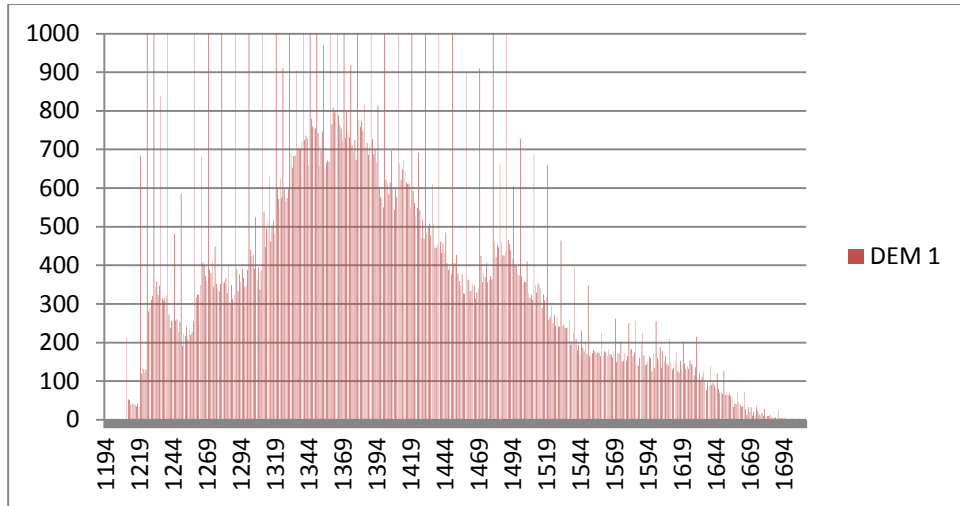
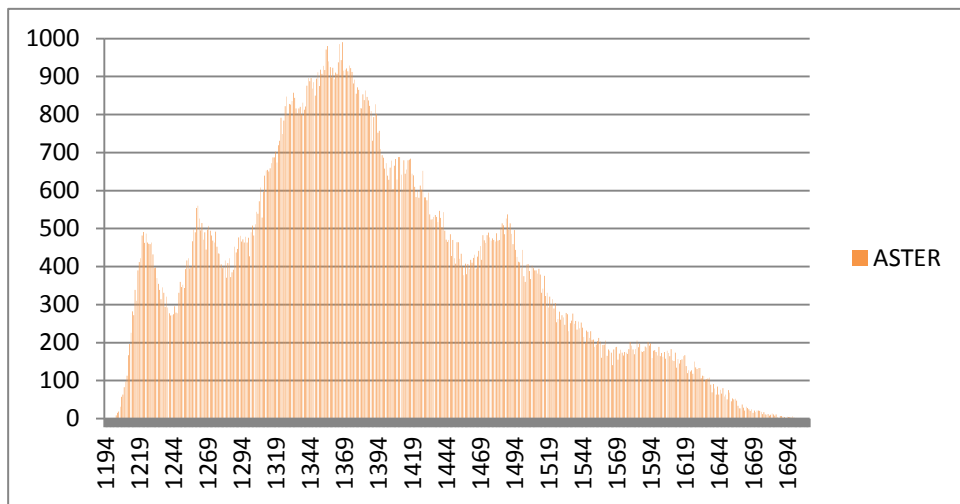**Figure 86 Histogram of Grid DEM (1 arc-second) obtained by TIN Algorithm**
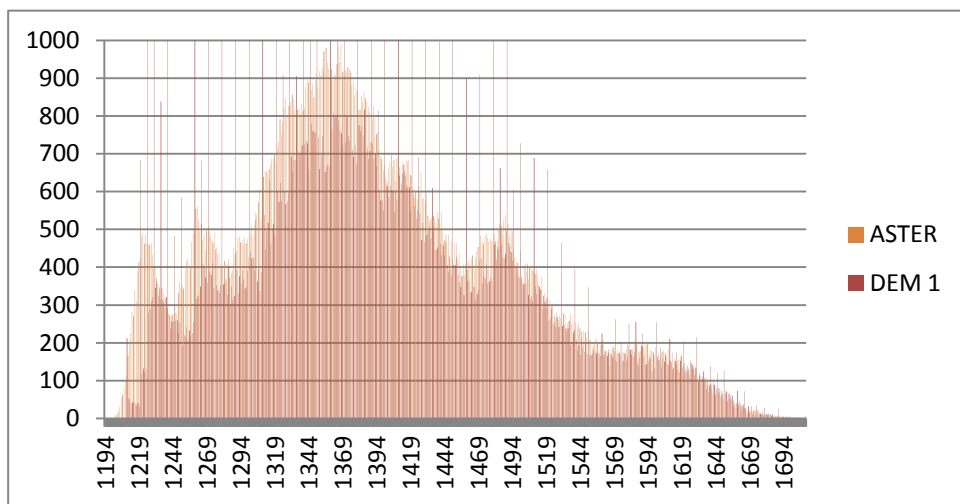

Figure 87 ASTER Grid DEM Histogram for the study area

Figure 88 Grid DEM 1 and ASTER Histograms simultaneously

CHAPTER 6

DISCUSSIONS, CONCLUSIONS AND RECOMMENDATIONS

Throughout the study, mainly one question is tried to be answered: 'Can the accuracy of the DEM be increased by using super resolution techniques?' The curiosity behind this study is that whether the combination of geography and digital image processing domains will help in increasing DEM accuracy or not.

Spatial resolution of grid DEM is determined by grid size. The primary parameter in choosing the grid size is the scale of the source data. The interpolation method, boundaries and the distribution of the data are the secondary ones. Selection of grid size depends on scale which brings new limits to the accuracy of grid DEM.

It is tried to prove that multi-frame super resolution helps in increasing the spatial resolution of DEM. From geometrical surfaces to actual land sites, to space-borne grid DEMs, it is tried to be proven that multi-frame super resolution helped to increase spatial resolution using low resolution images carrying non-redundant information. The results given in the previous section show that for synthetic data, although LR grid DEMs are obtained from the same source multi-frame super resolution shows a potential in increasing the spatial resolution of SR grid DEM. The level of enhancement is only a little higher than bi-cubic interpolation technique. For the actual land data, the above idea is somehow supported. However, the flat TINs occurred in the process of obtaining grid DEMs prevent us to draw a strong conclusion. The glass is half full for the results obtained from space-borne DEMs. From ASTER point of view, multi-frame super resolution enhanced ASTER when compared with real land data. On the contrary the level of enhancement with bi-cubic interpolation is higher than the multi-frame super resolution.

6.1 Discussions

Multi-frame super resolution is the algorithm of creating high resolution grid DEM from several low resolution grid DEMs provided that low resolution couples carry non-redundant information. As proved in chapter 4, although they have the same source, low resolution grid DEMs obtained from the same TIN configuration carry non-redundant information. Obviously, the level of enhancement is directly related to the amount of non redundant information. RMSD and NMI measures are graphed and correlation coefficients between these two measures are calculated. The examples of RMSD and NMI graphs can be seen in Figures 89 and 90. Graphs show inverse relation between NMI and RMSE. That is; as NMI decreases, RMSE value increases. The shapes of the graphs declare that the level of enhancement is directly related to the amount of non redundant information. If normalized mutual information value is high, then RMSD values would be low. In other terms if low resolution couples carry more non redundant information, than low RMSD value is expected. In order to find out the level of this relation, correlation coefficient between NMI and RMSD values are found. The correlation coefficient values for each test case can be seen in Table 54. Correlation coefficient obtained from 5 m METU area is regarded as an outlier, where as

can be seen in Table 50, the NMI values and RMSD values are very close. The minimum and maximum RMSD values are 3.082 and 3.103 respectively, whereas minimum and maximum NMI values are 1.317 and 1.320.

	SR	A	B	C	D	BC
RMSD	3.667	7.771	7.809	7.771	7.809	4.009
NMI	1.826	1.458	1.458	1.458	1.458	1.842
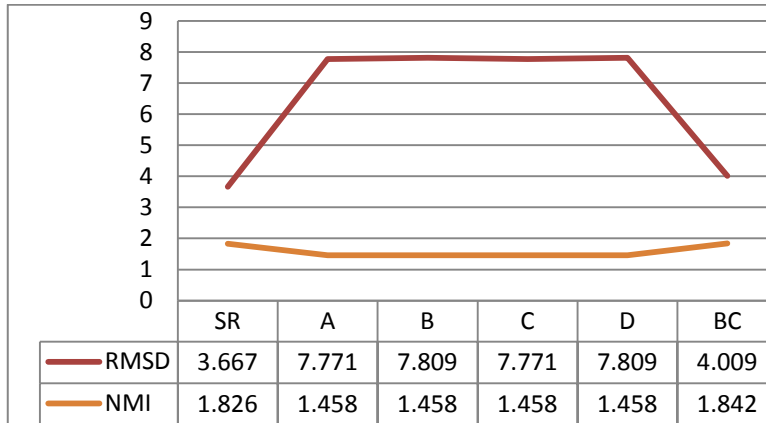
Figure 89 RMSD and NMI graph for 10 m Ellipsoidal Surface

	SR	A	B	C	D	BC
RMSD	8.183	8.323	8.323	8.324	8.324	8.17
NMI	1.49	1.484	1.484	1.484	1.484	1.491
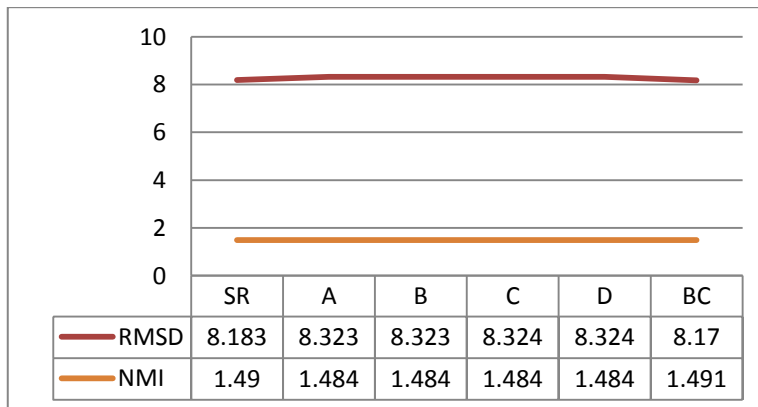
Figure 90 RMSD and NMI graph for 1 arc-second SRTM vs ASTER data

Table 54 Correlation Coefficient values for each test case

Test Case	Grid Size	Correlation Coefficient
Ellipsoid	10 m	-0.99685
Ellipsoid	5m	-0.99804
Gaussian	5 m	-0.98613
Gaussian	2.5 m	-0.99533
METU Area	10 m	-0.99914
METU Area	5 m	0.694601
SRTM+ASTER vs TIN	0.5 arc-second	-0.99953

Multi-frame super resolution algorithm uses low resolution grid DEMs. They are arranged as the grid centers of these LR grid DEMs which are half pixel away from each other. In grid DEM production for each grid cell, interpolation is applied and a value for that particular cell is obtained. For every different grid cell, new information is found. As explained in chapter 4, although they use the same base for interpolation, each coordinate brings new information. Especially in TIN, flat TINs create serious problems. In Figure 91, TIN and HR grid DEM can be seen, where in the middle near the big triangles, the small triangles are flat triangles. Corners of TINs have the same elevation value, so they have zero slope and they do not have a defined aspect. The values obtained from interpolation will bring the same value. However, multi-frame super resolution helps to solve this problem.
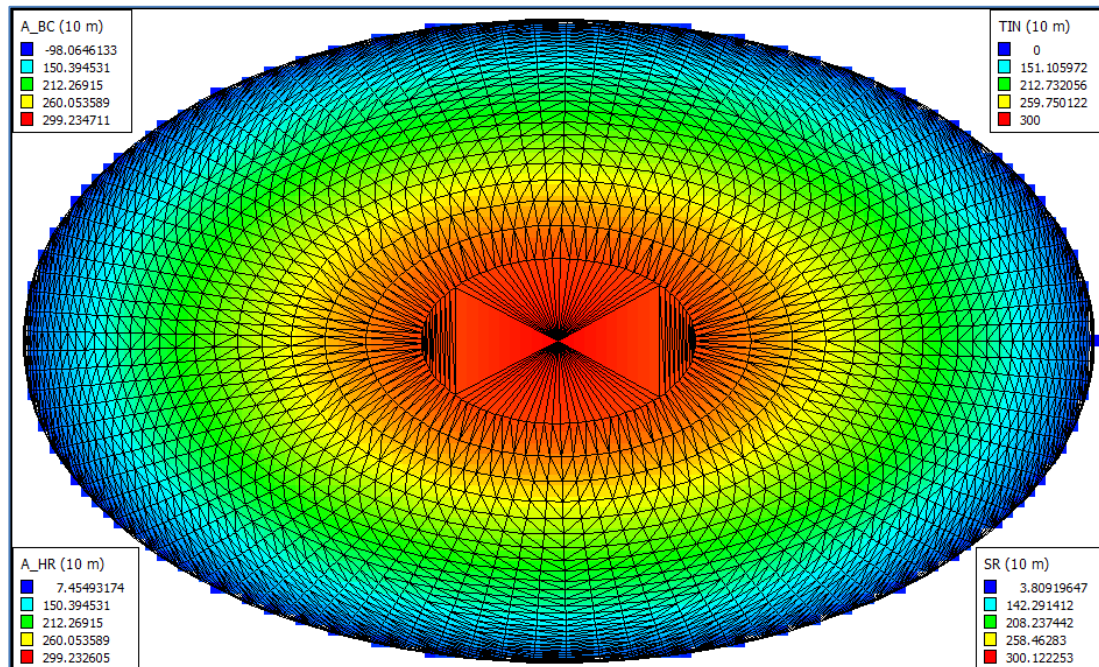
Figure 91 TIN, HR grid DEM and all legends for Ellipsoidal surface (10 m)

In Figures 92 and 93, four points are selected arbitrarily. Z value for the left point in Figure 92, which is on flat TIN, is miscalculated by traditional TIN algorithm. However multi-frame super resolution calculates the z value correctly. This point is between the 290 m and 300 m contours. The right point on the other hand is very near to 300 m elevation. Bi-cubic interpolation cannot find an extremity, as in the case of multi-frame super resolution, because the value is determined by 16 LR grid DEM values. Bi-cubic interpolation limits values because of 16 input values.

Figure 92 Selected point values on TIN, SR, A_HR, and A BC for ellipsoid (10 m)

Two points selected arbitrarily in Figure 93, show the level of enhancement made by multi-frame super resolution. Although the source of LR grid DEMs is the same, the result shows a spatial enhancement.

Figure 93 Selected point values on TIN, SR, A_HR, and A BC for ellipsoid (10 m)

Another point in discussion is the better enhancement by bi-cubic interpolation in Gaussian surface with 5 m grid size. The grid values in that case is very narrow. As indicated previously, ringing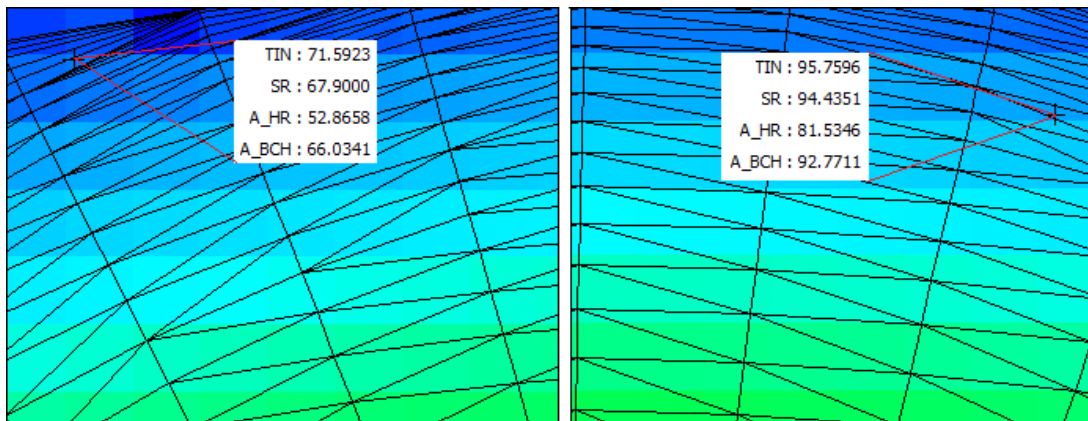 effect comes out and gives enormous mistake in multi-frame super resolution. The point in discussion is that why this effect is not seen in other parts. The answer to this question is hidden in the range of values. The range is very narrow and any little difference gets bigger by iteration and in the end it has greater results on overall. The roof of the hydraulic lab in Figure 18 shows this secondary ringing effect very clearly. The same effect is seen on multi-frame super resolution Gaussian surface with 5 m grid size. The range is very narrow so the neighboring grid cell values are very close, so the secondary ringing effect occurred. Then the question arouses that "Why we do not see the same effect on the others?" The answer is the width of the range of grid cell values. If the neighboring grid cell values are very close, then the secondary ringing effect occurs.

6.2 Conclusion and Recommendation

Higher accuracy can be obtained by using smaller grid sized DEMs. However, sampling accuracy limits DEM's accuracy; in turn decreasing the grid size is limited with the map scale. On the other hand, super resolution is one of the techniques by which more information can be obtained from limited samples. Super resolution on Grid DEM gives great chances to increase the accuracy from a limited sampling accuracy.

The main question in this study is "Can the accuracy of the DEM be increased by using super resolution techniques?" During the period of study, some other side questions arose like "Does super resolution work on grid DEMs?", "Having the same source of data, do low resolution pairs carry non-redundant information?"

The multi-frame super resolution on synthetic data shows a potential in increasing the spatial resolution of SR grid DEM even if LR grid DEMs are obtained from the same source. The level of enhancement competes with bi-cubic interpolation technique. This dissertation is weakly supported with the results obtained from the actual land.

This study showed that multi-frame super resolution can be applicable on grid DEMs and two items from each domain can be coupled. In this study Iterative Backward Projection (IBP) technique is used for super resolution and for DEM interpolation Triangulated Irregular

Network (TIN) method is used. At the end of the study in can be concluded that despite the "ill-posed nature of the inverse problem", iterative backward projection is only a start in coupling super resolution and digital elevation modeling domains.

As a recommendation; grid DEM and super resolution coupling, promises a good scientific study on grid DEM super resolution coupling. Need for high accuracy products from limited sampled data, will lead scientists to find a way for maximizing the productivity of limited samples. Even in the production stage of DEM, the coupling of super resolution will help to increase the productivity.

The objection made about "Single source of data" is very important and very crucial. In this study, adequate answers are tried to be given to this objection. Theoretical or practical scientific studies on multi source data will enlarge and strengthen the answers given in this study. Especially the suggestion done earlier, "the level of enhancement is directly related to the amount of non redundant information that LR grid DEM pairs carry" can be proved on multi source data environments.

REFERENCES

Aranoff, S. (1995). *Geographic Information Systems: A managemental Perspective.* WDL Publications, Ottowa, Canada.

Avcıbaş, İ., & Sankur, B. (2000). Statistical analysis of image quality measures. *Eurepean Signal Processing Conference EUSIPCO - 2000*, (pp. . 2181 - 2184). Tampere, Finland.

Avcıbaş, İ., Sankur, B., & Sayood, K. (2002). Statitical evaluation of image quality measures. *Journal of Electronic Imaging , 11* (2), 11 (2), 206 - 223.

Baker, S., & Kanade, T. (2002). Limits on Super-Resolution and How to Break Them. *IEEE Transactions on Pattern Recognition and Machine Intelligence* , Vol. 24, No. 9, 1167-1183.

Bulyshev, A., Hines, G., Vanek, M., Amzajerdian, F., Reisse, R., & Pierrottet, D. (2010). Computational experiments on super-resolution enhancement of FLASH LIDAR data. In M. Turner, & G. Kamerman (Ed.), *Laser Radar Technology and Applications XV. 7684*, p. doi:10.1117/12.853194. Orlando, FL: Proceedings of SPIE--the International Society for Optical Engineering.

Carlisle, B. H. (2005). Modelling the spatial distribution of DEM error. *Transactions in GIS* , 9 (4), 521- 540.

Fitzpatrick, J. M., Hill, D. L., & Maurer Jr., C. R. (2000). Image Registration. In M. Sonka, & J. M. Fitzpatrick, *Handbook of Medical Imaging Volume 2. Medical Image Processing and Analysis* (pp. 487-496). Bellingham, WA: SPIE - The International Society for Optical Engineering.

Flanagan, M., & Civco, D. (2001). Subpixel Impervious Surface Mapping. St. Louis, MO: ASPRS 2001 Annual Convention (April 23 - 27).

Grohmann, C. H. (2006). Resampling SRTM 03"- data with kriging. *GRASS/OSGeo-News Open Source GIS and Remote Sensing information* , 4, 21-25.

Hartlry, R. (1928). Transmission of Information. *The Bell System Technical Journal , 7* (3), 535-563.

Keeratikasikorn, C., & Trisirisatayawong, I. (2008). Reconstruction of 30m DEM from 90m SRTM DEM with Bicubic Polynomial Interpolation Method. *The International Archives of the Photogrammetry, Remote Sensing and Spatial Information Sciences, XXIst ISPRS Congress, XXXVII - Part B1*, pp. 791 - 794. Beijing.

Keren, D., Peleg, S., & Brada, R. (1988). Image sequence enhancement using sub-pixel displacements. *IEEE Conference on computer Vision and Pattern Recognition*, (pp. 742-746). Ann Arbor, MI.

Lucas, B., & Kanade, T. (1981). An iterative image registration technique with an application to stereo vision. *International Joint Conference on Artificial Intelligence*, (pp. 674 - 679). Vancouver, Canada.

Nguyen, N., & Milanfar, P. (2001). A Computationally Efficient Superresolution Image Reconstruction Algorithm. *IEEE Transactions on Image processing* , Vol. 10, No. 4, 573-583.

Oksanen, J., & Sarjakoski, T. (2005). Error propagation of DEM based surface derivative. *Computers and Geosciences* , 31, 1015-1027.

Park, S. C., Park, M. K., & Kang, M. G. (2003). Super-resolution image reconstruction: a technical overview. *Signal Processing Magazine, IEEE* , V. 20 (3), 21 - 36.

Paşaoğulları, O. (2002). Effect of scale and grid size for hydrological studies. *Master Thesis, Graduate School of Natural and Applied Sciences, METU, Ankara, Turkey* .

Sefercik, U., Jacobsen, K., Oruc, M., & Marangoz, A. (2007). Comparison of SPOT, SRTM and ASTER DEMs. In C. Heipke, K. Jacobsen, & M. Gerke (Ed.), *ISPRS Archives - Volume XXXVI-1/W51, 2007.* Hannover, Germany.

Shannon, C. (1948). A Mathematical Theory of Communication. *The Bell System Technical Journal , 27*, 379-423, 623-656.

Shepard, D. (1968). A two-dimensional interpolation function for irregularly-spaced data. *Proceedings of the 1968 23rd ACM National Conference*, (pp. 517–524). NY, USA.

Shi, W. Z., & Tian, Y. (2006). A hybrid interpolation method for the refinement of a regular grid digital elevation model. *International Journal of Geographical Information Science* , Vol. 20, No 1, 53 – 67.

Song, H., He, X., Chen, W., & Sun, Y. (2010). An Improved Iterative Back-projection Algorithm for Video Super-resolution Reconstruction. *2010 Symposium on Photonics and Optoelectronic (SOPO 2010) Proceedings*, (pp. 1-4). Chengdu, China.

SPOT 5, http://spot5.cnes.fr/gb/systeme/3110.htm. (2006). Retrieved May 21, 2006, from Supermode.

Tatem, A. J., Lewis, H. G., Atkinson, P. M., & Nixon, M. (2002). Super-resolution land cover pattern prediction using a Hopfield neural network. *Remote Sensing of Environment* , 79, 1-14.

Valeriano, M. M., Kuplich, T. M., Storino, M., Amaral, B. D., Mendes, J. N., & Lima, D. J. (2006). Modeling small watersheds in Brazilian Amazonia with shuttle radar topographic mission-90 m data. *Computers & Geosciences , 32* (8), 1169-1181.

Witten, I. H., & Frank, E. (2005). *Data Mining: Practical Machine Learning Tools and Techniques.* San Francisco, CA: Morgan Kaufmann Publishers.

Wu, J., Trivedi, M., & Rao, B. (2004). High frequency component compensation based on super-resolution algorithm for face video recognition. *Proceedings of the 17th International Conference on Pattern Recognition (ICPR'04). Vol. 3 pp. 598-601.* Cambridge, UK: IEEE Computer Society.

Zhou, Q., & Liu, X. (2004). Analysis of errors of derived slope and aspect related to DEM data properties. *Computers & Geosciences* , 30 369 - 378.

CURRICULUM VITAE

Onur PAŞAOĞULLARI was born in Konya on April 9, 1975. He graduated from Middle East Technical University Civil Engineering Department in 1998. He received his M.S. degree in Civil Engineering Department from the same University in 2002 with his thesis "Effect of scale and grid size for hydrological studies". He worked in Turkish Telecom for more than 10 years responsible from conducting the GIS Project. He worked in former State Planning Organization as an engineer responsible from establishing Spatial Decision Support Module. He is the Head of Planning and Coordination Department in General Directorate of Geographic Information Systems. He and his team are responsible from establishment of Turkish National Spatial Data Infrastructure, and establishment of Turkish Geo Portal. His primary research interests include geographic information systems, 2.5 and 3D modeling, Geo Portals.

Publications

- Effect of Map Scale and Grid Size in Hydrological Studies, 8th ESRI and ERDAS User Conference (Turkey), 6-7 June 2002 Ankara, Turkey
- Effect of map scale and grid size for hydrological modelling. (with Usul, N.) International Conference of GIS and Remote Sensing in Hydrology, Water Resources and Environment (ICGRSHWE), Three Gorges Dam, China, 16-19 September 2003 IAHS Publication